The Abdus Salam
International Centre for Theoretical Physics

United Nations
Educational, Scientific
and Cultural Organization

International Atomic
Energy Agency

World Year of PHYSICS 2005

H4.SMR/1642-2

"IAG-IASPEI Joint Capacity Building Workshop on Deformation Measurements and Understanding Natural Hazards in Developing Countries"

17 - 23 January 2005

The North Central Italian Upper Mantle Anomaly from Seismological, Petrological and Geodetic Data, Five Lustres after its Discovery

G.F. Panza[1, 2]

[1] Department of Earth Sciences
University of Trieste

[2] ICTP SAND Group, Trieste

The North Central Italian upper mantle anomaly, from seismological, petrological and geodetic data, five lustres after its discovery

G.F. Panza

ICTP, January 2005

12/21/2004

Reprinted from Nature, Vol. 296, No. 5854, pp.238-239, 18 March 1982

64

Delineation of the North Central Italian upper mantle anomaly

G. F. Panza*, St. Mueller†, G. Calcagnile‡ & L. Knopoff§

* Istituto di Geodesia e Geofisica, Università di Trieste, Trieste, Italy
† ETH-Geophysics, Zurich, Switzerland
‡ Istituto di Geodesia e Geofisica, Università di Bari, Bari, Italy
§ Institute of Geophysics and Planetary Physics, University of California, Los Angeles 90024, USA

The Italian peninsula is the focus of intense deformational tectonic activity. It is underlain by mantle material whose inferred, relatively anomalous properties[1,2] are not inconsistent with the seismic, volcanic and thermal activity that is manifested in this region. The most effective geophysical tool for mapping the structure of the uppermost 200–300 km of the Earth is the observation and analysis of seismic surface-wave dispersion on a regional scale. Here we synthesize the interpretations of Rayleigh wave dispersion measurements made by several authors, each for different parts of North Central Italy[3–8], to delineate the lateral extent of the upper mantle anomaly in this region.

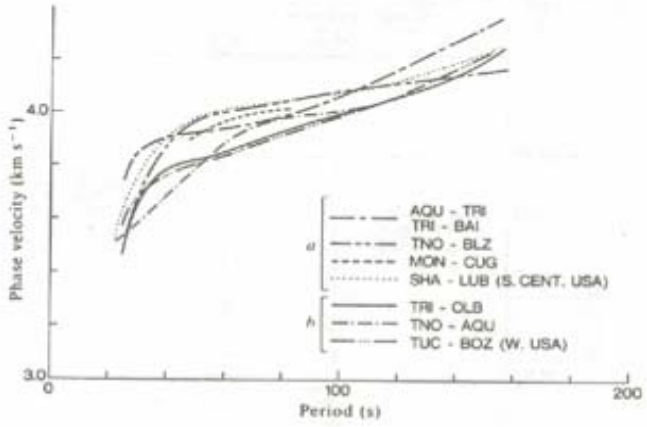

Fig. 2 Phase velocities used to delineate the North Central Italian anomaly and comparison with dispersion relations for western and South-Central USA. The r.m.s. errors for each curve are $\sim \pm 0.03$ km s^{-1} in the period range 40–60 s and are larger at the extremes of the period range[3,5–9]. Curves in group *a* are for regions without tectonic involvement and in group *b* for regions with tectonic involvement.

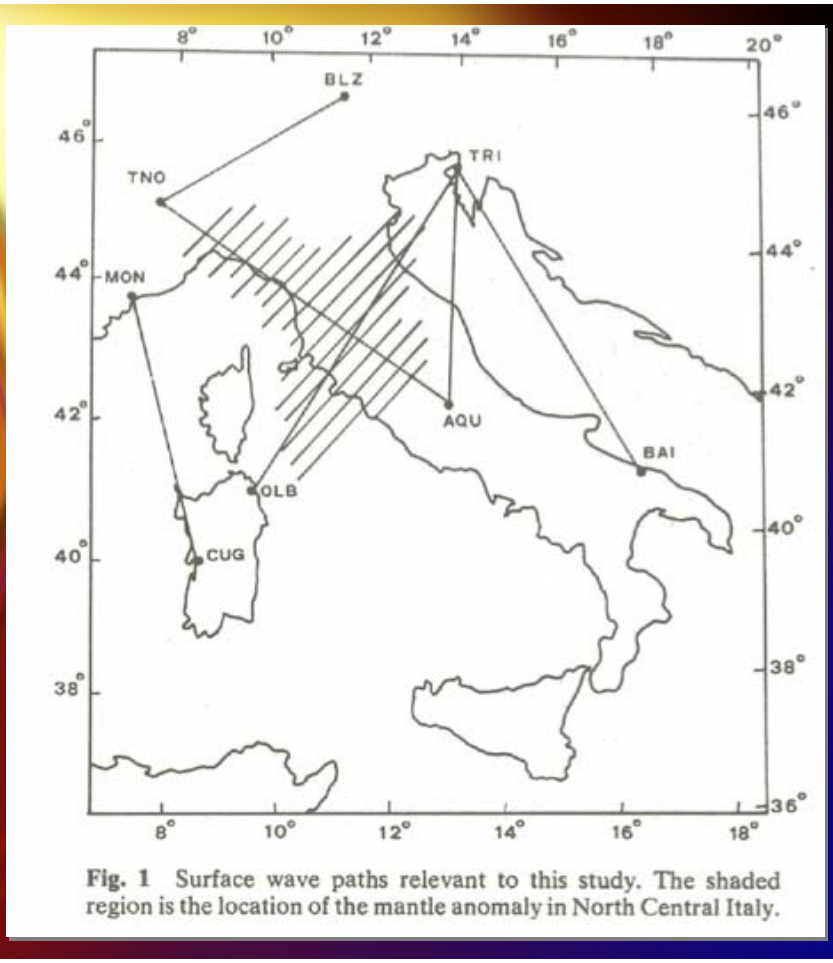

Fig. 1 Surface wave paths relevant to this study. The shaded region is the location of the mantle anomaly in North Central Italy.

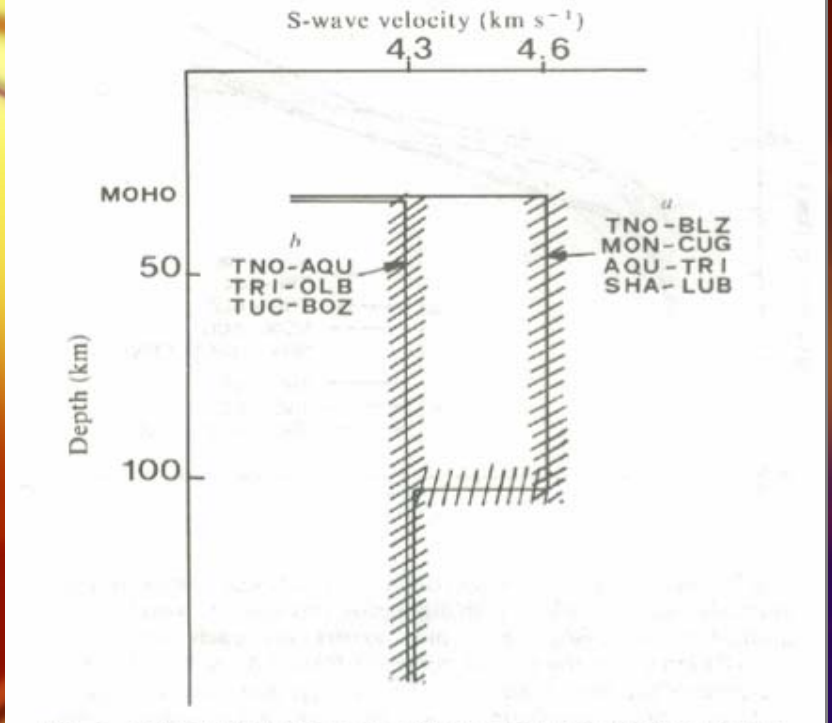

Fig. 3 Schematic shear wave velocity–depth distributions in the upper mantle for regions without *a* and with *b* major tectonic involvement today. The shading represents schematically the range of models satisfying each group of dispersion data.

We concluded that the anomalous low phase velocity region of nortehrn Italy lies to the east of the path MON-CUG, to the west of AQU-TRI, and south of the Alps.

Multiscale Surface waves tomography

Scale of the deforming plate

Phase and group velocity measurements

Station-Station paths

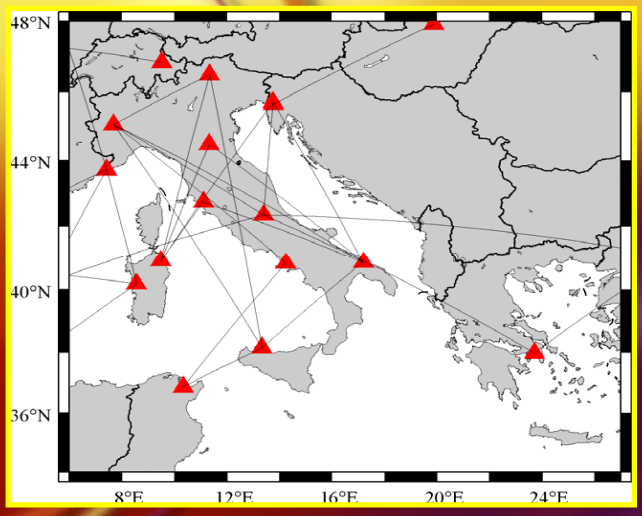

Epicentre-Station paths

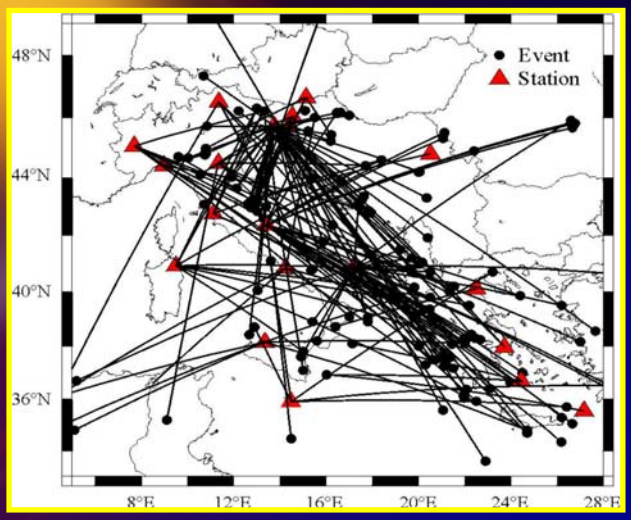

Broadband and LP Stations

Italy: TRI - GENV - AQU - NPL - GSO - TNO - BOL - OLB - BLZ - PAL - BAI - CUG; Slovenia: LJU - BISS - CEY; Greece: ATU - MIL - LIT - KAP; Malta: MLT; Tunisia: SBS; Monaco: MON; Switzerland: CHU; Hungary: PSZ

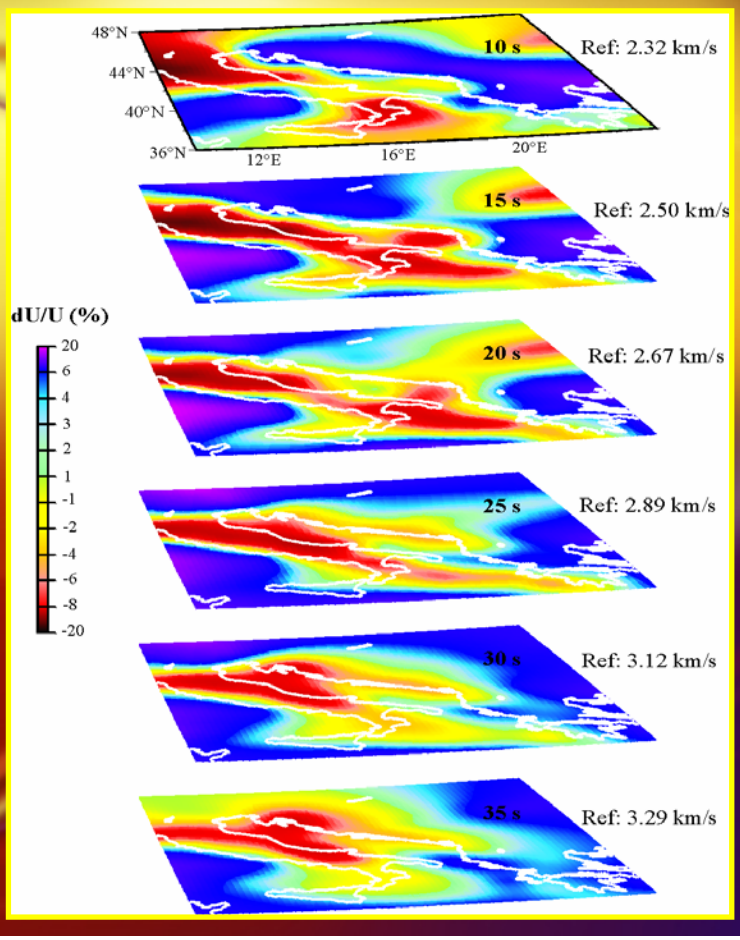

Group Velocity Tomography maps in the period range 10 s - 35 s

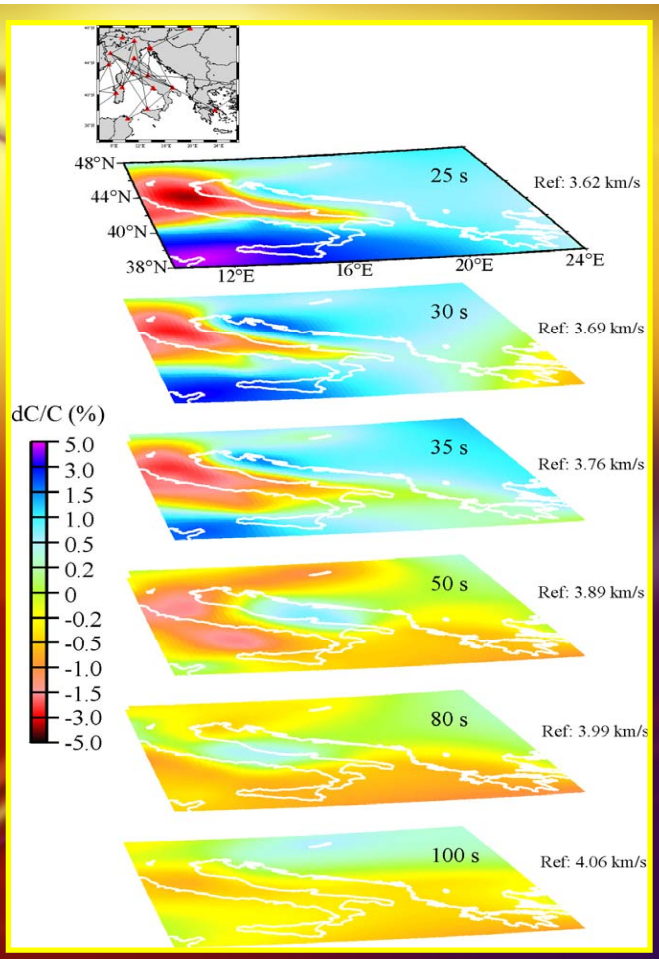

Phase Velocity Tomography maps in the period range 25 s - 100 s

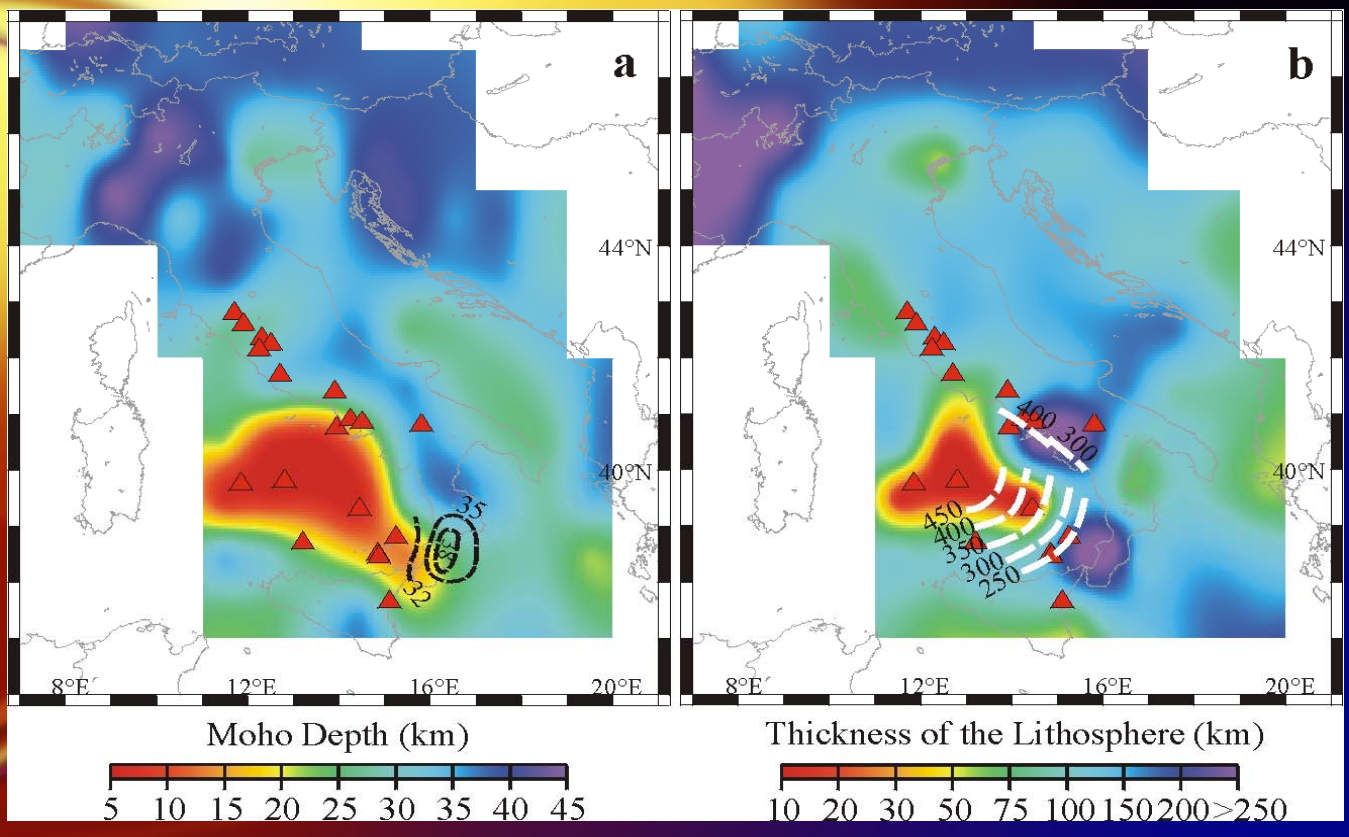

(a) Moho depth with contouring of the deeper Moho where lithospheric doubling is unambiguously detected;

(b) Thickness of the Lithosphere in km: the dashed lines schematize the subduction of the Ionian-Adria lithosphere, traced accordingly with ISC hypocenters distribution. The recent volcanoes in the study area are plotted as red triangles (from North to South): Amiata-Vulsini, Cimino-Vico-Sabatini, Albani, Roccamonfina, Phlegraean Fields-Vesuvio, Vulture, Ischia, Stromboli, Vulcano-Lipari, Etna, Ustica, Marsili, Magnaghi, Vavilov.

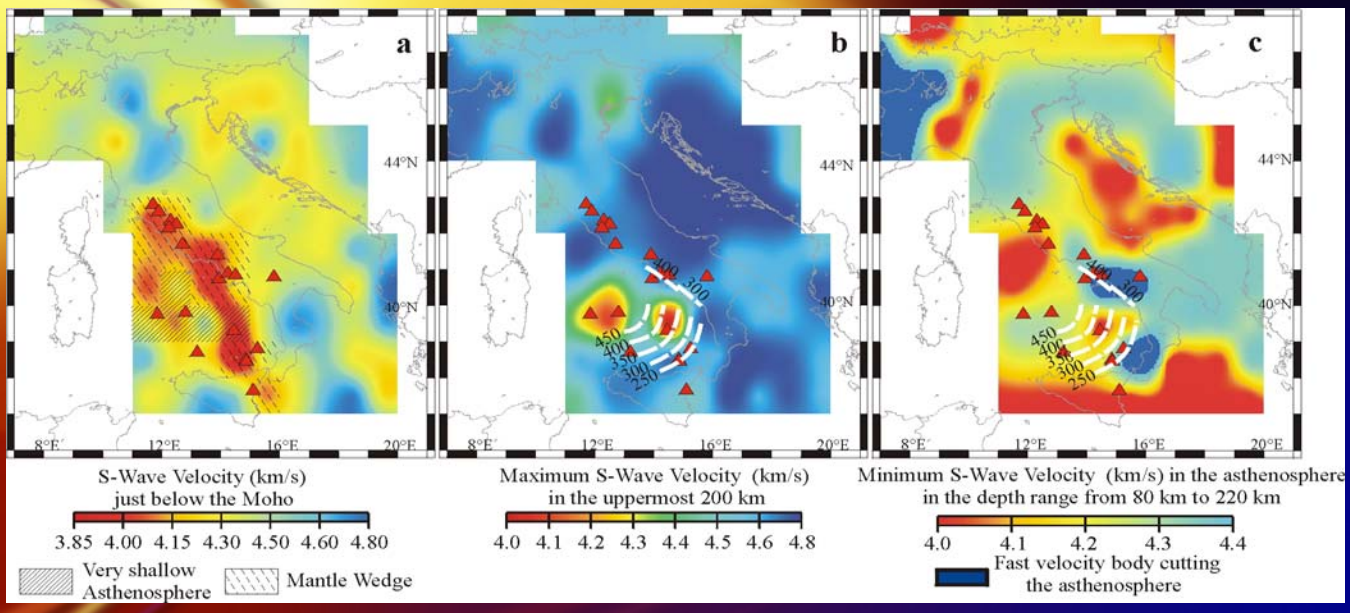

(a) V_s (km/s) just below the Moho - different dashed patterns outline where mantle wedge and a very shallow asthenosphere are detected;

(b) maximum V_s (km/s) in the uppermost 200 km;

(c) minimum V_s (km/s) in the asthenosphere, in the depth range from about 80 km to about 220 km.

In (b) and (c) the dashed lines schematize the subduction of the Ionian-Adria lithosphere, traced accordingly with ISC hypocenters distribution.

In (c) the dark blue areas indicate the fast velocity bodies cutting the asthenosphere, that can be extended to depths > 250 km, as indicated by the isolines. Red triangles represent the recent volcanoes.

Scale of the plate boundary

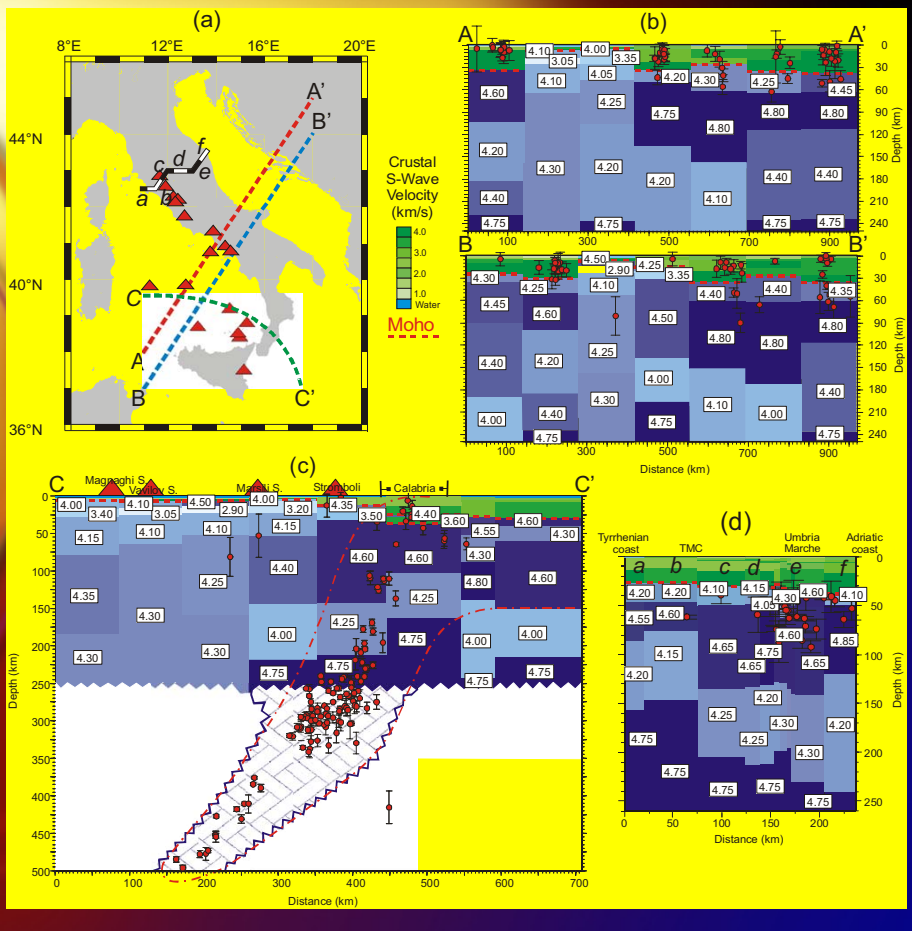

(a) Position of sections and of all recent volcanoes (triangles).

(b) Parallel vertical sections through the Tyrrhenian Sea, the Southern Apennines and the Dinarides. The pattern of high velocity is very different: the almost continuous high velocity body, that may be the Adriatic lithosphere subducted beneath the Apenninic belt, seen along profile BB', is not visible along AA'.

(c) The red dashed line outlines the subducted Ionian slab. From East to West the triangles delineate, in the order, the position of the volcanic edifices of Magnaghi-Vavilov, Marsili and Stromboli.

(d) Lithosphere-asthenosphere system from Tyrrhenian (*a*) to Adriatic coast (*f*); the mantle wedge presence supports the lithospheric delamination beneath Central Italy.

The shallow, intermediate and deep earthquakes that fall into a band, about 100 km wide, along each section, with the depth error bar, as given in the ISC catalogue, are shown.

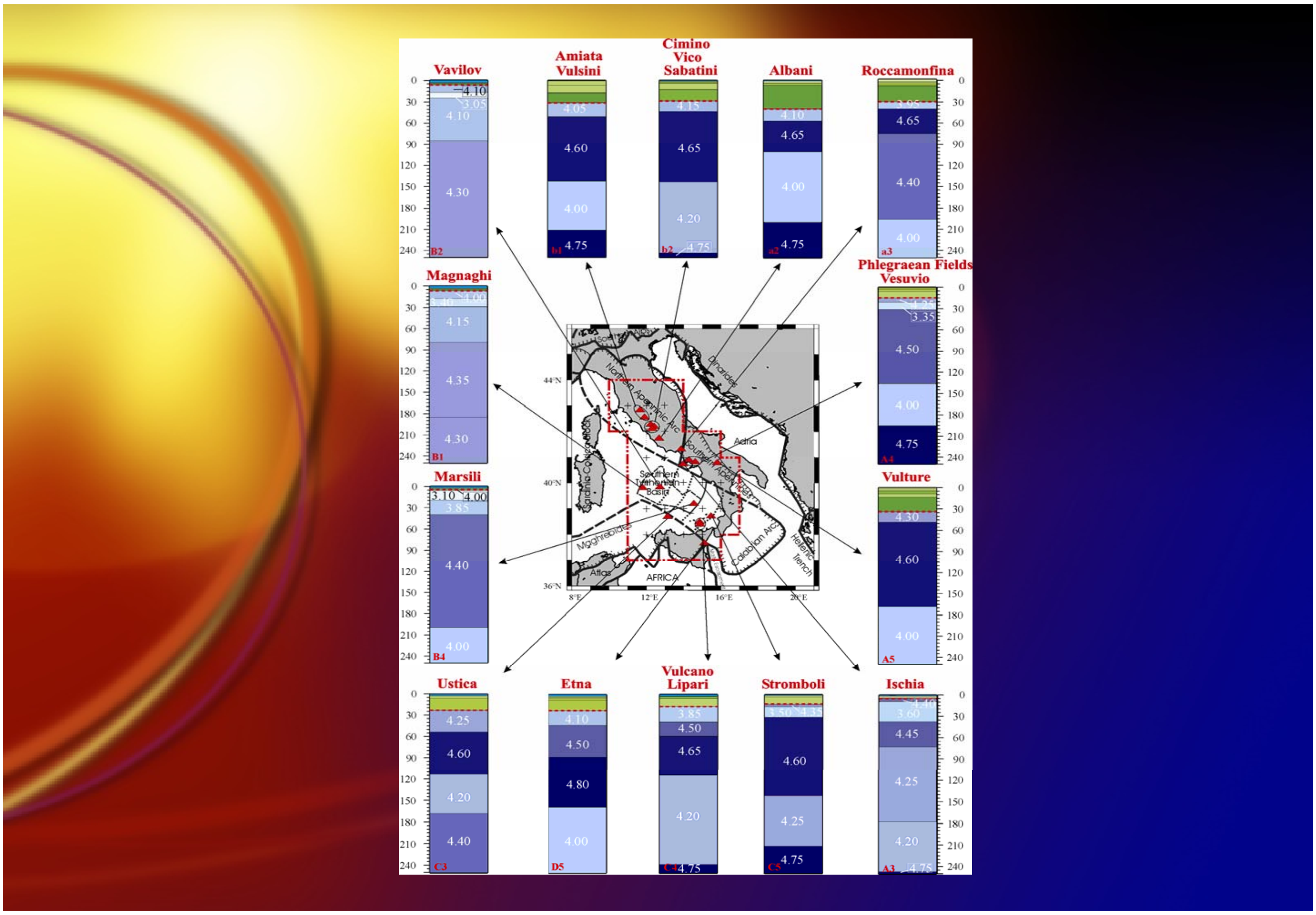
Vavilov
Amiata Vulsini
Cimino Vico Sabatini
Albani
Roccamonfina
Magnaghi
Phlegraean Fields Vesuvio
Marsili
Vulture
Ustica
Etna
Vulcano Lipari
Stromboli
Ischia

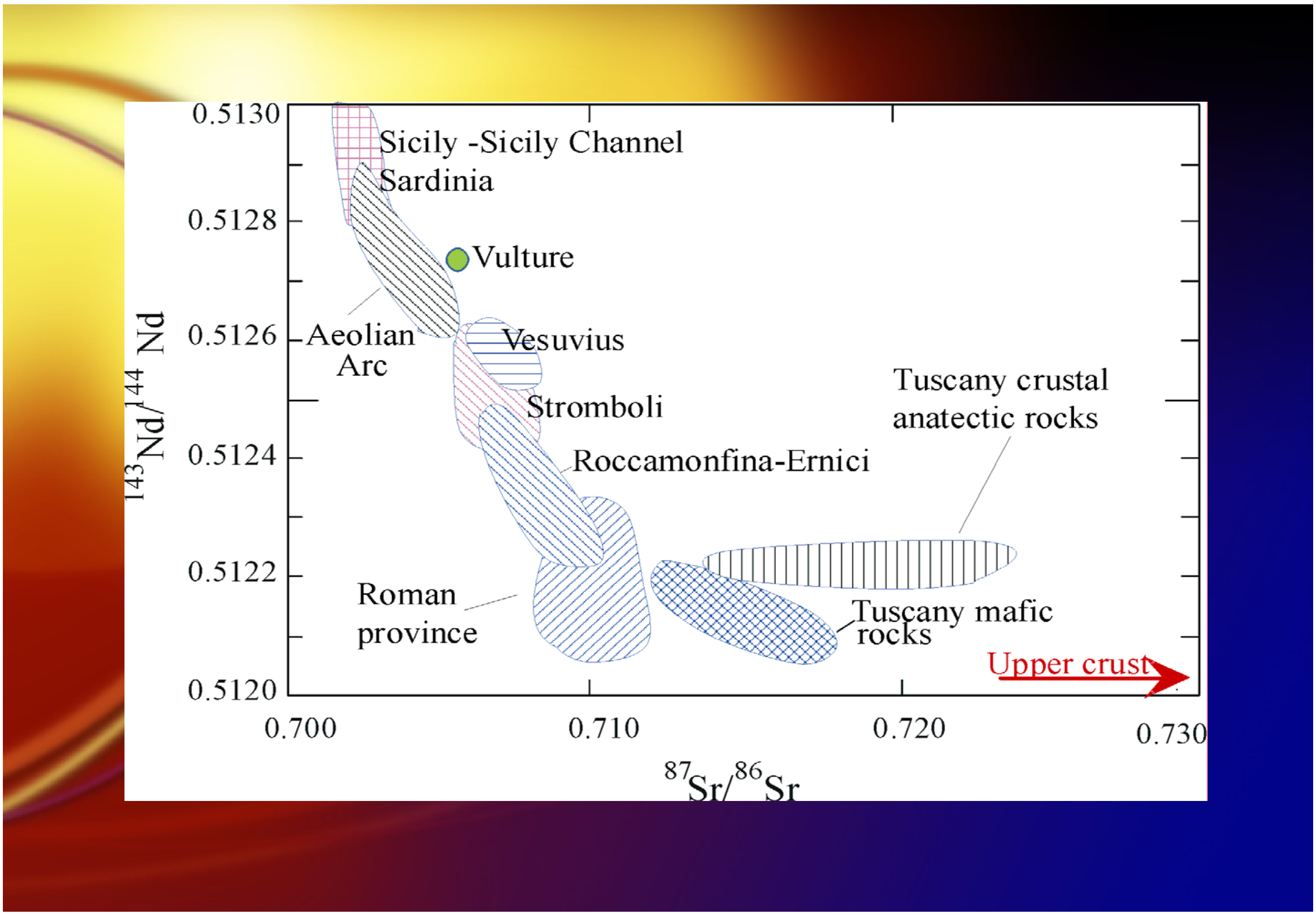
Sicily -Sicily Channel
Sardinia
Vulture
Aeolian Arc
Vesuvius
Stromboli
Roccamonfina-Ernici
Tuscany crustal anatectic rocks
Roman province
Tuscany mafic rocks
Upper crust
$^{143}Nd/^{144}Nd$
$^{87}Sr/^{86}Sr$
0.5130
0.5128
0.5126
0.5124
0.5122
0.5120
0.700
0.710
0.720
0.730

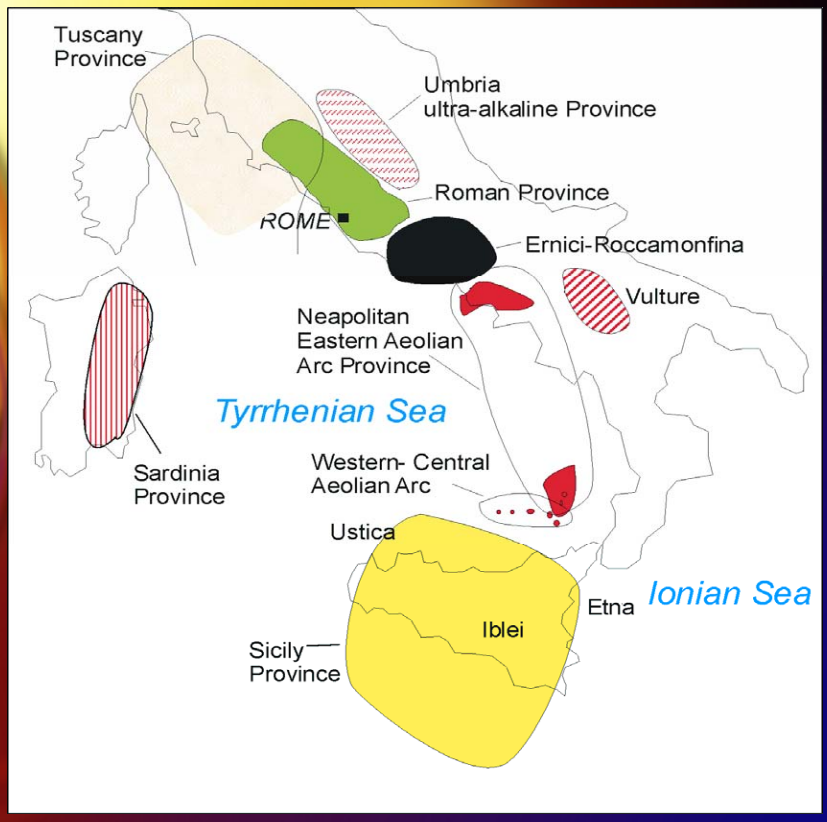

Geodynamic model of the Tyrrhenian basin and neighbouring volcanic areas

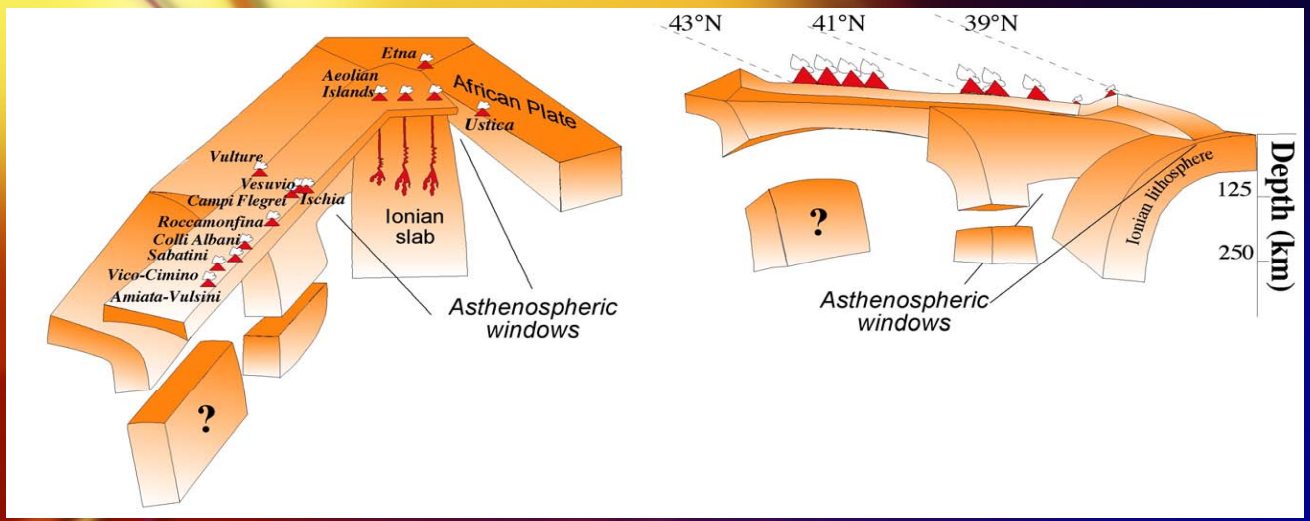

The 3-D model illustrates the possible thermo-mechanical detachment of part of the subducting lithosphere.

Local Scale: earthquake fault zones

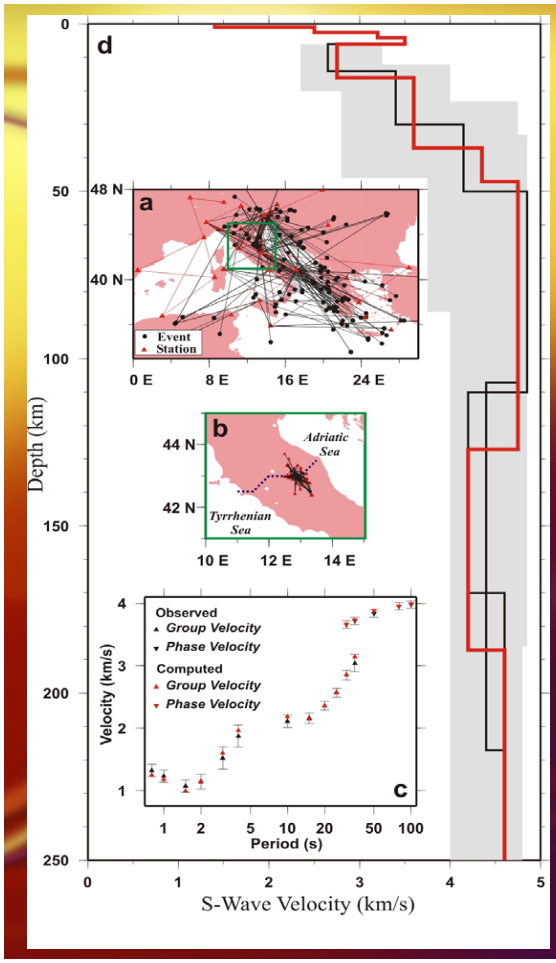

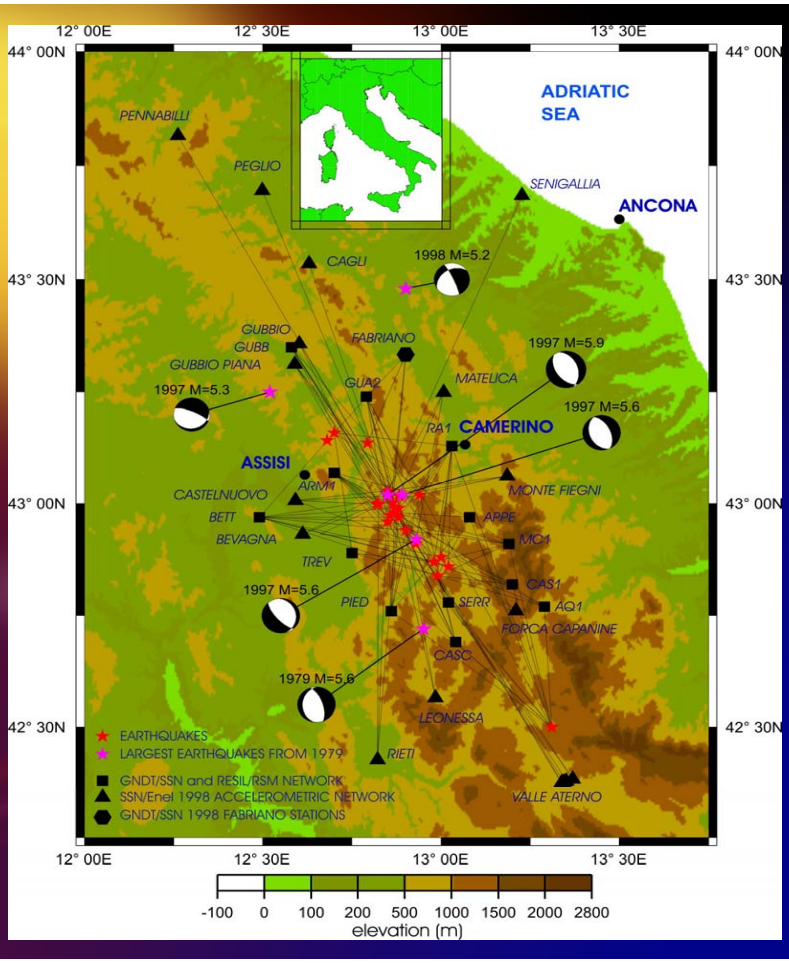

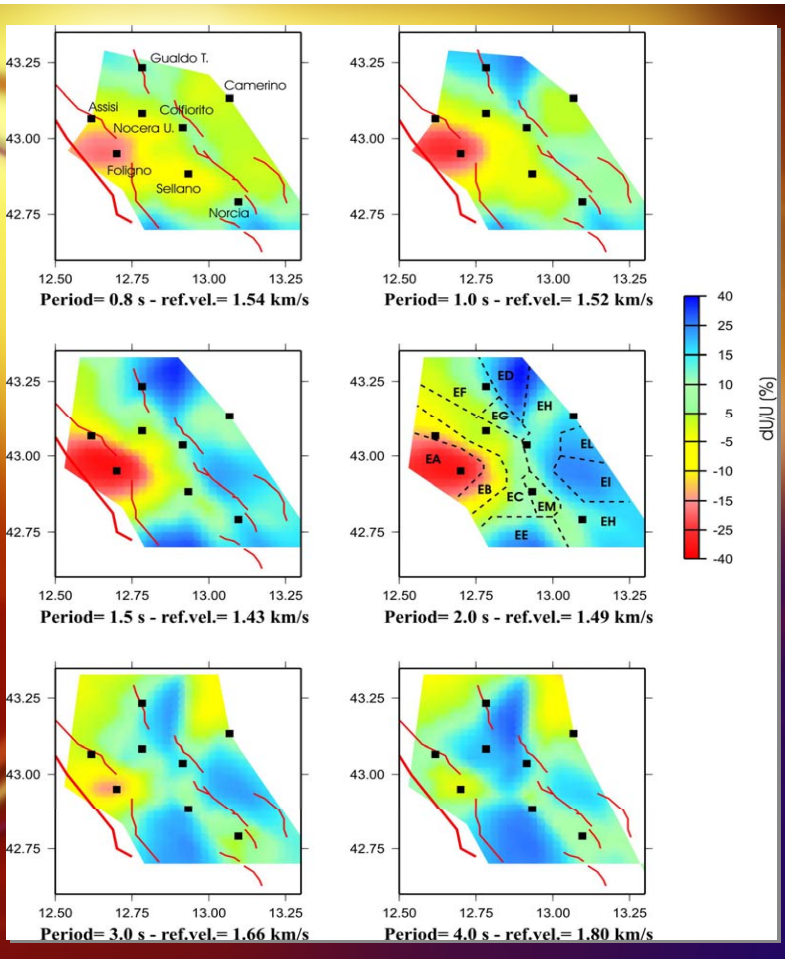

Local group velocity tomography

Section across the Umbria-Marche fault zone

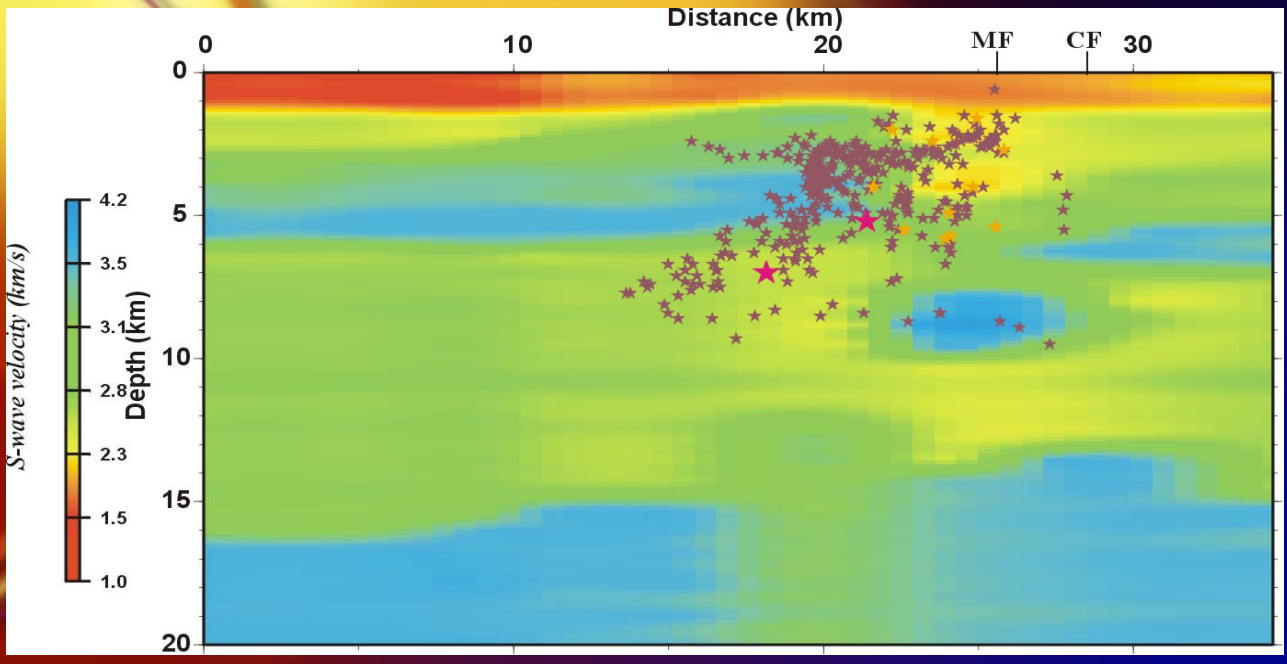

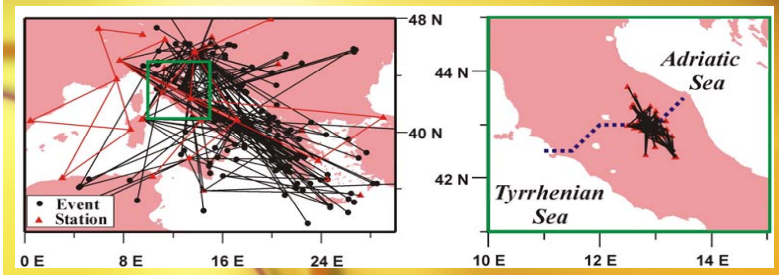

S-wave velocity image of the crust and upper mantle in the central Apennines

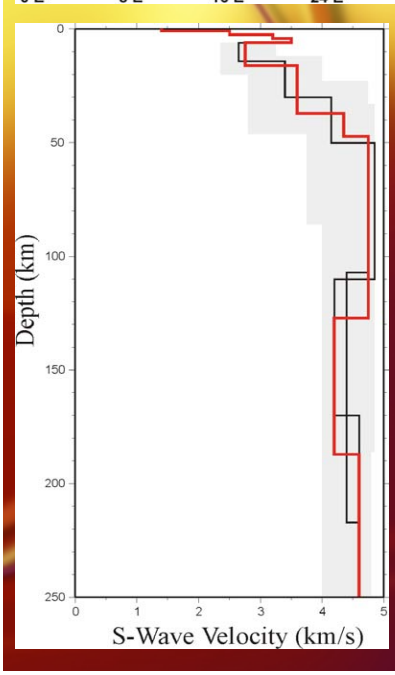

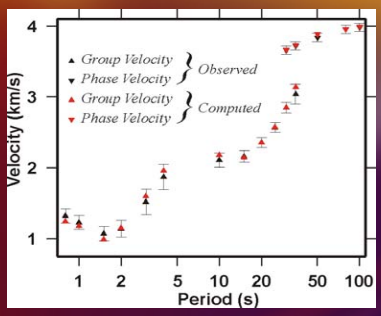

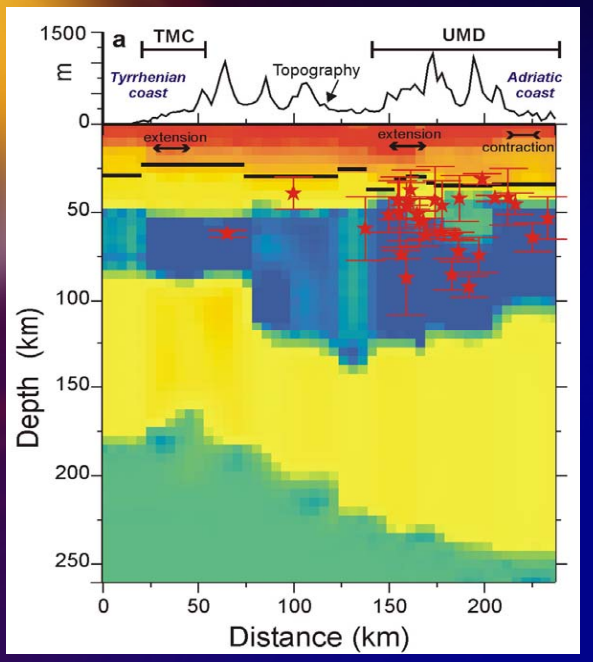

BUOYANCY-DRIVEN DEFORMATIONS IN THE CENTRAL APENNINES

The juxtaposed contraction and extension observed in the crust of the Italian Apennines and elsewhere has, for a long time, attracted the attention of geoscientists and is a long-standing enigmatic feature.

Several models, invoking mainly external forces, have been put forward to explain the close association of these two end-member deformation mechanisms clearly observed by geophysical and geological investigations.

These models appeal to interactions along plate margins or at the base of the lithosphere such as back-arc extension or shear tractions from mantle flow or to subduction processes such as slab pull, roll back or retreat and detachment.

BUOYANCY-DRIVEN DEFORMATIONS IN THE CENTRAL APENNINES

- Although external forces must have been important in the building up of the North-Central Apennines, we investigate the contribution of internal buoyancy forces with respect to the ongoing slow and complex lithospheric deformations, as revealed by very recent GPS solutions and by the unusual intermediate depth seismicity distribution [*Selvaggi and Amato, 1992*] that does not define a classical Benioff zone.
- In the uppermost 50 km of the model, we use density values estimated from a high-resolution gravimetry survey [*Marson et al., 1998*] made along the study profile. For the deeper structures we convert the S-wave velocity model [*Chimera et al., 2003*] into density [*Ludwig et al., 1970*] considering temperature effects. The concordance between the gravity anomaly directly computed from our density model (no data fitting) and the observed Bouguer anomaly is a measure of the reliability of our assumptions linked to the density estimates. Doing so, we fix the density and geometry of the crust-mantle structure, and the viscosity is the only variable parameter in our models.

V_s versus depth and hypocentres of the sub-crustal earthquakes (vertical bars indicate depth error) in the period 1965-1998 within a stripe 150 km wide along the study profile (red line in the inset). The bold black segment indicates the Moho depth.

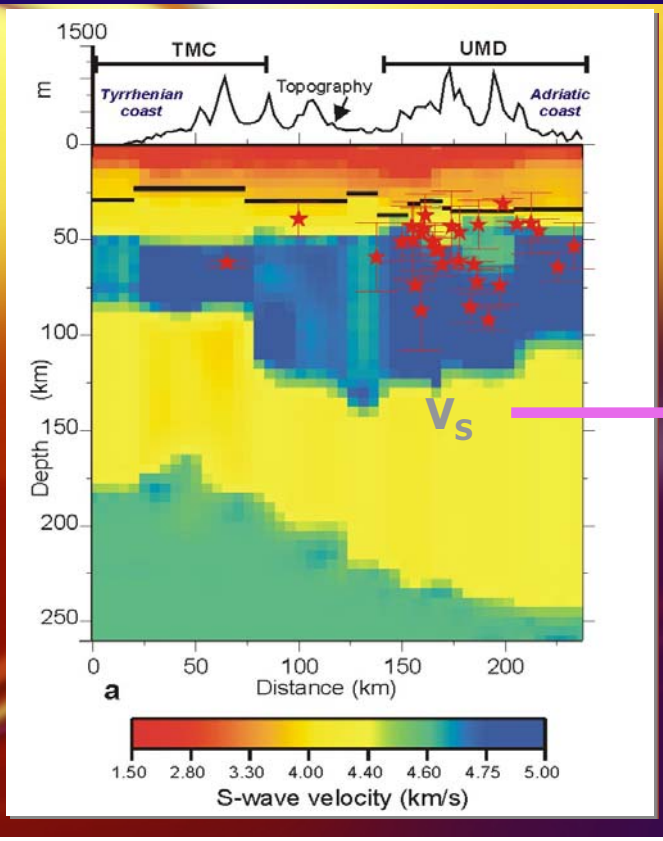

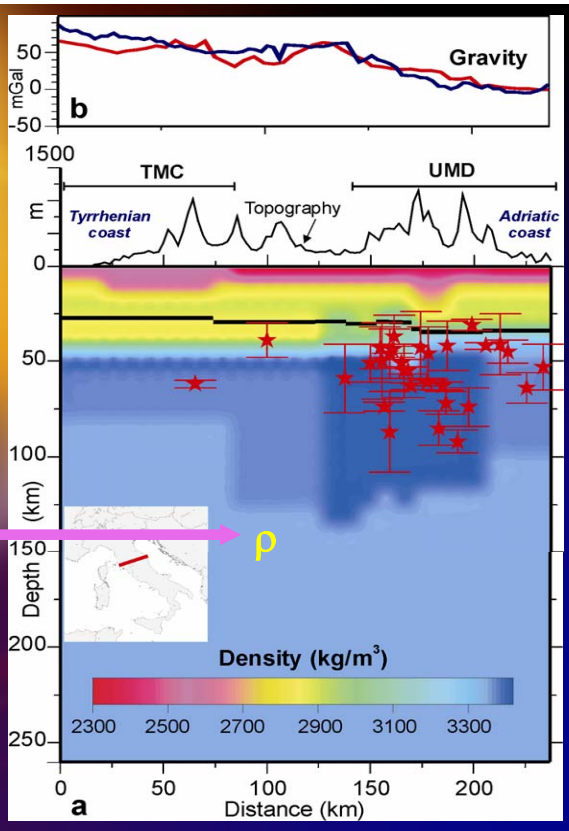

Density model. The topmost line represents the surface topography. Observed Bouguer gravity anomaly (blue) vs. gravity (red) predicted from our density model.

Postseismic deformation following the 1997 Umbria-Marche normal faulting earthquakes

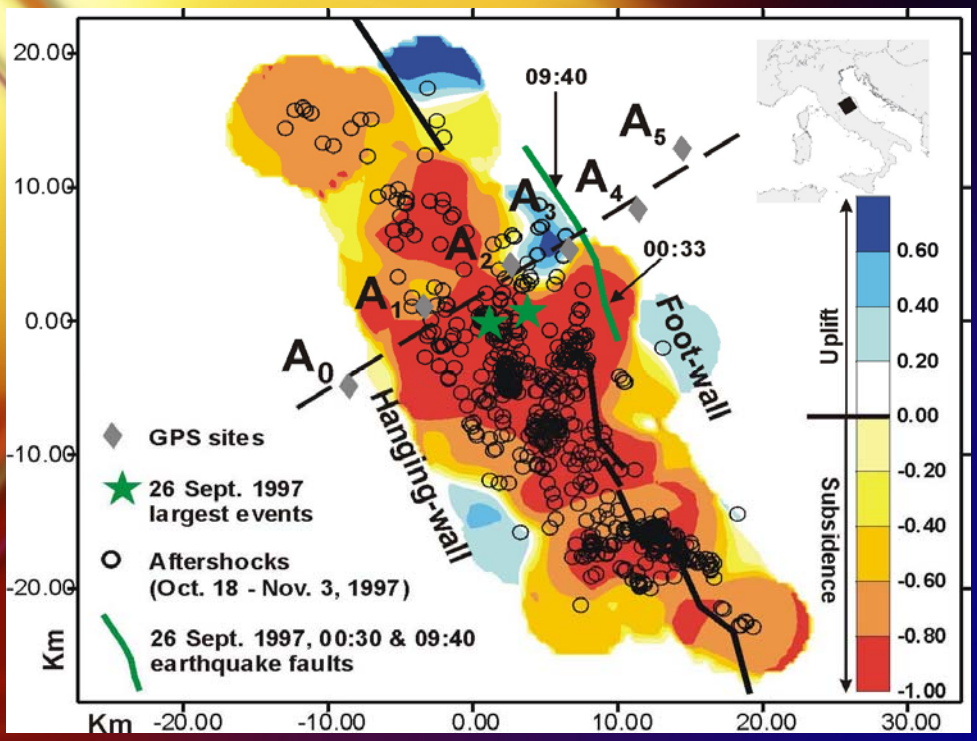

Vertical viscoelastic relaxation over 1 year for different fault models using different viscosity models

Layer	Thickness km	Viscosity Pa s
UC	8	Elastic
TZ	12	10^{19}-10^{17}
LC	15	10^{18}-10^{17}
Mantle	2856	10^{21}
Core	3480	Inviscid

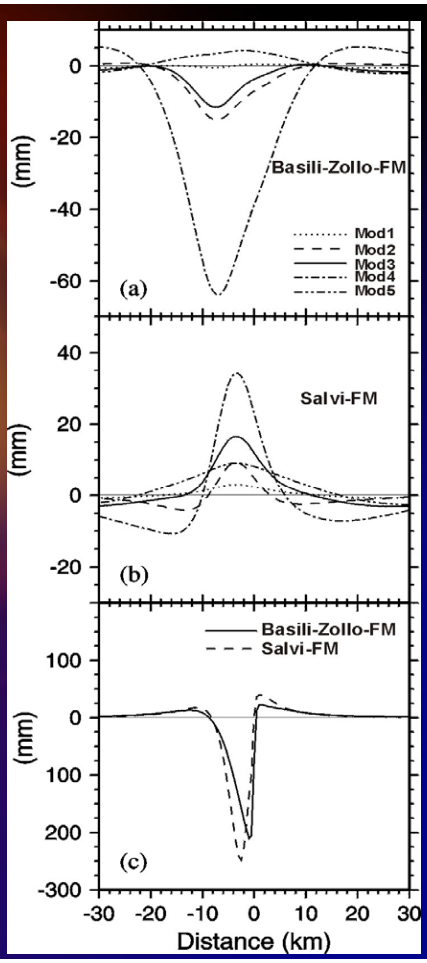

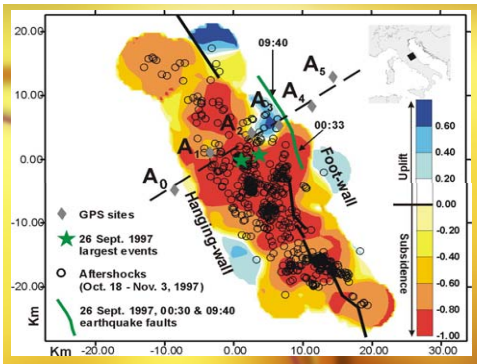

GPS (baseline length variations) vs. model predictions for different fault models using the preferred rheological model

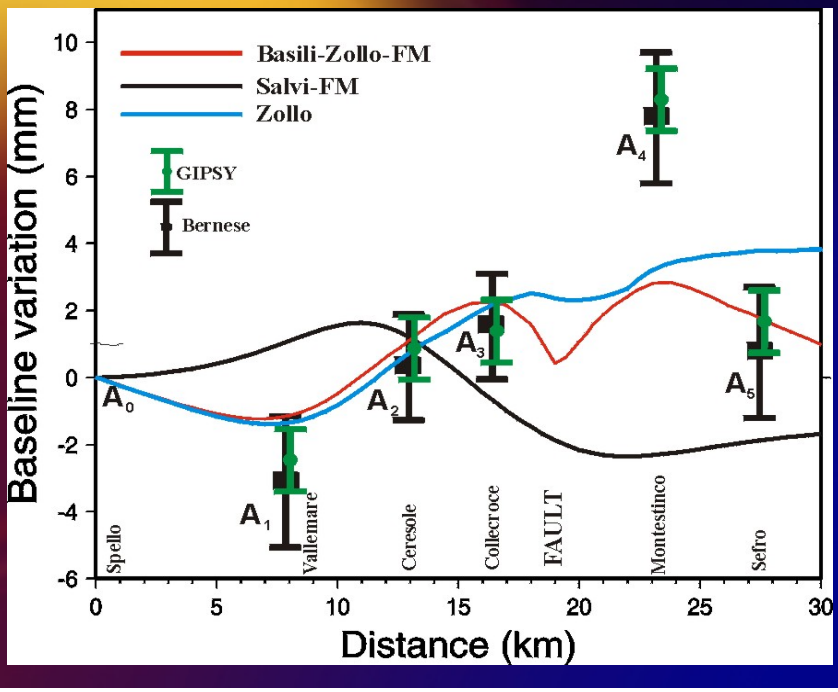

Slow viscous flow and tectonic (deviatoric) stress are found from the momentum conservation and continuity equations. By defining the stream function ψ as a velocity potential

$$v = (\partial\psi/\partial x_2, -\partial\psi/\partial x_1)^T$$

the governing equations can be combined to form:

$$\left(\frac{\partial^2}{\partial x_2^2} - \frac{\partial^2}{\partial x_1^2}\right)\eta\left(\frac{\partial^2\psi}{\partial x_2^2} - \frac{\partial^2\psi}{\partial x_1^2}\right) + 4\frac{\partial^2}{\partial x_1 \partial x_2}\eta\frac{\partial^2\psi}{\partial x_1 \partial x_2} = -g\frac{\partial\rho}{\partial x_1} \quad (1)$$

Where (x_1, x_2), ρ, η and g are the Cartesian co-ordinates, density, viscosity, and acceleration due to gravity, respectively.

The maximum shear stress is determined from the computed components of the tectonic stress tensor

$$\tau_{max} = \left[\frac{1}{2}\left(\tau_{11}^2 + \tau_{22}^2 + 2\tau_{12}^2\right)\right]^{1/2} = \eta\left[4\left(\frac{\partial^2\psi}{\partial x_1 \partial x_2}\right)^2 + \left(\frac{\partial^2\psi}{\partial x_2^2} - \frac{\partial^2\psi}{\partial x_1^2}\right)^2\right]^{1/2}$$

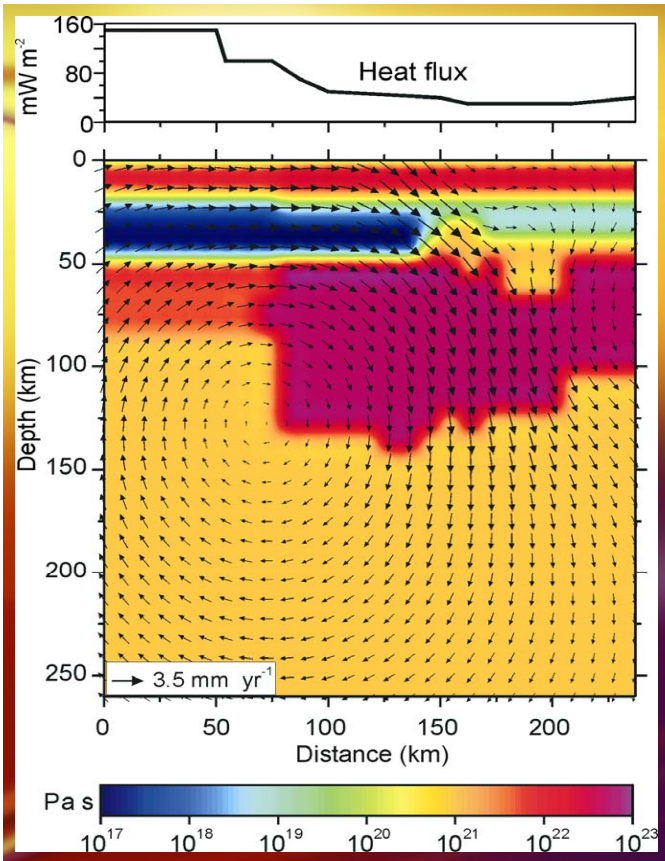

Effective viscosity of the lithospheric mantle can be constrained considering the observed regional strain rates. Sub-crustal earthquakes in the region provide an indirect measure of the rate of strain release within the seismogenic body. The seismic moment released beneath the UMD in the depth range from 30 km to 80 km, is estimated from the Harvard University CMT Catalog (1977-2002). Two large shocks occurred in the region: in 19.09.1979 (M_W=5.8) and in 26.03.1998 (M_W=5.4). The remaining sub-crustal earthquakes contribute very little to the cumulative seismic moment release, that is estimated to be about 8.5×10^{17} N×m. Using Kostrov's formula the strain rate, within a volume V (50 km × 50 km × 50 km) over a time interval t (20 years), is found to be 8.5×10^{-17} s^{-1}. This strain rate is used as a constraint on the viscosity of the lid in our test computations of the flow (and strain rate) for various viscosity ratios between lid and asthenosphere. We finally adopted the effective viscosity of the lid beneath the UMD to be 5×10^{22} Pa×s.

Effective viscosity used and predicted flow field. Reduction of the crust and lithospheric mantle effective viscosity at the left correlates with the high heat flow and recent magmatism.

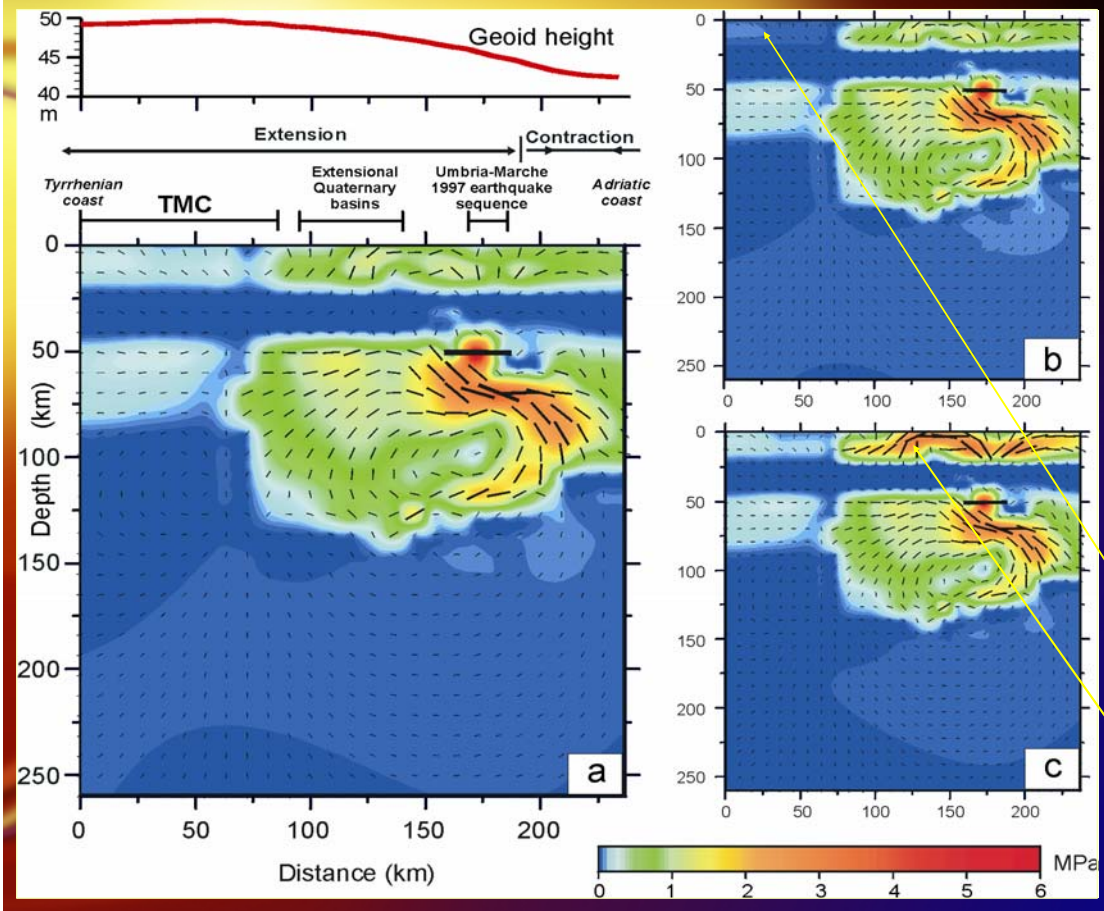

Tectonic shear stress and compressional axes (ticks) predicted by diffferent viscosity models along the studied profile (tensional axes are perpendicular to the compressional ones). The horizontal ticks indicate thrusting and vertical ticks indicate normal faulting. The geoid height exhibits its steepest gradient above the area of maximum deformation predicted in model (a); its viscosity profile has been shown before. In model b the viscosity of the Tuscan Metamorphic Complex upper crust is less than that in model a by a factor of 5; in model c, the viscosity of the Umbria-Marche Domain upper crust is higher than that in model a by a factor of 5.

RESULTS

The seismic tomography study provides a sound evidence of lithospheric delamination beneath the Apennines.

It is shown that buoyancy solely can explain recent and ongoing lithospheric deformations and the unusual distribution of intermediate depth earthquakes.

The coexistence of two end-member deformation mechanisms (contraction and extension) is explained, a geological enigma recognized in different geodynamic frameworks worldwide, but observed at the surface and active nowadays, hence better studied, only in the Italian Peninsula.

References

Panza, G.F., Mueller, S., Calcagnile, G. and Knopoff, L., (1982). Delineation of the north central Italian upper mantle anomaly. Nature, 296, 238-239.

Peccerillo, A. and Panza, G.F., (1999). Upper mantle domains beneath Central-Southern Italy: Petrological, geochemical and geophysical constraints. PAGEOPH, 156, 421-443.

Panza, G.F., Pontevivo, A., □Chimera, G., Raykova, R and Aoudia, A., (2003). The Lithosphere-Asthenosphere: Italy and surroundings. Episodes, 26, 169-174.

Chimera, G., Aoudia, A., Sarao', A. and Panza, G.F., (2003). Active tectonics in Central Italy: constraints from surface wave tomography and source moment tensor inversion. PEPI, 138, 241- 262.

Panza, G.F., Pontevivo, A., Sarao', A., Auodia, A., and Peccerillo, A., (2004). Structure of the lithosphere-asthenosphere and volcanism in the Tyrrhenian Sea and surroundings. APAT, Memorie descrittive della Carta Geologica d'Italia, vol LXIV, 29-56.


THE END

Reprinted from Nature, Vol. 296, No. 5854, pp.238-239, 18 March 1982

64

Delineation of the North Central Italian upper mantle anomaly

G. F. Panza*, St. Mueller†, G. Calcagnile‡ & L. Knopoff§

* Istituto di Geodesia e Geofisica, Università di Trieste, Trieste, Italy
† ETH-Geophysics, Zurich, Switzerland
‡ Istituto di Geodesia e Geofisica, Università di Bari, Bari, Italy
§ Institute of Geophysics and Planetary Physics, University of California, Los Angeles 90024, USA

The Italian peninsula is the focus of intense deformational tectonic activity. It is underlain by mantle material whose inferred, relatively anomalous properties[1,2] are not inconsistent with the seismic, volcanic and thermal activity that is manifested in this region. The most effective geophysical tool for mapping the structure of the uppermost 200–300 km of the Earth is the observation and analysis of seismic surface-wave dispersion on a regional scale. Here we synthesize the interpretations of Rayleigh wave dispersion measurements made by several authors, each for different parts of North Central Italy[3–8], to delineate the lateral extent of the upper mantle anomaly in this region.

Over the past 20 years intensive efforts have been made to study details of the cross-section of the crust and upper mantle in the European–Mediterranean area. As a result of these studies, several zones were delineated[1,2], such as the Western Mediterranean, the Tyrrhenian Sea, the Adriatic promontory of the African plate and the Central European Rift System, each with differing mantle structure. In addition to these structures, another conspicuous anomaly can be identified under the north-central part of the Apennine peninsula, that is the tectonically active region to the east and north of Corsica.

The properties of the upper mantle under North Central Italy (Fig. 1) have been delineated by Rayleigh wave dispersion measurements along two profiles TNO–AQU and TRI–OLB[5,6]. These profiles have unusually low phase velocities in the period range 40–60 s (Fig. 2). Velocities as low as these have been observed in the Western USA[9], as, for example, on the path TUC–BOZ, and the East African Rift[10], both regions of high heat flow. The correlation between the surface wave phase velocities in northern Italy and high heat flow is even stronger after the phase velocities have been inverted; cross-sections are found consistent with the absence of a lid to the low-velocity channel (Fig. 3) and anomalously low S-wave velocities that extend up to, or close to the Mohorovicic discontinuity. In these cases the high surface heat flows are probably thus derived from high temperatures at shallow depth in the mantle and hence are a surface expression of tectonic involvement on a scale extending into the mantle.

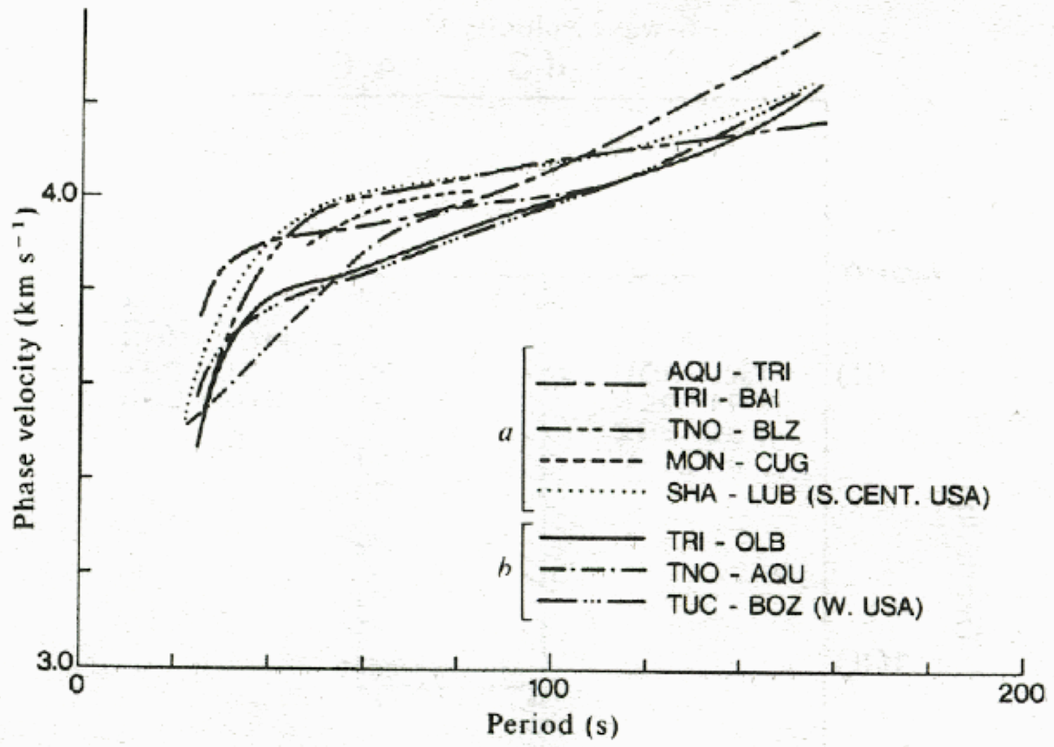

Fig. 2 Phase velocities used to delineate the North Central Italian anomaly and comparison with dispersion relations for western and South-Central USA. The r.m.s. errors for each curve are $\sim\pm0.03$ km s^{-1} in the period range 40–60 s and are larger at the extremes of the period range[3,5–9]. Curves in group *a* are for regions without tectonic involvement and in group *b* for regions with tectonic involvement.

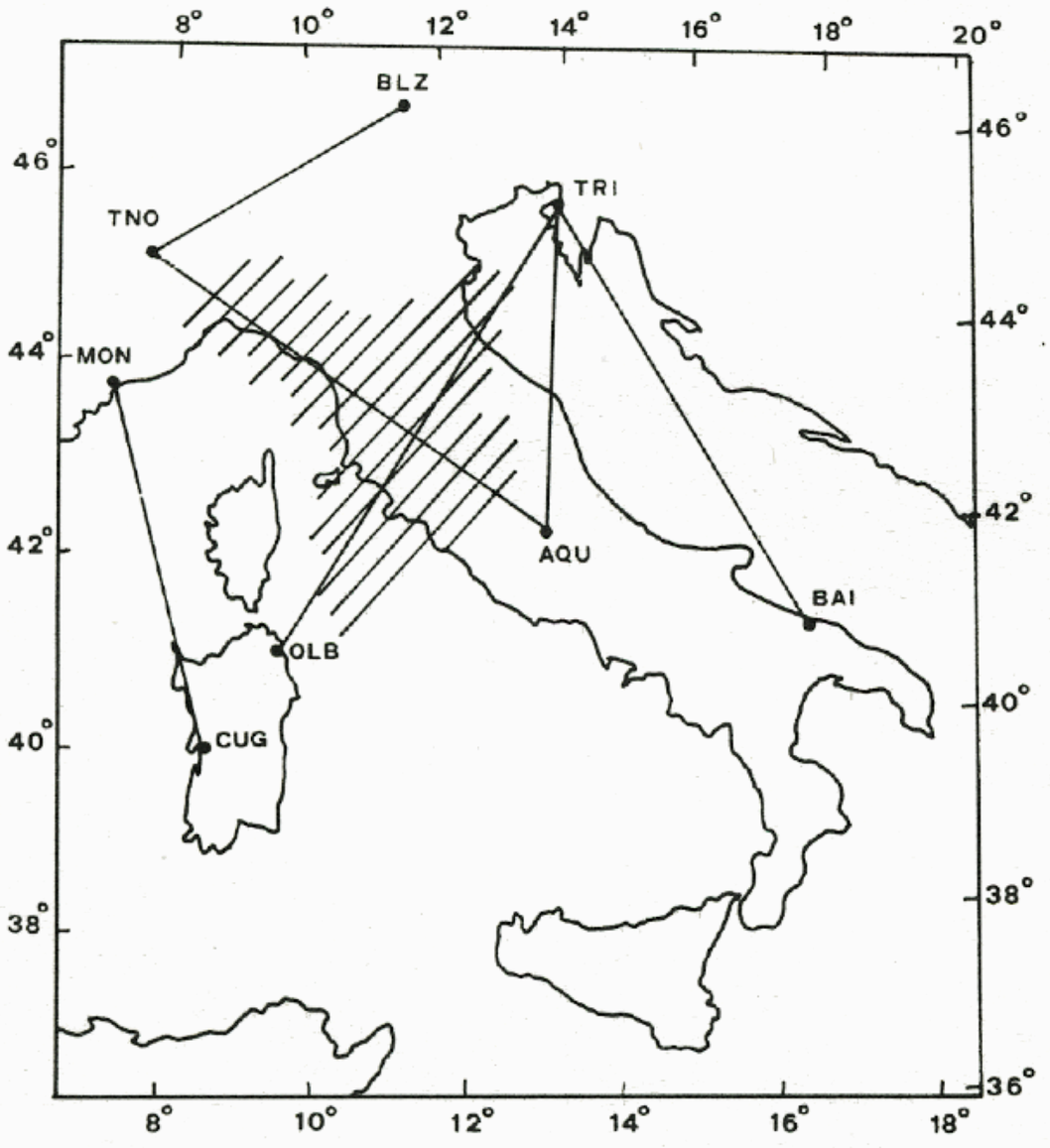

Fig. 1 Surface wave paths relevant to this study. The shaded region is the location of the mantle anomaly in North Central Italy.

The phase–velocity profile TNO–AQU (Fig. 2) differs in shape from the other two examples and would seem to provide an example of the danger of a literal interpretation of phase velocity curves in the period range 40–60 s. This curve differs from the others because of the influence of a larger crustal thickness under the axis of the Apennines than in the other regions described by low-phase velocities. Inversion of this phase velocity curve indeed indicates that a lid to a low S-wave velocity channel is absent[5], and that this curve is properly catalogued with TRI–OLB, TUC–BOZ and others.

We can provide a rough limit to the lateral extent of the Italian anomaly. To the south, the region is abutted by the Tyrrhenian Sea and still farther south by the Sicilian crossing of the Mediterranean by the contact between the African and European plates. High heat flows, volcanism, low surface-wave phase velocities, deep focus earthquakes, and an inferred subduction[11] give the Tyrrhenian region the appearance of a back-arc basin. Thus the anomaly of the northern Italian peninsula seems to continue southward; the southern limit to the Tyrrhenian extension of the anomaly would appear to be at or near the plate boundary with North Africa. An exploration of this region will be described elsewhere.

To the west, surface-wave profiles near Corsica and Sardinia on path MON–CUG[3], as well as to the north in the Italian Alpine foothills on path TNO–BLZ[4,7], have shown rather higher phase velocities in the period range characteristic of mantle depths. Similar phase velocities have been found elsewhere in relatively older, stable continental regions with more-or-less normal heat flows, that is, regions without major tectonic involvement today[9,12,13] including the US Gulf Coast, such as on path SHA–LUB, and Western Europe. While inversion of

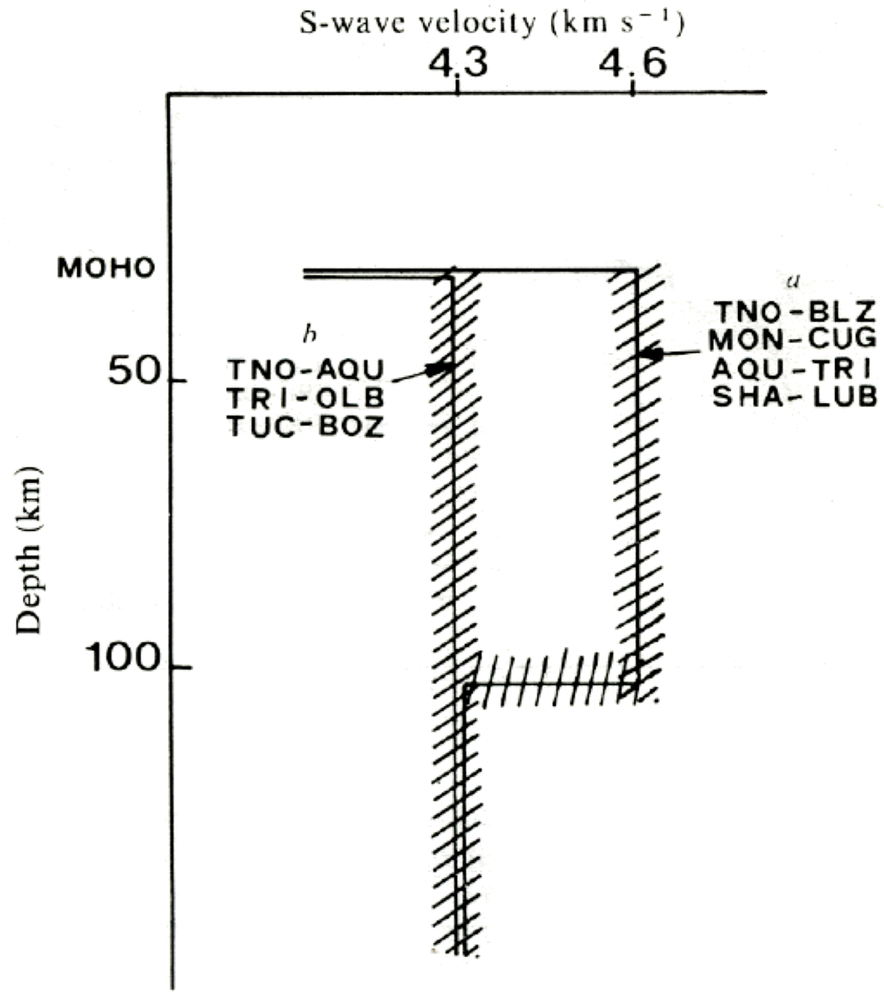

Fig. 3 Schematic shear wave velocity–depth distributions in the upper mantle for regions without *a* and with *b* major tectonic involvement today. The shading represents schematically the range of models satisfying each group of dispersion data.

these latter phase velocities may differ in some detail, especially in view of the non-uniqueness of the inversions, all successful inversions yield an upper mantle cross-section which has a broad low-velocity channel of significant contrast to an overlying high-velocity lid (Fig. 3); the channel-lid interface is found around a depth of 100 km. As indicated, this cross-section is evidently well correlated with the age and stability of these regions, characterized by their 'normal' heat flows and relatively low seismicity.

The values of phase velocities at periods between 40 and 60 s are diagnostic between the two groups. The errors in measurement are in every case less than the phase velocity interval between the groups of curves. It follows that the inversions of these phase velocity data yield structures for the two typical regions that are completely resolved from one another; the differences between the geophysical and geological environments of these two groups of regions are equally large.

The eastern edge of the Italian anomaly is delineated by surface-wave phase velocities that were determined along two Adriatic two-station paths, TRI–BAI and TRI–AQU[8]. The two phase velocity curves are indistinguishable over their common period range and are plotted as a single curve in Fig. 2. They are clearly members of the family of curves associated with young, stable continental regions, such as those for Western Europe. Such regions have well defined lids to channels. Cross-sections such as those for northern Italy, in which high-velocity lids are absent, are excluded. The inversion of these curves is no different, within errors of measurement, from those derived for other regions and sketched in Fig. 3.

We conclude that the anomalous low phase velocity region of northern Italy lies to the east of the path MON–CUG, to the west of the path AQU–TRI, and south of the Alps.

This work was supported by grants from CNR, Rome (80.2213) and NATO (1497), the Deutsche Forschungsgemeinschaft and the Schweizerischer Nationalfonds zür Forderung der wissenschaftlichen Forschung.

Received 20 July 1981; accepted 19 January 1982.

1. Panza, G. F., Mueller, St. & Calcagnile, G. *Pure appl. Geophys.* **118,** 1209–1213 (1980).
2. Panza, G. F., Calcagnile, G., Scandone, P. & Mueller, St. *Le Scienze* May, 60–69 (1980).
3. Berry, M. J. & Knopoff, L. *J. geophys. Res.* **72,** 3613–3626 (1967).
4. Panza, G. F., Mueller, St. & Knopoff, L. *Rapp. Commun int. mer. Medit.* **23,** 50 (1975).
6. Calcagnile, G., Panza, G. F. & Knopoff, L. *Tectonophysics* **56,** 51–63 (1979).
7. Sprecher, Ch. thesis, Swiss fed. Inst. Technol. (1976).
8. Calcagnile, G. & Panza, G. F. *Pure appl. Geophys.* **118,** 823–830 (1980).
9. Biswas, N. N. & Knopoff, L. *Geophys. J. R. astr. Soc.* **36,** 515–519 (1974).
10. Knopoff, L. & Schlue, J. W. *Tectonophysics* **15,** 157–163 (1972).
11. Caputo, M., Panza, G. F. & Postpischl, D. *J. geophys. Res.* **75,** 4919–4923 (1970).
12. Knopoff, L. *Tectonophysics* **13,** 497–515 (1972).
13. Seidl, D. & Mueller, St. *J. Geophys.* **42,** 283–328 (1977).

Printed in Great Britain by Macmillan Production Ltd., Basingstoke, Hampshire

by Giuliano F. Panza[1,2], Antonella Pontevivo[1], Giordano Chimera[1], Reneta Raykova[1], and Abdelkrim Aoudia[1,2]

The lithosphere-asthenosphere: Italy and surroundings

1 Department of Earth Sciences, University of Trieste, Via Weiss 4, 34127 - Trieste, Italy. *panza@dst.units.it*
2 The Abdus Salam International Centre for Theoretical Physics, SAND Group, Trieste, Italy.

The velocity-depth distribution of the lithosphere-asthenosphere in the Italian region and surroundings is imaged, with a lateral resolution of about 100 km, by surface wave velocity tomography and non-linear inversion. Maps of the Moho depth, of the thickness of the lithosphere and of the shear-wave velocities, down to depths of 200 km and more, are constructed. A mantle wedge, identified in the uppermost mantle along the Apennines and the Calabrian Arc, underlies the principal recent volcanoes, and partial melting can be relevant in this part of the uppermost mantle. In Calabria, a lithospheric doubling is seen, in connection with the subduction of the Ionian lithosphere. The asthenosphere is shallow in the Southern Tyrrhenian Sea. High velocity bodies, cutting the asthenosphere, outline the Adria-Ionian subduction in the Tyrrhenian Sea and the deep-reaching lithospheric root in the Western Alps. Less deep lithospheric roots are seen in the Central Apennines. The lithosphere-asthenosphere properties delineate a differentiation between the northern and the southern sectors of the Adriatic Sea, likely attesting the fragmentation of Adria.

Introduction

The first definition of the gross features of the lithosphere-asthenosphere system in Italy and surroundings dates back to Panza et al. (1980) and it is chiefly based on the analysis of Rayleigh wave dispersion. More recent models are based both on surface waves (e.g. Marquering and Snieder, 1996; Martinez et al., 1997, 2000, 2001; Ritzwoller and Levshin, 1998; Yanovskaya et al., 1998, 2000; Pasyanos et al., 2001; Karagianni et al., 2002; Pontevivo and Panza, 2002) and body waves tomography (e.g. Gobarenko, 1990; Spakman, 1990; Babuska and Plomerova, 1990; Alessandrini et al., 1995, 1997; Papazachos et al., 1995; Papazachos and Kiratzi, 1996; Cimini and De Gori, 1997; Parolai et al., 1997; Piromallo and Morelli, 1997; Bijwaard et al., 1998; Lucente et al., 1999). Based on the existing information derived both from refraction and reflection experiments, and body-wave and surface-wave tomography, a compilation of the compressional velocity (V_p), shear velocity (V_s), and density (ρ) distribution in space is due to Du et al. (1998).

We show here features of the lithosphere-asthenosphere system that characterize Italy and surroundings, with a multiscale lateral resolution, as obtained from the simultaneous inversion of regionalized surface wave tomography (e.g. Pontevivo and Panza, 2002; Panza and Pontevivo, 2002; Chimera et al. 2003) and refraction and reflection seismology data (e.g. Aljinovic and Blaskovic, 1987; Bally et al., 1986; Blundell et al., 1992; Catalano et al., 1996, 2001; Cernobori et al., 1996; Cristofolini et al., 1985; De Voggd et al., 1992; Doglioni et al., 2001; Ferrucci et al., 1991; Finetti et al., 2001; Gentile et al., 2000; Improta et al., 2000; Kissling and Spakman, 1996; Morelli, 1998; Mostaanpour, 1984; Pepe et al., 2000; Pialli et al., 1995, 1998; Scarascia and Cassinis, 1997).

Data and method

The data and methods used to obtain the tomographic maps are described by Pontevivo and Panza (2002), Panza et al. (2003a), Chimera et al. (2003), Levshin et al. (1972, 1992), Ditmar and Yanovskaya (1987) and Yanovskaya and Ditmar (1990). The tomographic maps can be discretized with a proper grid and for each cell of the grid the cellular average group or phase velocity curve is computed. The cellular dispersion curves can be grouped according to their shape and average value (e.g. Panza et al., 2003b) to define regional properties. The lateral resolving power common to most of the available surface-wave tomography (Pontevivo and Panza, 2002) is of about 200 km, but if some parameters of the uppermost part of the crust are fixed on the base of *a priori* independent geological and geophysical information, the lateral resolving power of the cellular mean dispersion curves can be improved and this justifies the choice to perform the inversion for cells of 1°×1° (Panza and Pontevivo, 2002; Panza et al., 2003a). If dispersion relations are available for periods as low as 1 sec, local studies can be performed at the scale of a few tens of km.

Due to the complexity of the area we prefer non-linear inversion, since it is independent from the initial model. Through the non-linear inversion, known as the hedgehog method (Valyus et al., 1969; Valyus, 1972; Knopoff, 1972), of the group and phase velocity curves at regional, cellular and local scale, average multiscale lithospheric models that reach a depth of about 250 km are obtained. As *a priori* information, we use the existing literature. In the inversion, the unknown Earth model is replaced by a set of parameters and the definition of the structure is reduced to the determination of the numerical values of these parameters. In the elastic approximation, the structure is modelled as a stack of N homogeneous isotropic layers, each one defined by four parameters: V_p, V_s, ρ and thickness. Each parameter can be fixed (during the inversion the parameter is held constant accordingly to independent geophysical evidences—the *a priori* information), independent (the variable parameters that can be well resolved by the data) or dependent (the parameter has a fixed relationship with an independent parameter). For each cell, a set of solutions, which are consistent with the observations and with the resolving power of the data (Knopoff and Panza, 1977; Panza 1981), is obtained.

Retrieval of multiscale structural models

In Figure 1, three examples of models of the crust and of the upper mantle are presented. In each frame, the inverted dispersion data, the set of solutions (thin lines) V_s versus depth, the explored part of the parameters space (grey area), and the chosen solution (bold line) are shown. It could be attractive to consider as solution a median of all solutions, but this is formally not correct. At the base of our choice

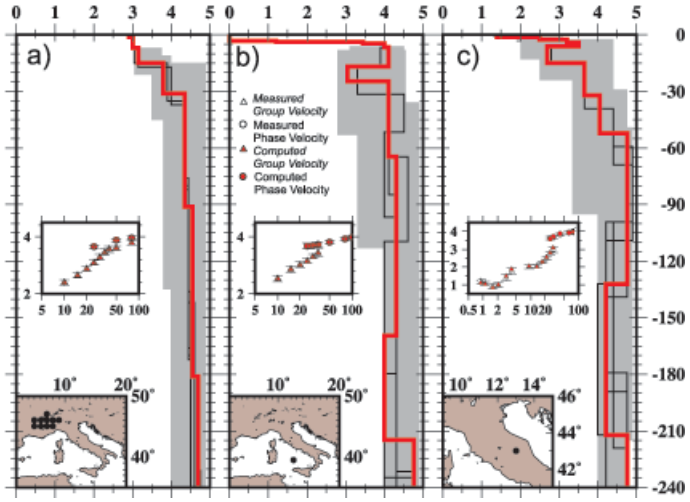

***Figure 1** Models (V_S) of crust and upper mantle for: (a) Western Alps, (b) 1°×1° cell containing Vavilov Seamount, (c) part of UMD; as marked by dots. In each frame, measured (with error bars) and computed dispersion relations are given; thin lines: set of solutions; grey area: explored part of the parameters space; bold line: chosen solution.*

of the representative solution there is a tenet of modern science known as Occam's razor: it is vain to do with more what can be done with fewer (Russel, 1946). To reduce the effects of the projection of possible systematic errors into the inverted model, the root mean square (r.m.s.) of the chosen solution is as close as possible to the average r.m.s. computed from all the solutions.

The set of solutions in Figure 1a corresponds to the Western Alps region defined by Panza et al. (2003b). Due to the complexity of the Alpine domain, at crustal level, the model is formally correct but has no straightforward geological significance. On the other side at mantle level, the slight increase of V_S from about 4.35 km/sec, just below the Moho, to about 4.7 km/sec, at depths larger than 180 km, is consistent with the presence of lithospheric roots, as first indicated by Panza and Mueller (1979).

In Figure 1b, the solutions correspond to the 1°×1° cell in the central area of the Southern Tyrrhenian Sea, which contains the Vavilov Seamount (Panza and Pontevivo, 2002). The Moho is very shallow (about 7 km deep) and the lid thickness is less than 10 km, with V_S about 4.1 km/sec. Below this lid, there is a very well developed low velocity layer, centred at a depth of about 20 km, with V_S about 3.0 km/sec and thickness of about 8 km. This value of V_S is consistent, accordingly with Bottinga and Steinmetz (1979), with about 10% of partial melting. The V_S just below this very low velocity layer, about 4.1 km/sec, defines the uppermost asthenosphere. In the asthenosphere, V_S varies between 4.1 km/sec and 4.3 km/sec.

In Figure 1c, the chosen structure corresponding to the Umbria-Marche geological Domain (UMD) is characterized by a layered crust, about 32 km thick, with a relatively high velocity upper and lower crust (V_S about 3.20–3.65 km/sec) separated by a low-velocity transition zone (V_S about 2.75 km/sec) about 10 km thick. The Moho is followed by a relatively low velocity layer (V_S of about 4.0 km/sec), about 20 km thick. Below this layer, a lithospheric root, with V_S about 4.75 km/sec, reaches the depth of about 130 km, which is the top of the asthenosphere, with V_S about 4.2 km/sec and about 70 km thick. The outlined V_S sequence versus depth in the uppermost mantle is consistent with the concept of mantle wedge, decoupling the crust from the underlying lithosphere. Therefore, we define mantle wedge the low velocity zone (V_S less than about 4.2 km/sec) in the uppermost mantle that overlies the high velocity lid (V_S greater than about 4.5 km/sec).

Selected cross sections

Examples of sections, crossing key areas, are given in Figure 2 (Panza and Pontevivo, 2002; Panza et al., 2003a; Chimera et al., 2003). In Figure 2b, two vertical sections trending NE-SW from the Tyrrhenian Sea across the Southern Apennines to the Dinarides are plotted. In the same sections, the shallow and intermediate-depth seismicity, with the depth error bars as given by ISC and falling in a stripe about 100 km wide and centred on the profiles, is shown.

The northernmost section AA' crosses Vavilov seamount in the Tyrrhenian Sea, Apennines, middle Adriatic Sea and Dinarides. Starting from A', the most evident feature is the presence of a high velocity lid, with V_S about 4.8 km/sec. This lid reaches the maximum depth of about 155 km in the zone that goes from the western side of the Apennines to the Tyrrhenian coast. More to the southwest, this thick high velocity lid is missing. The section BB', less than about 100 km southeast of AA', crosses the Tyrrhenian Sea, the Vesuvio and Phlegraean Fields zone, the Gargano region, the Adriatic Sea and the Dinarides. Along BB', the high velocity body with $4.6 \le V_S \le 4.8$ km/sec reaches depths of about 110 km under the Dinarides, about 170 km under the Adriatic Sea and about 150 km under the western side of the Apennines. More to the southwest, below Vesuvio and Phlegraean Fields, the high velocity body extends to depths not less than 250 km.

In Figure 2c, a balanced cross section from the Tyrrhenian to the Ionian Seas, along CC', is plotted down to 500 km. Our data do not resolve deeper than about 250 km, therefore, below this depth, the subducting Ionian lithosphere is outlined on the basis of the

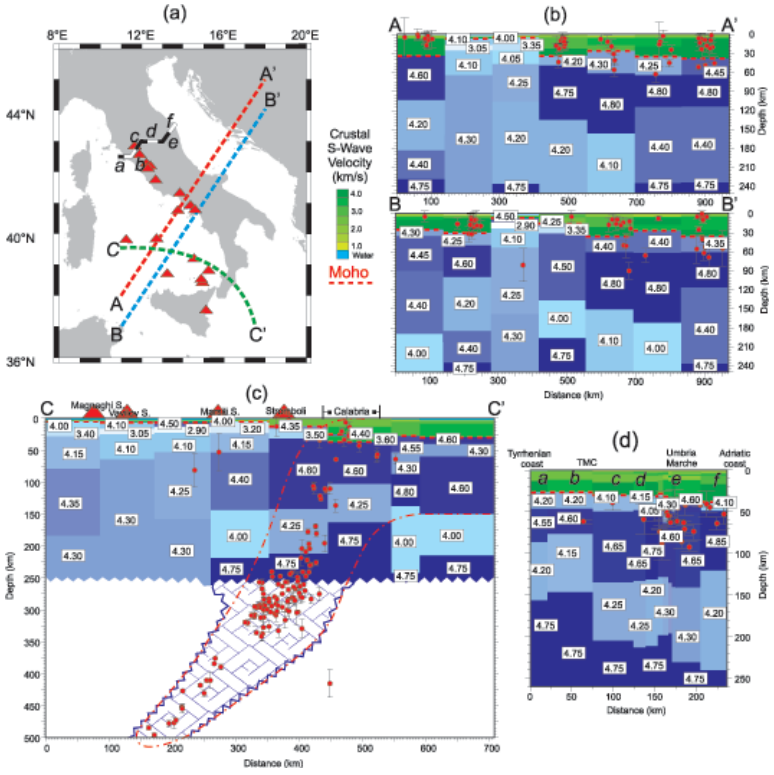

***Figure 2** (a) Position of sections and of all recent volcanoes (triangles) (Amiata-Vulsini, Cimino-Vico-Sabatini, Albani, Roccamonfina, Phlegraean Fields-Vesuvio, Vulture, Ischia, Stromboli, Vulcano-Lipari, Etna, Ustica, Marsili, Magnaghi, Vavilov); (b) Tyrrhenian Sea-Southern Apennines-Dinarides: the almost continuous high velocity body seen along BB' is not visible along AA'; (c) Tyrrhenian-Ionian Sea: outlined Ionian slab; shallow, intermediate-depth and deep earthquakes that fall into a band, about 100 km wide, along sections in (b) and (c), with the depth error bars being shown; (d) lithosphere-asthenosphere system from the Tyrrhenian (a) to the Adriatic coast (f) and related intermediate-depth seismicity; the mantle wedge supports the lithospheric delamination beneath Central Italy.*

hypocenters distribution of the intermediate-depth and deep seismicity. In correspondence to the shallow-mantle magma sources of the volcanic bodies Magnaghi-Vavilov and Marsili, low V_s layers (very shallow asthenosphere) below the very soft thin lid are detected. A very low velocity layer (mantle wedge) below a thin uppermost lid in the Stromboli area and a lithospheric doubling beneath Calabria are seen. In the southernmost part of CC', the crustal thickness is about 30 km and the lithospheric upper mantle is characterized by a layering where a relatively low velocity body (V_s about 4.3 km/sec) lies between two fast ones. At depths greater than about 150 km, a very well developed low velocity (V_s about 4.0 km/sec) asthenospheric layer is present. Crossing Calabria, the low velocity asthenospheric layer is absent and the relatively low velocity body (V_s about 4.25 km/sec) in the lithospheric mantle becomes deeper and thicker going towards west.

Figure 2d shows the lithosphere-asthenosphere system along a stripe from the Tyrrhenian to the Adriatic coasts (Chimera et al., 2003), particularly detailed in UMD (see zone *e* in Figure 2d). Beneath Central Italy high velocity bodies reach at least a depth of 130 km with a width of about 120 km. The crust exhibits clear V_s layering and lateral variation in thickness: less than 30 km below the Tuscan Metamorphic Complex (TMC) and about 35 km below UMD. The lid is thin (about 30 km) below the TMC, while it is about 70 km thick below UMD. Along the profile, particularly in the western part where it gets shallower, a developed mantle wedge separates the crust from the high velocity lid.

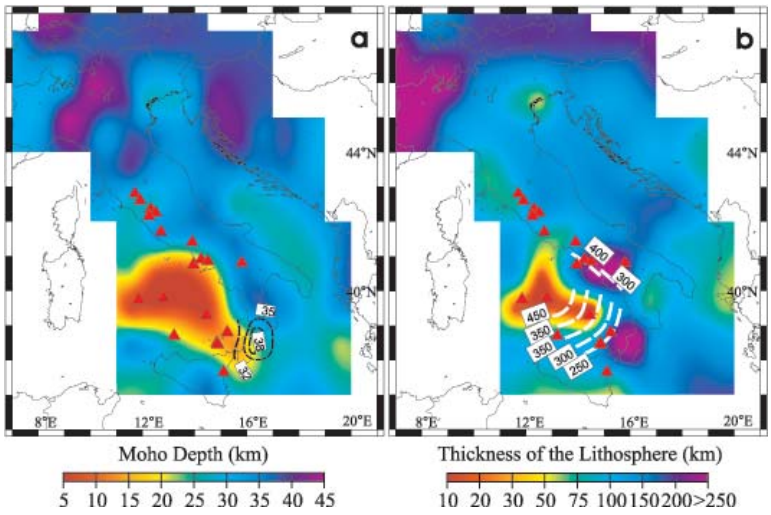

***Figure 3** (a) Moho depth with contouring of the deeper Moho where lithospheric doubling is unambiguously detected; (b) thickness of the lithosphere. Here and in Figure 4, the dashed lines schematise the subduction of the Ionian-Adria lithosphere, traced accordingly with ISC hypocenters distribution, and red triangles mark the recent volcanoes.*

Maps of the lithosphere-asthenosphere

The horizontal resolution of our maps is about 100 km and the vertical penetration reaches a depth of about 250 km. All the features shown at depth larger than 250 km are schematically based on the intermediate-depth and deep seismicity, as given by ISC, schematised by dashed segments in Figures 3b and 4b,c.

In Figures 3a,b, the Moho depth and the thickness of the lithosphere are shown, together with the recent volcanoes (red triangles). In Figure 3a, the contouring of the deeper Moho indicates where lithospheric doubling is unambiguously detected by our data. In the northernmost area of the map in Figure 3b, the lithospheric thickness is about 200 km, while in the Western Alps it is at least 250 km. The lithospheric thickness varies in the range of about 100–150 km along the Northern Apennines, around the Padan plain and in the Dinarides area, except in its westernmost part, where the lithosphere is only about 80 km thick. The Northern Adriatic Sea has a lithosphere thinner than the Central-Southern Adriatic Sea. In the southernmost Adriatic Sea and in the Otranto channel area, the lithosphere is less than about 100 km thick. In the Calabrian and Campanian areas the lithospheric thickness exceeds 250 km.

The two different dashing patterns in Figure 4a, where the V_s just below the Moho is shown, indicate the presence of the mantle

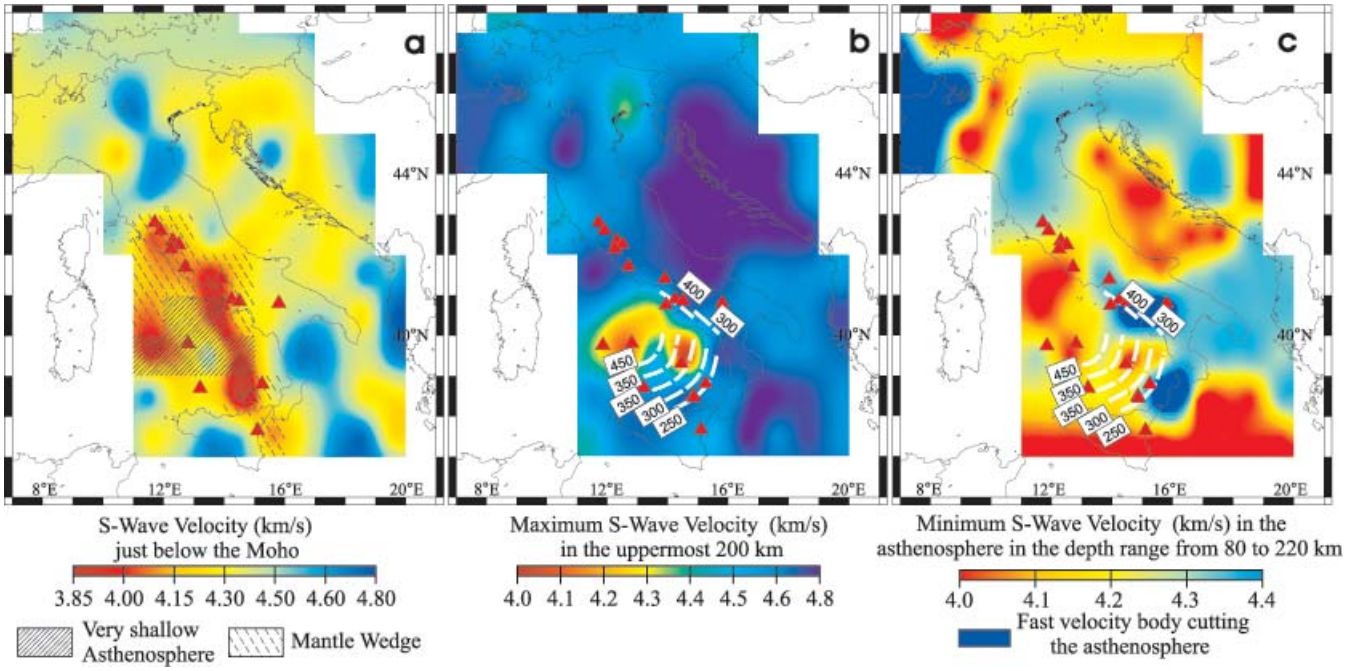

***Figure 4** (a) V_s just below the Moho (different dashed patterns outline where mantle wedge and a very shallow asthenosphere are detected); (b) maximum V_s in the uppermost 200 km; (c) minimum V_s in the asthenosphere, in the depth range from about 80 km to about 220 km. In (c) the dark blue areas indicate the fast velocity bodies cutting the asthenosphere.*

wedge and of a very shallow asthenosphere, respectively. Large lateral variations (Figure 4b) characterize the maximum V_s in the uppermost 200 km. Peak values are found in the western Alps, central Po valley, Dinarides, Central Adria, Southern-Central Apennines, Northern Tyrrhenian and Ionian Seas. In correspondence to all the volcanoes, except the Tyrrhenian Seamounts, the maximum lithospheric V_s exceeds about 4.6 km/sec. Magnaghi-Vavilov and Marsili are separated by a region with relatively high V_s, but in correspondence to these volcanoes V_s is very low. The high-velocity bodies of the Ionian-Adria subducting slabs extend below the volcanoes of the Aeolian Arc and of the Campanian province. The minimum V_s in the asthenosphere, in the depth range from about 80 km to about 220 km, is shown in Figure 4c. The dark blue area in the northern part of the map corresponds to the fast velocity bodies present in the western Alps. East of this lithospheric body, the V_s in the asthenosphere is as low as in the Northern Adriatic. The properties of the asthenosphere in the Northern Adriatic Sea (V_s between 4.0–4.1 km/sec), are different from those of the Southern Adriatic Sea and around the Otranto channel (V_s larger than about 4.3 km/sec). Low asthenospheric V_s is seen in Sicily and in the Tyrrhenian and Ionian Sea. The dark blue areas around the Tyrrhenian Sea indicate the fast velocity Ionian-Adria slabs that cut the asthenosphere, and that can be traced at depth larger than 250 km from the distribution of subcrustal seismicity.

Discussion

In BB' (Figure 2b) the high-velocity body extending to depths not less than 250 km can be related to the westward subduction of the Adriatic lithosphere towards the Tyrrhenian Basin. This feature is in agreement with the results of De Gori et al. (2001). Along a section very close to AA' (Figure 2b) they find a weak velocity perturbation in the mantle beneath the mountain belt with a small high velocity anomaly dipping southwestward. This feature can be correlated with the layer with V_s about 4.75 km/sec, whose top is at about 220 km, in AA'. The rising of the bottom of the asthenosphere could be caused by remnants of high velocity bodies probably detached (Wortel and Spakman, 2002 and references therein) from the lithospheric roots, through thermo-mechanical processes. The remarkable difference between the two sections of Figure 2b, confirmed by completely independent data, indicates that the subducted lithosphere has a very complex morphology.

In CC' (Figure 2c), the body with V_s about 4.4 km/sec near the center, above the slab, is probably due to thermal effects induced by the mechanical interaction between the Ionian lithosphere and the hot Tyrrhenian upper mantle. In the center of the section, the layer with V_s around 4.0 km/sec, extending from about 140 km to 220 km depth, can be explained by dehydration processes and melting along the down-going slab (e.g. Goes et al., 2000 and references therein). The layering along the easternmost half of CC', in the Ionian area, seems to be consistent with the subduction of serpentinized and attenuated continental lithosphere, formed in response to the Jurassic extensional phase. During the tensional phase, the relatively low velocity (V_s in the range 4.25–4.30 km/sec) layer could be formed as a result of the serpentinization of peridotites. Such process produces V_s retardations of a few percent (Christensen, 1966). The presence of a low velocity layer of chemical and not of thermal origin is consistent with the low heat flow in the Ionian Sea (Della Vedova et al., 1991). This layer, when subducted, gets thicker, consistently with the dehydration of serpentine, which is responsible for the weakening of the neighboring material. The seismicity is distributed along the slab and it seems to decrease, but it is not absent, in correspondence with the serpentinized layer. In the studied part of the Ionian Sea, the lithosphere is attenuated continental, thermally relaxed after the Jurassic extensional phase, while in the Southern Tyrrhenian Sea it is very young oceanic.

Beneath Central Italy (see Figure 2d) there is clear evidence of lithospheric roots surmounted by a well-developed mantle wedge. Young magmatism at the surface and high heat flow in the TMC region suggest that, in agreement with petrological and geochemical data (Peccerillo et al., 2001), this layer may represent a partially molten mantle. In Tuscany, the mantle wedge is underlined by a thin lithosphere and an up-risen asthenosphere roof, in agreement with the heat flow data (Della Vedova et al., 1991). Along the same vertical section, the rising of the bottom of the asthenosphere may have the same origin discussed for section AA' (Figure 2b). The subcrustal earthquakes (ISC) cluster in the shallower part of the thick Adriatic lid and in the eastern part of the lithospheric root, consistently with a slab-like geometry, while the part of the lithospheric root and thin lid to the west seems to be almost free of seismic activity. The absence of deep seismicity and the non-in-depth continuity of the fast velocity body below Central Apennines (Figure 2d) and Southern Apennines (Figure 2b) clearly highlight a major difference when compared to the structure and related deep seismicity of the Calabrian arc, where there is sound evidence of a continuous slab.

The complex crustal structure, where shearing and thrusting involve the whole crust and the upper mantle, causing the occurrence of more than one Moho, as described by Nicolich and Dal Piaz (1990), is confirmed by our data and the map in Figure 3a reproduces several other features identified by the same authors. Near the Otranto channel the Moho is in the range of 25–30 km, i.e. shallower with respect to the results of Nicolich and Dal Piaz (1990), but well in agreement with the Moho depth proposed by Herak and Herak (1995).

In Figure 3b, the Western Alps lithosphere at least 250 km thick is consistent with the presence of the lithospheric root (Panza and Mueller, 1979). The Northern Adriatic Sea has a lithosphere thinner than the Central-Southern Adriatic Sea, where a band with moderate seismicity can be identified. The lithosphere is very thin, less than 20 km, in correspondence to Magnaghi, Vavilov and Marsili. The lithospheric thickness exceeding 250 km in the Campanian and Calabrian areas is associated with the subduction of the Ionian-Adria lithosphere, schematically represented, for depths larger than 250 km, by the isolines in Figure 3b.

The mantle wedge area shown in Figure 4a is in agreement with what proposed by Meletti et al. (2000) in their structural and kinematic model of Italy. In some cases, the lowest velocity material is not just below the Moho but below a thin mantle lid, possibly formed by thermal underplating. All the volcanic areas (see the caption of Figure 2), except those with the inactive volcanoes of Vulture and Ustica, are characterized by the presence of a low velocity layer just below the Moho or below a very thin lid.

The dark blue area in the northern part of Figure 4c, due to the plate collision process between Eurasian and African plates, contains the so-far proposed locations of the rotation pole of Adria versus Europe (Meletti et al., 2000 and references therein).

Acknowledgements

Research funded by Italian MIUR Cofin-2001 (2001045878_007), Cofin-2002 (2002047575_002), CNR (CNRC007AF8), and INGV-2001. We thank F. Wezel for critically reading the manuscript.

References

Alessandrini, B., Beranzoli, L., and Mele, F.M., 1995, 3D crustal P-wave velocity tomography of the Italian region using local and regional seismicity data, Ann. Geof., v. 38, no 2, pp. 189-211.

Alessandrini, B., Beranzoli, L., Drakatos, G., Falcone, C., Karantonis, G., Mele, F.M., and Stavrakakis, G.N., 1997, Tomographic image of the crust and uppermost mantle in the Ionian and Aegean regions, Annali di Geofis., v. 40, no 1, pp. 151-160.

Aljinovic, B., and Blaskovic, I., 1987, Some characteristics of the carbonate complex in the offshore Adriatic area, Mem. Soc. Geol. It., v. 40, pp. 327-334.

Babuska, V., and Plomerova, J., 1990, Tomographic studies of the upper mantle beneath the Italian region, Terra Nova, v. 2, pp. 569-576.

Bally, A.W., Burbi, L., Cooper, C., and Ghelardoni, R., 1986, Balanced sections and seismic reflection profiles across the Central Apennines, Mem. Soc. Geol. It., v. 35, pp. 257-310.

Bijwaard, H., Spakman, W., and Engdahl, E.R., 1998, Closing the gap between regional and global travel time tomography, J. Geophys. Res., v. 103, pp. 30.055-30.078.

Blundell, D., Freeman, R., and Mueller, St., 1992, A continent revealed, The European geotraverse, University press, Cambridge.

Bottinga, Y., and Steinmetz, L., 1979, A geophysical, geochemical, petrological model of the sub-marine lithosphere, Tectonophysics, v. 55, pp. 311-347.

Catalano, R., Di Stefano, P., Sulli, A., and Vitale, F.P., 1996, Paleogeography and structure of the central Mediterranean: Sicily and its offshore area, Tectonophysics, v. 260, pp. 291-323.

Catalano, R., Doglioni, C., and Merlini, S., 2001, On the Mesozoic Ionian Basin, Geophys. J. Int., v. 144, pp. 49-64.

Cernobori, L., Hirn, A., McBride, J.H., Nicolich, R., Petronio, L., Romanelli, M., and STREAMERS/PROFILES Working Groups, 1996, Crustal image of the Ionian basin and its Calabrian margin, Tectonophysics, v. 264, pp. 175-189.

Chimera, G., Aoudia, A., Saraò, A., and Panza, G.F., 2003, Active tectonics in central Italy: constraints from surface wave tomography and source moment tensor inversion, Phys. Earth Planet. Int. (in press).

Christensen, N.I., 1966, Elasticity of Ultrabasic Rocks, J. Geophys. Res., v. 71, no 24, pp. 5921-5931.

Cimini G.B., and De Gori, P., 1997, Upper mantle velocity structure beneath Italy from direct and secondary P-wave teleseismic tomography, Annali di Geofis., v. XL, no 1, pp. 175-194.

Cristofolini, R., Ghisetti, F., Scarpa, R., And Vezzani, L., 1985, Character of the stress field in the Calabrian Arc and Southern Apennines (Italy) as deducted by geological, seismological and volcanological information, Tectonophysics, v. 117, pp. 39-58.

De Gori, P, Cimini, G.B., Chiarabba, C., De Natale, G., Troise, C., and Deschamps, A., 2001, Teleseismic tomography of the Campanian volcanic area and surrounding Apenninic belt, J. Volc. and Geoth. Res., v. 109, pp. 55-75.

Della Vedova, B., Marson, I., Panza, G.F., and Suhadolc, P., 1991, Upper mantle properties of the Tuscan-Tyrrhenian area: a framework for its recent tectonic evolution, Tectonophysics, v. 195, pp. 311-318.

De Voggd, B., Truffert, C., Chamot-Rooke, N., Huchon, P., Lallermant, S. and Le Pichon, X., 1992, Two-ship deep seismic soundings in the basins of the Eastern Mediterranean Sea (Pasiphae cruise), Geophys. J. Int., v. 109, pp. 536-552.

Ditmar, P.G., and Yanovskaya, T.B., 1987, A generalization of the Backus-Gilbert method for estimation of lateral variations of surface wave velocity, Izv. AN SSSR, Fiz. Zemli (Physics of the Solid Earth), v. 23, no 6, pp. 470-477.

Doglioni, C., Innocenti, F., and Mariotti, G., 2001, Why Mt. Etna? Terra Nova, v. 13, pp. 25-31.

Du, Z.J., Michelini, A., and Panza, G.F., 1998, EurID: a regionalised 3-D seismological model of Europe, Phys. Earth Planet. Inter., v. 105, pp. 31-62.

Ferrucci, F., Gaudiosi, G., Hirn, A., and Nicolich, R., 1991, Ionian Basin and Calabrian Arc: some new elements from DSS data, Tectonophysics, v. 195, pp. 411-419.

Finetti, I.R., Boccaletti, M., Bonini, M., Del Ben, A., Geletti, R., Pipan, M., and Sani, F., 2001, Crustal section based on CROP seismic data across the North Tyrrhenian-Northern Apennines-Adriatic Sea, Tectonophysics, v. 343, pp. 135-163.

Gentile, G., Bressan, G., Burlini, L., and De Franco, R., 2000, Three-dimensional V_p and V_p/V_s models of the upper crust in the Friuli area (northeastern Italy), Geophys. J. Int., v. 141, pp. 457-478.

Gobarenko, V.S., Nikolova, S.B., and Sokolova, S.J., 1990, Velocity structure of the western Mediterranean from inversion of P-wave traveltimes, Geophys. J. Int., v. 101, pp. 557-564.

Goes, S., Govers, R., and Vacher, P., 2000, Shallow mantle temperatures under Europe from P and S wave tomography, J. Geophys. Res., v. 105, pp. 11.153-11.169.

Herak, D., and Herak, M., 1995, Body-wave velocities in the circum-Adriatic region, Tectonophysics, v. 241, pp. 121-141.

Improta, L., Iannaccone, G., Capuano, P., Zollo, A., and Scandone, P., 2000, Inferences on the upper crustal structure of Southern Apennines (Italy) from seismic refraction investigations and surface data, Tectonophysics, v. 317, pp. 273-297.

ISC.International Seismological Centre On-line Bulletin, http://www.isc.ac.uk/Bull, Internat. Seis. Cent., Thatcham, United Kingdom.

Karagianni, E.E., Panagiotopoulos, D.G., Panza, G.F., Suhadolc, P., Papazachos, C.B., Papazachos, B.C., Kiratzi, A., Hatzfeld, D., Makropoulos, K., Priestley, K., and Vuan, A., 2002, Rayleigh Wave Group Velocity Tomography in the Aegean area, Tectonophysics, v. 358, pp. 187-209.

Kissling E., and Spakman, W., 1996, Interpretation of tomographic images of uppermost mantle structure: examples from the western and central Alps, J. Geodyn., v. 21, pp. 97-111.

Knopoff, L., 1972, Observations and inversion of surface-wave dispersion, *in*: The Upper Mantle, Tectonophysics, Ritsema A.R. ed., v. 13, pp. 497-519.

Knopoff, L., and Panza, G.F., 1977, Resolution of Upper Mantle Structure using higher modes of Rayleigh waves, Annales Geophysicae , v. 30, pp. 491-505.

Levshin, A.L., Pisarenko, V.F., and Pogrebinsky, G.A., 1972, On a frequency time analysis of oscillations, Annales Geophysicae, v. 28, pp. 211-218.

Levshin, A.L., Ratnikova, L., and Berger, J., 1992, Peculiarities of surface wave propagation across Central Eurasia, Bull. Seismol. Soc. Am., v. 82, pp. 2464-2493.

Lucente, F.P., Chiarabba, C., Cimini G.B., and Giardini, D., 1999, Tomographic constraints on the geodynamic evolution of the Italian region, J. Geophys. Res., v. 104, pp. 20.307-20.327.

Marquering, H., and Snieder, R., 1996, Shear-wave velocity structure beneath Europe, the north-eastern Atlantic and western Asia from waveform inversion including surface-wave mode coupling, Geophys. J. Int., v. 127, pp. 283-304.

Martinez, M.D., Lana, X., Badal, J., Canas, J.A., and Pujades, L., 1997, Preliminary objective regionalization of the Mediterranean basin derived from surface-wave tomography, Annali di Geofis., v. XL, no 1, pp. 43-59.

Martinez, M.D., Lana, X., Canas, J.A., Badal, J., and Pujades, L., 2000, Shear-wave velocity tomography of the lithosphere-asthenosphere system beneath the Mediterranean area, Phys. Earth and Plan. Int., v. 122, pp. 33-54.

Martinez, M.D., Canas, J.A., Lana, X., and Badal, J., 2001, Objective regionalization of Rayleigh wave dispersion data by clustering algorithms: an application to the Mediterranean basin, Tectonophysics, v. 330, pp. 245-266.

Meletti, C., Patacca, E., and Scandone, P., 2000, Construction of a Seismotectonic Model: The Case of Italy, Pure Appl. Geophys., v. 157, pp. 11-35.

Morelli, C., 1998, Lithospheric structure and geodynamics of the Italian peninsula derived from geophysical data: a review, Mem. Soc. Geol. It., v. 52, pp. 113-122.

Mostaanpour, M.M., 1984, Einheitliche Auswertung krustenseismicher daten in Westeuropa. Darstellung von Krustenparametern und Laufzeitanomalien. Verlag von Dirtrich Reimer in Berlin.

Nicolich, R., and Dal Piaz, R., 1990, Moho isobaths. *in* Structural model of Italy and Gravity Map, Sheet 2, Consiglio Nazionale delle Ricerche.

Panza, G.F., and Mueller, S., 1979, The plate boundary between Eurasia and Africa in the Alpine area, Memorie di Scienze Geologiche, Università di Padova, v. 33, pp. 43-50.

Panza, G.F., Mueller, S., and Calcagnile, G., 1980, The gross features of the lithosphere-asthenosphere system in Europe from seismic surface waves and body waves, Pure Appl. Geoph., v. 118, pp. 1209-1213.

Panza, G.F., 1981, The resolving power of seismic surface waves with respect to crust and upper mantle structural models, *in* The solution of the inverse problem in geophysical interpretation. Cassinis R. ed., Plenum Publ. Corp., pp. 39-77.

Panza, G.F., and Pontevivo, A., 2002, The Lithosphere-Asthenosphere System in the Calabrian Arc and surrounding seas, Preprint ICTP, IC/2002/141.

Panza, G.F., Pontevivo, A., Saraò, A., Aoudia, A., and Peccerillo, A., 2003a, Structure of the Lithosphere-Asthenosphere and Volcanism in the Tyrrhenian Sea and surroundings, Preprint ICTP, IC/2003/8.

Panza, G.F., Raykova, R., Chimera, G., and Aoudia, A., 2003b, Multiscale surface wave tomography in the Alps (abs), Transalp Conference, Trieste, February 2003.

Papazachos, C.B., Hatzidimitriou, P.M., Panagiotopoulos, D.G., and Tsokas, G.N., 1995, Tomography of the crust and upper mantle in southeast Europe, J. Geophys. Res., v. 100, pp. 12405-12422.

Papazachos, C.B., and Kiratzi, A.A., 1996, A detailed study of the active crustal deformation in the Aegean and surrounding area, Tectonophysics, v. 253, pp. 129-153.

Parolai, S., Spallarossa, D., and Eva C., 1997, Bootstrap inversion for Pn wave velocity in North-Western Italy, Annali di Geofis., v. XL, no 1, pp. 133-150.

Pasyanos, M.E., Walter, W.R., and Hazler, S.E., 2001, A surface wave dispersion study of the Middle East and North Africa for Monitoring the Compressive Nuclear-Test-Ban Treaty, Pure Appl. Geophys., v. 158, pp. 1445-1474.

Peccerillo, A., 2001, Geochemical similarities between the Vesuvius, Phlegraean Fields and Stromboli Volcanoes: petrogenetic, geodynamic and volcanological implications, Mineralogy and Petrology, v. 73, pp. 93-105.
Pepe, F., Bertotti, G., Cella, F., and Marsella, E., 2000, Rifted margin formation in the south Tyrrhenian Sea: a high-resolution seismic profile across the north Sicily passive continental margin, Tectonics, v. 19, no 2, pp. 241-257.
Pialli, G., Alvarez, W., and Minelli, G., 1995, Geodinamica dell'Appennino settentrionale e sue ripercussioni nella evoluzione tettonica miocenica, Studi geol. Camerti, Volume speciale 1995, no 1, pp. 523-536.
Pialli, G., Barchi, M., and Minelli, G., 1998, Results of the CROP03 deep seismic reflection profile, Mem. Soc. Geol. It., v. 52.
Piromallo, C., and Morelli, A., 1997, Imaging the Mediterranean upper mantle by P-wave travel time tomography, Ann. Geof., v. 40, no 4, pp. 963-979.
Pontevivo, A., and Panza, G.F., 2002, Group Velocity Tomography and Regionalization in Italy and bordering areas, Phys. Earth Planet. Inter., v. 134, pp. 1-15.
Ritzwoller, M.H., and Levshin, A.L., 1998, Eurasian surface wave tomography: Group velocities, J. Geophys. Res., v. 103, pp. 4839-4878.
Russell, B., 1946, History of western philosophy, George Allen and Unwind, Ltd.
Scarascia, S., and Cassinis, R., 1997, Crustal structures in the central-eastern Alpine sector: a revision of the available DSS data, Tectonophysics, v. 271, pp. 157-188.
Spakman, W., 1990, Tomographic images of the upper mantle below central Europe and the Mediterranean, Terra Nova, v. 2, pp. 542-553.
Valyus, V.P., Keilis-Borok, V.I., and Levshin, A., 1969, Determination of the upper-mantle velocity cross-section for Europe, Proc. Acad. Sci. USSR, v. 185, no 3.
Valyus, V.P., 1972, Determining seismic profiles from a set of observations. *in* Computational Seismology, Keilis-Borok ed., Consult. Bureau, New-York, pp. 114-118.
Yanovskaya, T.B., and Ditmar, P.G., 1990, Smoothness criteria in surface-wave tomography, Geophys. J. Int., v. 102, pp. 63-72.
Yanovskaya, T.B., Kizima, E.S., and Antonova, L.M., 1998, Structure of the crust in the Black Sea and adjoining regions from surface wave data, J. Seismol., v. 2, pp. 303-316.
Yanovskaya, T.B., Antonova, L.M., and Kozhevnikov, V.M., 2000, Lateral variations of the upper mantle structure in Eurasia from group velocities of surface waves, Phys. Earth Planet. Inter., v. 122, pp 19-32.
Wortel, M.J.R., and Spakman, W., 2002, Subduction and Slab Detachment in the Mediterranean-Carpathian Region, Science, v. 290, pp. 1910-1916.

***Giuliano F. Panza**, Professor of seismology in the Department of Earth Sciences - University of Trieste, and head of SAND Group ICTP-Trieste. Laurea in physics from the University of Bologna in 1967; PostDoc at UCLA. He is fellow of Academia Nazionale dei Lincei, of Academia Europea, and Third World Academy of Sciences. He is winner of the EGS Beno Gutermberg medal in 2000, and received Laurea Honoris Causa in Physics in 2002 from the University of Bucharest. He is leader of several projects funded by EC related to seismic hazard assessment.*

***Antonella Pontevivo**, PhD from the Department of Earth Sciences -University of Trieste in 2003. Laurea in physics from the University of Trieste in 1999. At present PostDoc in the Geological Institute - University of Copenhagen. Her PhD thesis is on surface-wave tomography, non-linear inversion and geophysical implications in the Italian area and surroundings.*

***Giordano Chimer**a is PhD-student in the Department of Earth Sciences - University of Trieste. He received his Laurea in physics from the University of Trieste in 1998. His interests are: tomography and non-linear inversion in the Apenninic and Alpine areas.*

***Reneta Raykova**, Laurea in physics from the University of Sofia in 1994. As PhD student in the Department of Seismology at the Geophysical Institute of Sofia, she received in 2003 from the Department of Earth Sciences - University of Trieste, a one year EU - Marie Curie fellowship. Her interests are surface wave tomography and structure of the crust and upper mantle.*

***Abdelkrim Aoudia**, research scientist at the International Centre for Theoretical Physics at Trieste. He received his PhD in geophysics from the University of Trieste in 1998. His research interests revolve around using geophysical, geodetic and tectonic data to understand the mechanical behavior of earthquake faults and to constrain better conceptual and quantitative models for lithospheric deformation.*

Available online at www.sciencedirect.com
SCIENCE DIRECT®
Physics of the Earth and Planetary Interiors 138 (2003) 241–262
PHYSICS OF THE EARTH AND PLANETARY INTERIORS
www.elsevier.com/locate/pepi

Active tectonics in Central Italy: constraints from surface wave tomography and source moment tensor inversion

G. Chimera [a,*], A. Aoudia [a,b], A. Saraò [a], G.F. Panza [a,b]

[a] *Dipartimento di Scienze della Terra, Università degli Studi di Trieste, via Weiss 4, 34127 Trieste, Italy*
[b] *SAND Group, Abdus Salam International Center for Theoretical Physics, Trieste, Italy*

Received 12 August 2002; received in revised form 28 February 2003; accepted 12 June 2003

Abstract

We investigate the lithosphere–asthenosphere structure and active tectonics of Central Italy, with emphasis on the Umbria–Marche area, by means of surface wave tomography and seismic moment tensor inversion.

The data include: a large number of short period local and regional group velocity measurements sampling the Umbria–Marche Apennines and the Adria margin, respectively; incorporation of published phase velocity measurements sampling Italy and surroundings; results from deep seismic soundings which go through the Umbria–Marche area.

The local group velocity maps, covering the area reactivated by the 1997–1998 Umbria–Marche earthquake sequence, suggest an intimate relationship between the lateral earth structure variations and the distribution of the active fault systems and related sedimentary basins.

The upper crustal models reveal the importance of inherited compressional tectonics on the recent extensional deformation and associated seismic activity.

Source inversion studies of the main events of the 1997 earthquake sequence show the dominance of normal faulting mechanisms, whereas selected aftershocks between the fault segments, at the step-over, reveal that the prevailing deformation is of strike-slip faulting type.

At the regional scale, the crust exhibits clear layering and varies in thickness from about 25 km below the Tuscan Metamorphic Complex (TMC), to about 30 km below the Val Tiberina extensional thick sedimentary basin and reaches about 35 km below the Umbria–Marche geological domain (UMD). The lithospheric mantle (lid) is thin (about 30 km) below TMC, while it is about 70 km thick below UMD. A lithospheric root about 120 km wide, between the TMC and UMD, reaches a depth of at least 130 km. A low-velocity zone, defined mantle wedge (V_S less than 4.2 km/s) in the uppermost mantle overlying the high velocity lid is detached. This wedge is about 20 km thick and decouples the underlying lid from the crust. The retrieved crust and upper mantle structure beneath Central Italy is in agreement with Bouguer anomaly and heat flow data and supports a delamination process. The high velocity upper mantle underlying the mantle wedge is inferred to be subcrustal lithospheric material delaminated from the overlying crust.

Keywords: Crust; Lithosphere; Asthenosphere; Surface wave tomography; Source moment tensor; Central Italy; Umbria–Marche

1. Introduction

The study of the Apennines structure in Central Italy is important to the understanding of the relationships

* Corresponding author. Fax: +39-040-5582111.
E-mail address: giordano@dst.units.it (G. Chimera).

0031-9201/$ – see front matter © 2003 Elsevier B.V. All rights reserved.
doi:10.1016/S0031-9201(03)00152-3

between recent and inherited shallow and deep processes in the crust and upper mantle. The geodynamic complexity of this geological domain makes the kinematics of the present-day deformation and its relationships with the seismicity less well understood. The recent 1997–1998 Umbria–Marche earthquake sequence (Amato et al., 1998; Cattaneo et al., 2000) clearly highlighted complex deformation processes (Hunstad et al., 1999; Riva et al., 2000), acting within the crust and the upper mantle. The Umbria–Marche crustal normal faulting seismic sequence, which consisted of three moderate earthquakes (26 September 1997 at 00:33 h, $M_W = 5.7$; 26 September 1997 at 09:40 h, $M_W = 6.1$ and 14 October 1997 at 15:23 h, $M_W = 5.6$), ruptured three distinct fault segments (Galadini et al., 1999; Meghraoui et al., 1999; Barba and Basili, 2000), whereas previous large earthquakes with similar faulting geometries (e.g. $M_W = 6.9$; Irpinia, 1980), occurred on single fault segments (Pantosti and Valensise, 1990). In the same region of Umbria–Marche, an earthquake occurred in the upper mantle, on 28 March 1998, $M_W = 5.2$ (Olivieri and Ekstrom, 1999), indicative of complex processes acting at the crust mantle transition. Deep seismic sounding profiles (Bally et al., 1986; Pialli et al., 1998; Finetti et al., 2001) and P-wave tomography (Amato et al., 1993; Lucente et al., 1999; Piromallo and Morelli, 1997; Spakman et al., 1993) resolve fairly well the main features of the crust and mantle structures, respectively. Nevertheless, a sound description of the physical properties of the uppermost mantle and its boundary with the crust is still missing. In this paper we intend to improve the lateral and vertical definition of the crust/lithosphere–asthenosphere system (Calcagnile and Panza, 1981; Panza et al., 1982; Suhadolc and Panza, 1989), in Central Italy and propose new constraints for the geodynamic modeling of the area. We employ well established surface wave tomography methods (Ditmar and Yanovskaya, 1987; Yanovskaya and Ditmar, 1990) along with non-linear inversion of dispersion relations for structure retrieval (Panza, 1981; Valyus et al., 1969) and waveform inversion for the moment tensors (Sileny et al., 1992) to: (1) image the Umbria–Marche fault zone; (2) investigate the lateral and vertical heterogeneity within the upper crust (in terms of structural and physical properties); (3) image the lithosphere–asthenosphere system beneath Central Italy.

2. Structural setting

Two major events affected the geologic history of the Central Apennines. The first was the eastward compression which occurred during the convergence and subsequent collision between the European margin (represented by the Corsican eastern margin) and the Adria microplate, in the late Cretaceous–late Oligocene, early Miocene (Boccaletti et al., 1971; Castellarin et al., 1992; Scandone, 1979). The second is a regional extension that affected the inner zone of the North-Central Apennines since early–middle Miocene (Carmignani et al., 1994; Jolivet et al., 1990). These two events gave rise to two belts of different age and geodynamic significance: a western, inner and older, Etruscan belt, and an eastern, outer and younger, Umbrian belt (Barchi et al., 1998). The Etruscan belt consists of an antiformal stack of crustal slices whose crest is now in the Tyrrhenian sea and extends from the eastern boundary of the Corsica basin to Perugia where the front of the Tuscan nappes is localized (Barchi et al., 1998 and references therein). This belt sits above the so-called Tuscan upper mantle anomaly (Della Vedova et al., 1991; Panza et al., 1982). The Umbrian belt consists of hierarchically disposed crustal, basement and sedimentary cover duplexes, showing discontinuity between shallow and deep structures (Pialli et al., 1998). Doglioni et al. (1998) argue that the North-Central Apennines underwent both Alpine and Apenninic subduction events. A probable temporary coexistence of the opposite subductions during the late Oligocene–early Miocene, discussed by Doglioni et al. (1998) using the CROP03 seismic data, could add complexity to the crust–lithosphere system in this area. These geodynamic inheritances of the Apennines belt and its structural settings make the kinematics of the ongoing deformation and its relationships with the seismicity less well understood. It is widely accepted that the North-Central Apennines formed while the Adriatic subduction zone rolled back toward the east (Doglioni, 1991; Royden et al., 1987; Scandone, 1979). Several seismological studies show that subduction is still active (Amato et al., 1993; Margheriti et al., 1996; Selvaggi and Chiarabba, 1995) but the dynamic mechanisms that led to its recent evolution, characterized by the coexistence of extension and compression (Frepoli and Amato, 1997; Montone

et al., 1997; Negredo et al., 1999), are still under discussion. The main forces acting underneath the Central Apennines have been interpreted as due either to slab pull (Royden et al., 1987) or/and to the eastward relative mantle flow (Doglioni et al., 1999), or to slab detachment (Carminati et al., 1998; Wortel and Spakman, 1992, 2000). The data provided by the recent Umbria–Marche normal faulting earthquake sequence, located just to the west of the transition between the extensional and compressional zones, contributed to our understanding of the relationships between moderate earthquakes and the faults that are recognizable in the geological record (Boncio and Lavecchia, 2000; Cello et al., 2000; Galadini et al., 1999; Meghraoui et al., 1999; Barba and Basili, 2000). However, some key issues related to possible conceptual models of the structural deformation that would match the Umbria–Marche epicentral area remain still a matter of debate. Some authors (e.g. Bally et al., 1986) argue that the prevailing type of deformation is of thin-skinned type, where the thrust faults are rooted to a regional detachment between the basement and the overlying deformed sedimentary sequence, gently dipping toward west, while others are in favor of a thick-skinned type of deformation involving the basement (Lavecchia et al., 1994). Another important question, which is still open, is whether or not the recognized normal faults are reactivated pre-existing thrust faults. This study along with other data reported in the literature will allow us to bring additional constraints to the structure and geodynamic evolution of the Central Apennines.

3. Data

To determine the surface wave dispersion relations of the fundamental mode of Rayleigh waves in the period range 0.8–4.0 s, we use the data recorded during the 1997 Umbria–Marche shallow depth earthquake sequence, by the following networks:

(i) strong motion network installed from 3 September to 14 October 1997 by the National Seismic Survey (SSN) and the Italian ENEL (SSN and ENEL, 1998);
(ii) geophone network installed from 18 October to 3 November 1997 by the National Group for the Defense against Earthquakes (GNDT) and SSN (Govoni et al., 1999);
(iii) stations of the local permanent networks: three stations managed by the Osservatorio Geofisico Sperimentale of Macerata (RSM), and five RESIL stations managed by the "Regione Umbria-Oss. Bina of Perugia" (Govoni et al., 1999);
(iv) geophones installed in Fabriano in the period 4–14 November 1997 (GNDT and SSN, 1998).

At the stage of inversion, in addition to our short-period data, we use: group (10–35 s) and phase (30–100 s) velocity dispersion relations from Pontevivo and Panza (2002) and Panza et al. (1980), respectively; deep seismic sounding data (Bally et al., 1986; Pialli et al., 1998; Finetti et al., 2001), Bouguer anomaly (Marson et al., 1998) and heat flow (Della Vedova et al., 2001) data.

4. Surface wave tomography and non-linear inversion

4.1. Group velocity measurements and tomography

We use the frequency–time analysis (FTAN) to extract the group velocity dispersion curve of the fundamental mode (Levshin et al., 1972, 1992) of Rayleigh waves in the period range 0.8–4 s from the signals of events with magnitude greater than 3.0, corresponding to the event–station paths shown in Fig. 1. The basic characteristics of the current measurement procedure are based on a long history of development of surface wave analysis (e.g. Dziewonski et al., 1969; Levshin et al., 1972, 1992; Cara, 1973; Keilis-Borok (Ed.), 1989).

To our dispersion relations, we associate the measurement errors corresponding to the difference between dispersion values obtained from distinct paths with similar length and position as shown in Table 1.

Other errors that can affect our measurements arise from the straight-line approximation of the event–station path and from the source phase term (e.g. Panza et al., 1973, 1975a,b). The results obtained from the eight worse path test cases, covering distances in the ranges 19–63 km, can be summarized as follows: the percentage difference in length reaches a maximum of 0.5% with an average of about 0.15%,

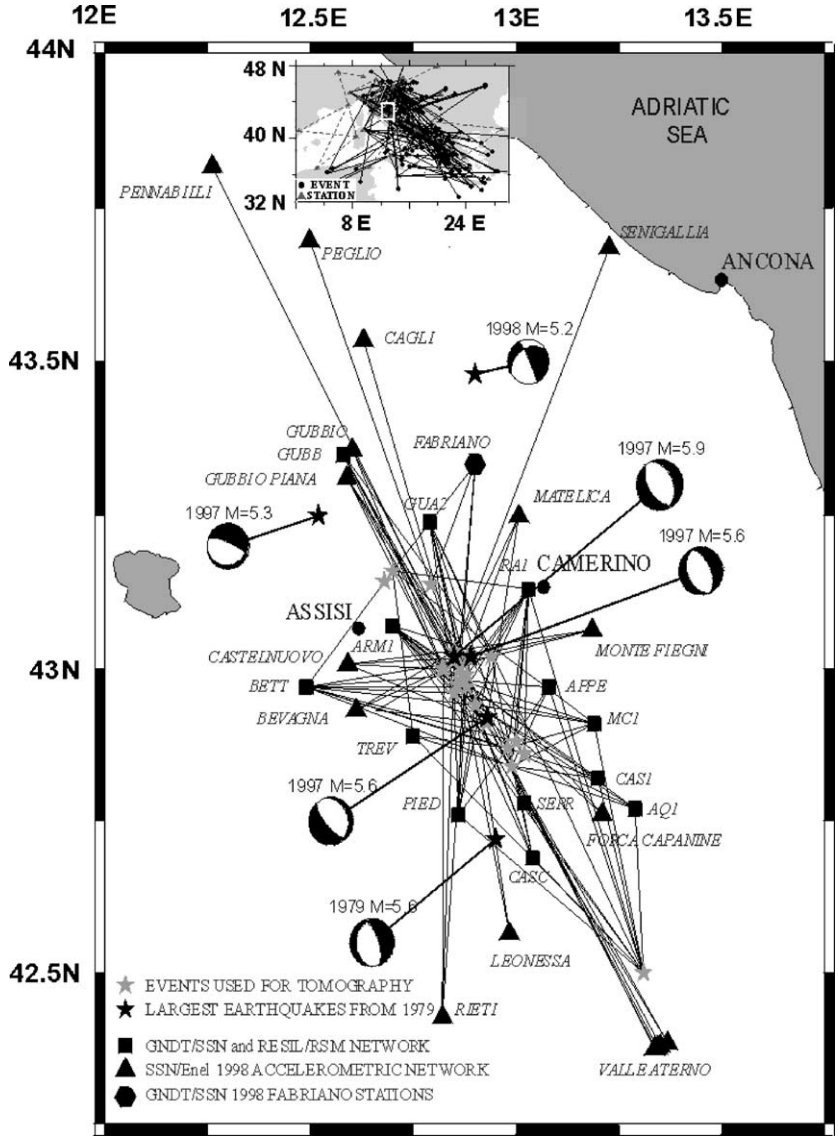

Fig. 1. Stations, earthquakes and seismic paths selected for surface wave tomography. The fault-plane solutions of the largest events in Umbria–Marche (Central Italy), since 1979, are also shown. In the frame at the top, both the paths from epicenter to station (solid bold lines) for the long period group velocity tomography (Pontevivo and Panza, 2002) and the paths from station to station (grey dashed lines) for the phase velocity tomography (Panza et al., 1980) are plotted.

the maximum path deviation from the straight line is about 7 km with an average of 2 km, the resulting percent variations in velocity and time have a maximum of about 0.5% with average value of about 0.15%. Therefore, the errors due to straight-line approximation of the event–station path are negligible with respect to the measurement errors. The effects of the source term on the group velocity measurements have been investigated computing synthetic seismograms keeping fixed the structural model and varying the source parameters, strike, dip and rake around the well-constrained focal mechanisms shown in Section 5. The resulting synthetic and measured dispersion curves differ negligibly within the measure-

Table 1
Group velocity dispersion data and measurement errors of the fundamental mode of the Rayleigh waves for the 11 regions in Umbria–Marche

Period (s)	Group velocity (km/s)											Measurement error (km/s)
	Region EA	Region EB	Region EC	Region ED	Region EE	Region EF	Region EG	Region EH	Region EI	Region EL	Region EM	
0.8	1.32	1.45	1.50	1.67	1.60	1.70	1.61	1.59	1.59	1.58	1.45	±0.10
1.0	1.23	1.42	1.50	1.84	1.58	1.73	1.65	1.61	1.67	1.59	1.50	±0.10
1.5	1.07	1.31	1.48	1.76	1.64	1.59	1.56	1.61	1.73	1.64	1.52	±0.10
2.0	1.14	1.39	1.57	1.86	1.66	1.55	1.62	1.71	1.88	1.84	1.60	±0.12
3.0	1.52	1.77	1.92	2.04	2.01	1.76	1.94	1.82	2.02	1.97	1.84	±0.18
4.0	1.87	2.07	2.20	2.36	2.27	1.93	2.25	1.97	2.10	2.02	2.01	±0.18

ment errors and therefore the source effects may safely be ignored in the considered distance and period range.

The compiled group velocity database represents the input for the tomography algorithm. We apply the method of Ditmar and Yanovskaya (1987) and Yanovskaya and Ditmar (1990) to compute group velocity maps at fixed periods. The tomography algorithm is the generalization of the one-dimensional inversion method of Backus and Gilbert (1968, 1970) and it does not require a priori parameterization or truncation of any expansion since the basis functions for the model are superpositions of the kernels of the group travel time integrals. We obtain, for each period, the group velocity $U(\theta, \phi)$ as a function of the position on the earth surface, i.e. of latitude and longitude (θ, ϕ). We estimate the horizontal resolution $a(\theta, \phi)$ and the stretching $\varepsilon(\theta, \phi)$ (example in Fig. 2) following the method of Yanovskaya and coworkers

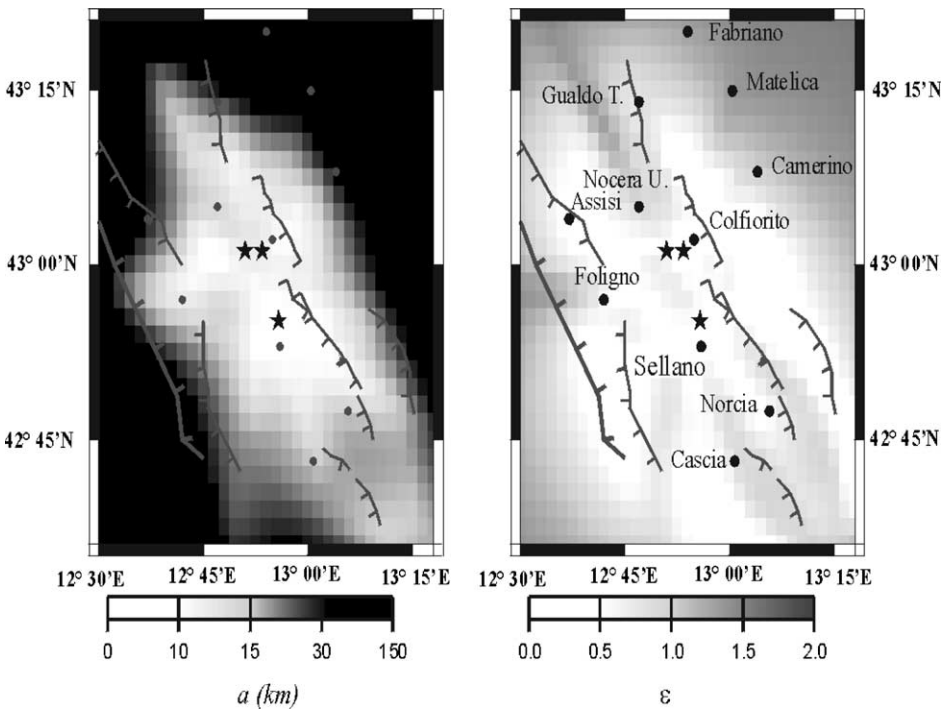

Fig. 2. Fault system (Galadini et al., 2000; Barchi et al., 2000) in the investigated area and epicenters (stars) of the events of 26 September and 14 October 1997 plotted on the map of the horizontal resolution, a, and on the map of the stretching parameter, ε, at 0.8 s.

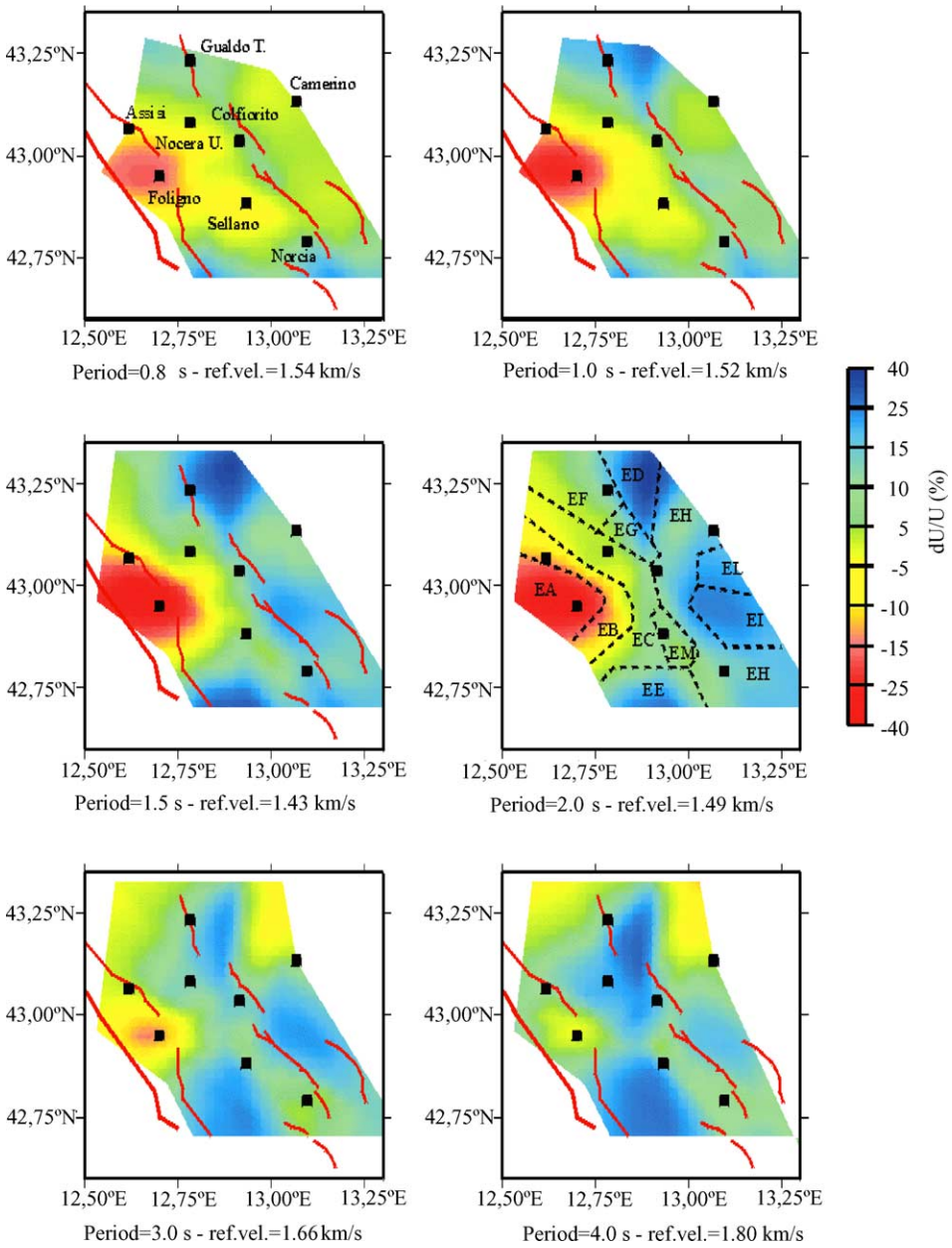

Fig. 3. Rayleigh waves group velocity tomography maps at the different periods shown as percent deviation from the average reference velocity (ref. vel.). The 11 regions, marked from EA to EM and obtained by grouping the dispersion curves, are plotted on the 2.0 s map.

(Yanovskaya et al., 1998, 2000; Yanovskaya and Antonava, 2000). The stretching parameter controls how uniformly the paths are distributed in all directions: where the stretching value is large, the paths have a preferred orientation and the tomography does not provide any additional information to the original results obtained by FTAN.

The maps shown in Fig. 3 represent the group velocity percent variation with respect to the mean velocity at each of the selected periods.

We focus where the horizontal resolution is smaller than 20 km for all periods.

4.2. Regionalization

We regionalize the dispersion curves by grouping those that differ by less than the measurement error at each period. Accordingly, we subdivide the Umbria–Marche zone in 11 homogeneous regions, most of them compatible with the resolution length, following the procedure of Pontevivo and Panza (2002).

The lateral anisotropy suggested by this subdivision is supported by the distribution of the main faults, which follow the borders of most of the regions (Fig. 3).

For each homogeneous region we calculate a locally averaged dispersion curve to which we associate the measurement errors as listed in Table 1.

4.3. Non-linear inversion

We apply the non-linear inversion method, independent from the starting model, known as "hedgehog" (Valyus et al., 1969; Knopoff, 1972; Knopoff and Panza, 1977; Panza, 1981), that is an optimized Monte Carlo non-linear search of velocity–depth distributions, to the observational data represented by group and phase velocity dispersion curves. Following this procedure, in the elastic approximations, the structure is parameterized and modeled as a stack of N homogeneous isotropic layers, each one defined by compressional and shear-wave velocities (V_P, V_S), thickness (h) and density (ρ). Each parameter may be fixed, independent or dependent. Fixed parameters are held constant during the inversion, accordingly with relevant geophysical evidences. Independent parameters are those for which acceptable models are sought by the inversion, taking into account the resolving power of the data (Panza, 1981). Dependent parameters maintain a fixed relationship with the independent ones. As a rule, in the well-resolved depth range, V_S and h are independent, ρ is fixed, and V_P is fixed if the information is available or dependent on V_S so that the $V_P/V_S = \sqrt{3}$.

To our Umbria–Marche regionalized dispersion measurements we add other information available in the literature. In particular, we use group velocity values in the range from 10 to 35 s from Pontevivo and Panza (2002) and phase velocities from 30 to 100 s from Panza et al. (1980) (Table 2). Therefore, the phase and group velocity curves of the 11 regions of Umbria–Marche cover a wide range (0.8–100 s) of periods.

From our non-linear inversion, we retrieve a set of solutions compatible with the dispersion data. We do not choose the solutions of the inverse problem corresponding to the minimum root mean square (rms), since they are the most affected by the presence of possible systematic errors. From the set of solutions, we accept the one corresponding to the rms closest to the average value, which was computed from all solutions, and hence reduce the projection of possible systematic errors (Panza, 1981) into the structural model. If alternatively, although it may not represent a formally acceptable solution of the inversion process, a median of all solutions (Shapiro and Ritzwoller, 2002) in a set is used as representative, the resulting picture is not significantly different from our selected solution.

The depth resolution of our dataset is determined by the partial derivatives (Urban et al., 1993) of the dispersion curves with respect to the shear-wave velocity of the Rayleigh wave fundamental mode for different periods. As can be seen from Fig. 4 our data are not sensitive to the structural properties at depths larger than about 250 km. To optimize the resolving power of the whole dataset, we perform the inversion through four different steps.

The three first inversion steps are restricted to the Umbria–Marche area, while the last inversion step considers the whole strip from the Tyrrhenian to the Adriatic.

In the first step, the group velocities from 10 to 35 s and the phase velocities from 30 to 100 s are inverted in the depth range from 10 to about 250 km, with V_S and h as independent parameters, V_P dependent and ρ fixed. In all the layers we have fixed $V_P/V_S = \sqrt{3}$, while ρ is taken from Marson et al. (1998) for the crustal layers and consistent with the Nafe and Drake relation (Ludwig et al., 1970) in the upper mantle. The uppermost 10 km of the model being fixed from the results of CROP03 profile (Pialli et al., 1998).

In the second step of the inversion, the 11 dispersion relations, defined for the 11 regions of Umbria–Marche in Section 4.2, are inverted. The model deeper

Table 2
Phase and group velocity and error ranges of Rayleigh fundamental mode from Panza et al. (1980) and Pontevivo and Panza (2002)

Period (s)	Velocity and measurement error (km/s)											
	Region A: Tyrrhenian coast 42.5°N, 11.0°E		Region B: Orbetello zone 42.5°N, 11.5°E		Region C: Chiusi zone 43.0°N, 12.0°E		Region D: Perugia zone 43.0°N, 12.5°E		Region E: Umbria–Marche zone 43.0°N, 13.0°E		Region F: Ancona zone 43.5°N, 13.5°E	
	Group	Phase	Group	Phase	Group	Phase	Group	Phase	Group	Phase	Group	Phase
10	2.16 ± 0.22	–	2.17 ± 0.21	–	2.11 ± 0.10	–	2.15 ± 0.11	–	2.11 ± 0.10	–	2.18 ± 0.11	–
15	2.45 ± 0.22	–	2.39 ± 0.19	–	2.25 ± 0.09	–	2.24 ± 0.08	–	2.16 ± 0.08	–	2.22 ± 0.10	–
20	2.72 ± 0.20	–	2.63 ± 0.18	–	2.47 ± 0.09	–	2.45 ± 0.07	–	2.36 ± 0.07	–	2.42 ± 0.08	–
25	2.89 ± 0.19	–	2.80 ± 0.17	–	2.67 ± 0.08	–	2.64 ± 0.07	–	2.57 ± 0.07	–	2.63 ± 0.08	–
30	3.19 ± 0.19	3.63 ± 0.09	3.13 ± 0.18	3.63 ± 0.09	2.97 ± 0.10	3.62 ± 0.09	2.93 ± 0.08	3.63 ± 0.09	2.85 ± 0.08	3.64 ± 0.09	2.85 ± 0.08	3.67 ± 0.09
35	3.37 ± 0.33	3.69 ± 0.08	3.32 ± 0.33	3.68 ± 0.08	3.17 ± 0.17	3.68 ± 0.08	3.13 ± 0.16	3.69 ± 0.08	3.04 ± 0.16	3.70 ± 0.08	3.02 ± 0.16	3.73 ± 0.08
50	–	3.82 ± 0.06	–	3.82 ± 0.06	–	3.82 ± 0.06	–	3.83 ± 0.06	–	3.84 ± 0.06	–	3.86 ± 0.06
80	–	3.93 ± 0.06	–	3.94 ± 0.06	–	3.95 ± 0.06	–	3.95 ± 0.06	–	3.95 ± 0.06	–	3.95 ± 0.06
100	–	3.97 ± 0.06	–	3.97 ± 0.06	–	3.97 ± 0.06	–	3.97 ± 0.06	–	3.98 ± 0.06	–	3.98 ± 0.06
rms	0.130	0.040	0.130	0.040	0.070	0.040	0.070	0.040	0.070	0.040	0.070	0.040

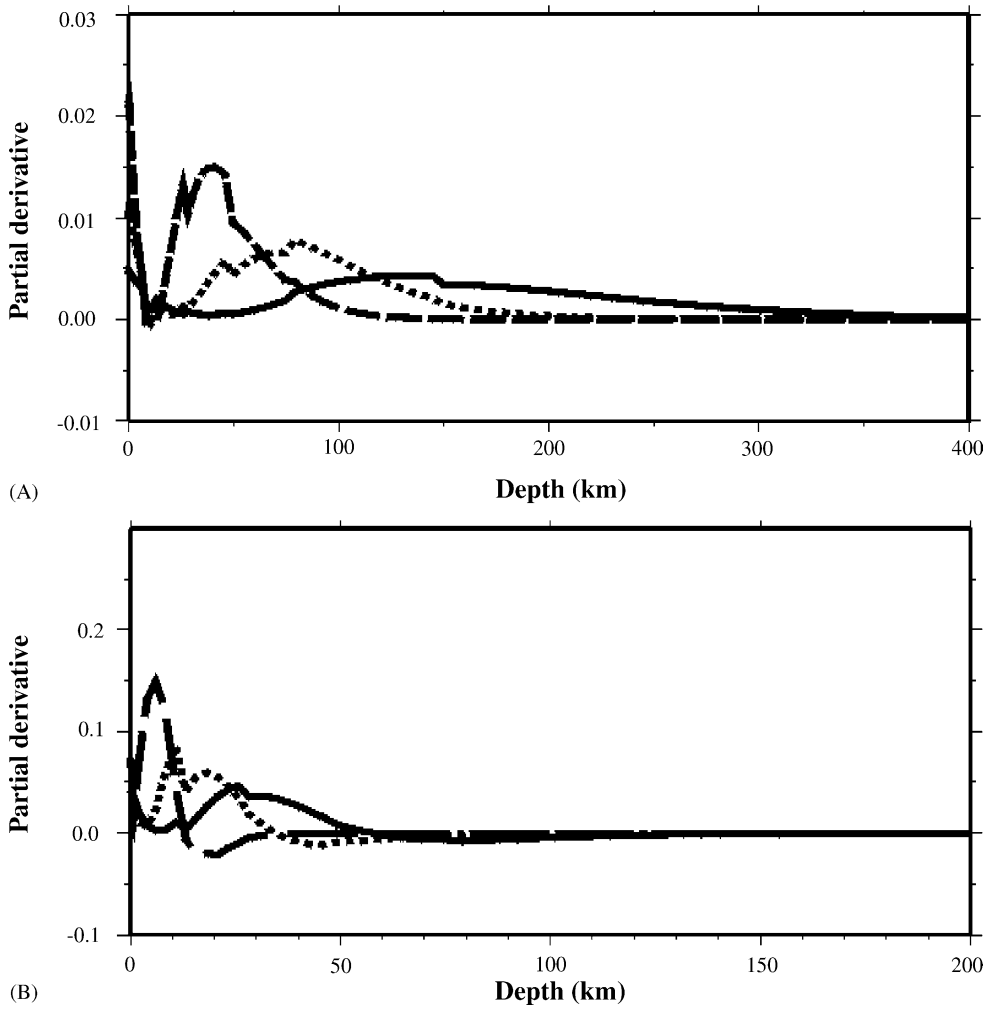

Fig. 4. (A) Partial derivatives of the phase velocity of Rayleigh waves with respect to shear-wave velocity of the fundamental mode at 100 s (solid line), 50 s (dotted line) and 30 s (dashed line) for structure B (Fig. 10). The partial derivatives are normalized with respect to the layer thickness. (B) Partial derivatives of the group velocity of Rayleigh waves with respect to shear-wave velocity of the fundamental mode at 30 s (solid line), 20 s (dotted line) and 10 s (dashed line) for structure B (Fig. 10). The partial derivatives are normalized with respect to the layer thickness.

than 10 km is fixed according to the results of the first step, while for the shallow model a finer parameterization that takes into account the resolving power of the data (Panza, 1981) is used. The CROP03 profile defines the sequence of the stratigraphic units, their ρ (Marson et al., 1998) and V_P (Bally et al., 1986; Barchi et al., 1998). In Table 3, we summarize the elastic properties of the main lithotypes along CROP03 profile. Therefore, the fixed parameters are V_P and ρ while the independent ones are h, V_S and consequently the V_P/V_S ratio of the layers in the uppermost three layers. The selected solutions (Fig. 5) allowed us to construct the cross-section sketch AB shown in Fig. 6 along the profile reported in Fig. 7.

In the third step, the inversions are repeated keeping the uppermost 10 km of each region fixed according to the results of step 2, and V_S and h are the independent parameters in the depth range 10–250 km (Fig. 8).

In Fig. 9, we show an example of the locally averaged dispersion measurements (vertical bars

Table 3
Elastic properties for different lithotypes along CROP03 profile. Bold data refer to the results of the present investigation

Stratigraphic units as in CROP03	Geologic period	$V_P \pm \Delta G V_P$ (km/s)	$V_S \pm \Delta G V_S$ (km/s)	$(V_P/V_S) \pm \Delta G(V_P/V_S)$ (km/s)	ρ (g/cm^3)
MPQ-US9	Quaternary–Pliocene, late Miocene	2.65 ± 0.20	**1.6 ± 0.2**	**1.7 ± 0.3**	2.30
CM-US8-US5-7	Miocene–Oligocene	3.6 ± 0.4	**2.3 ± 0.4**	**1.6 ± 0.5**	2.35
L-TN2-4-US2-4	Early Miocene–Paleocene, Cretaceous–Jurassic	5.5 ± 0.5	**3.0 ± 0.2**	**1.8 ± 0.3**	2.55

represent measurement errors), compared with the group and phase velocity values computed for the selected solution of the inverse problem for the region EA (see Figs. 3 and 8).

As a final step, we extend the inversion to the region from the Tyrrhenian to the Adriatic sea (broken red–black line in Fig. 10 and red dots labeled from A to F) fixing the geometry of the shallow layers accordingly to CROP03 profile, and the V_P and V_S of the lithotypes accordingly with the results of step 2. In all the layers inverted in the third and fourth step, we assume that these are made by Poissonian material and the density is inferred from empirical average relations with seismic wave velocities (Ludwig et al., 1970). The juxtaposition of the selected solutions sketches the lithosphere–asthenosphere system from the Tyrrhenian to the Adriatic as shown in Fig. 10. The lateral variations imaged in Fig. 10 are mainly the results of a constrained parameterization by a priori information.

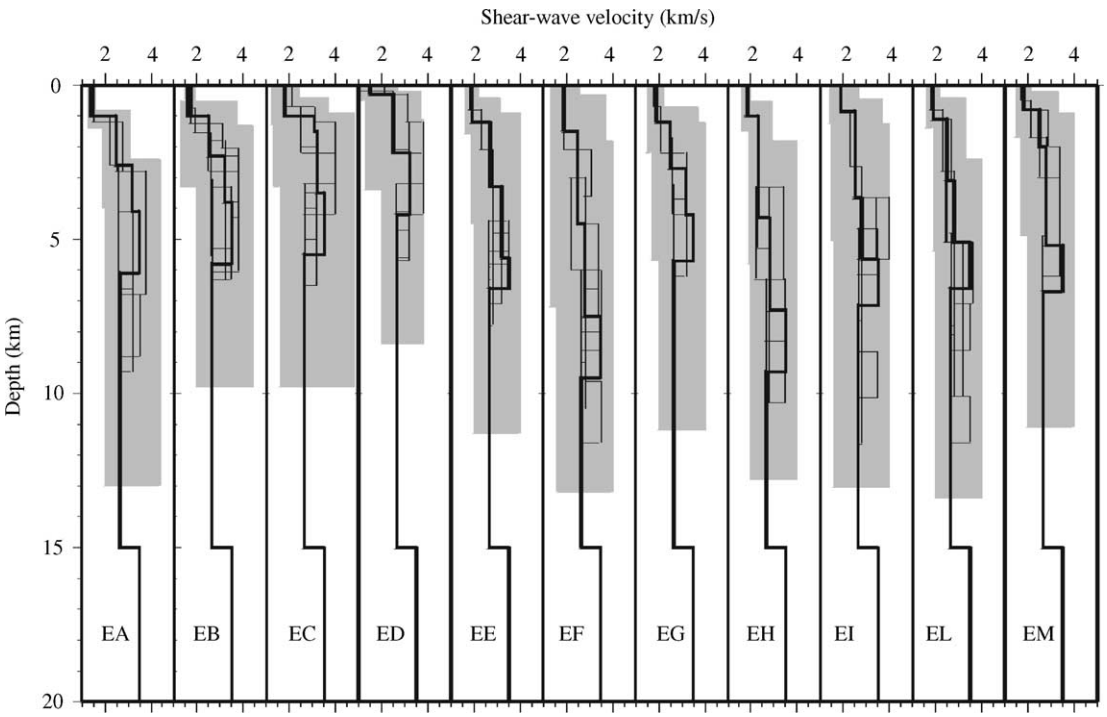

Fig. 5. The solutions of the 'hedgehog' inversions for the 11 regions (shown and named as in Fig. 3) of Umbria–Marche area. For each inversion, all the solutions (thin lines), the selected solution (bold line) and the investigated parameters space (gray area) are shown.

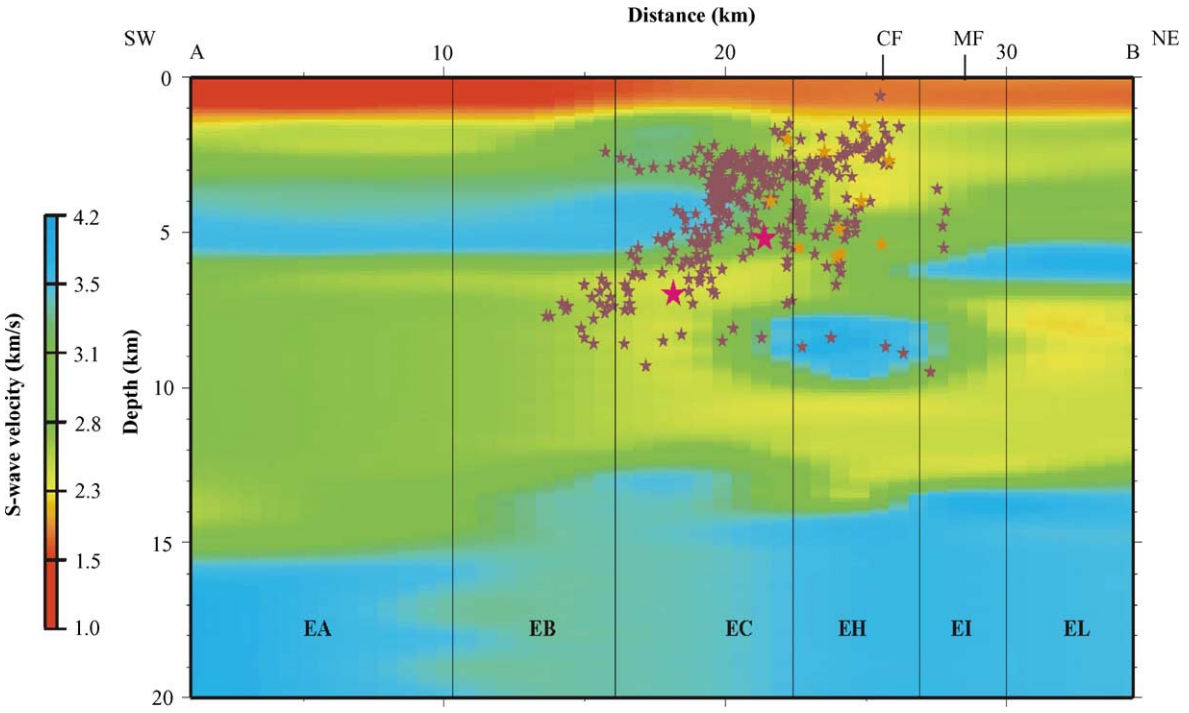

Fig. 6. V_S section across the Umbria–Marche fault zone (see Fig. 7 for its location). The stars represent the seismicity recorded (within the area shown by the rectangle in Fig. 7) by SSN/GNDT temporary network. Orange stars are the events studied in this paper, while red stars are the large events of 26 September 1997 (MF: Monte Prefolio fault, CF: Costa-Cesi fault). This plot has been obtained from the chosen solutions (Fig. 5) juxtaposed by a standard minimum curvature gridding algorithm.

Normally, surface wave inversion requires some assumptions of smoothness in the Earth model so that the accumulated phase can be interpreted in some sense, as a path average. In fact, grouping of similar dispersion relations as done by Pontevivo and Panza (2002) allowed us to identify areas with "homogeneous" dispersion properties, but not necessarily with laterally homogenous structures. The resolution of dispersion measurements is, in fact, only indirectly connected with the lateral structural resolution: a given dispersion relation can correspond different structural models, depending upon the a priori information that is used to constrain the inversion. In our case, it has been possible to outline the lateral variations reported in our section (Fig. 10) by introducing the relevant a priori information given by the CROP03 crustal profile (Pialli et al., 1998). In other words, the introduction of this independent information about the crustal parameters improves the resolving power of our tomography data. The same applies to the lateral variations observed at a smaller scale, across the Umbria–Marche fault zone (Fig. 6), where the fixed parameters were taken from a crustal profile made by Bally et al. (1986). Therefore, the lateral variations we mapped are mainly the results of the constrained parameterization by relevant independent datasets. The outlined lateral variations in our models give rise to surface wave refractions whose effects on travel times and ray paths are negligible with respect to measurement errors as discussed in Section 4.1.

Velocity profiles like the ones shown in Figs. 5, 8 and 10c, as bold lines, represent the point estimation of the parameters corresponding to the chosen solutions. On the base of mathematical statistics they have little sense without the associated confidence interval. Therefore, since the representation of the solution with its confidence interval is a graphical problem of some complexity, the sections (Figs. 6 and 10d) have been drawn for the purpose of being simply indicative of the main features. For example, representative

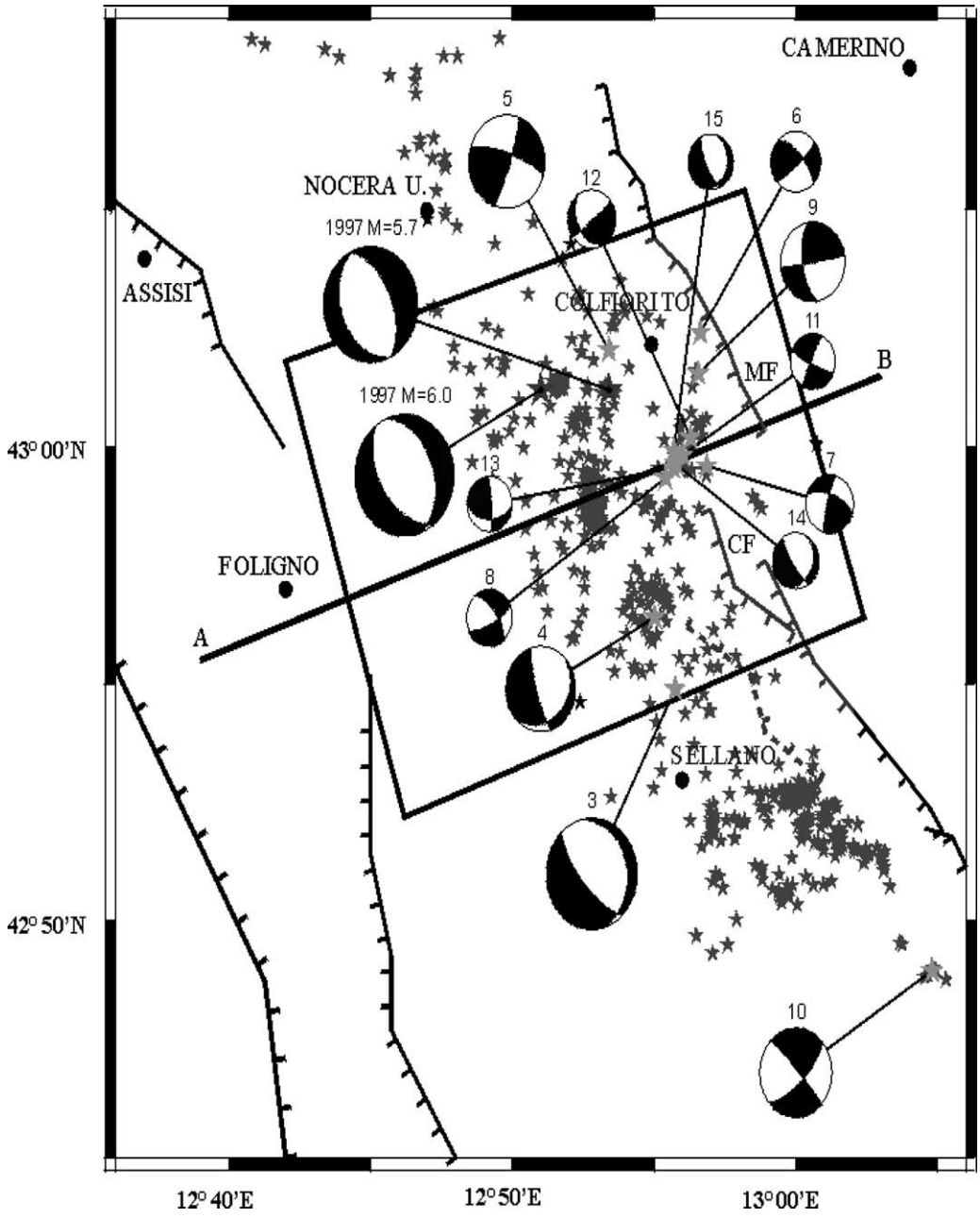

Fig. 7. Fault-plane solutions determined by the seismic source moment tensor inversion. The beach balls are labeled as in Table 4. The fault system (MF: Monte Prefolio fault, CF: Costa-Cesi fault) and the section (line AB perpendicular to the fault system) are plotted. The rectangle bounds the events, which are projected on the section shown in Fig. 6.

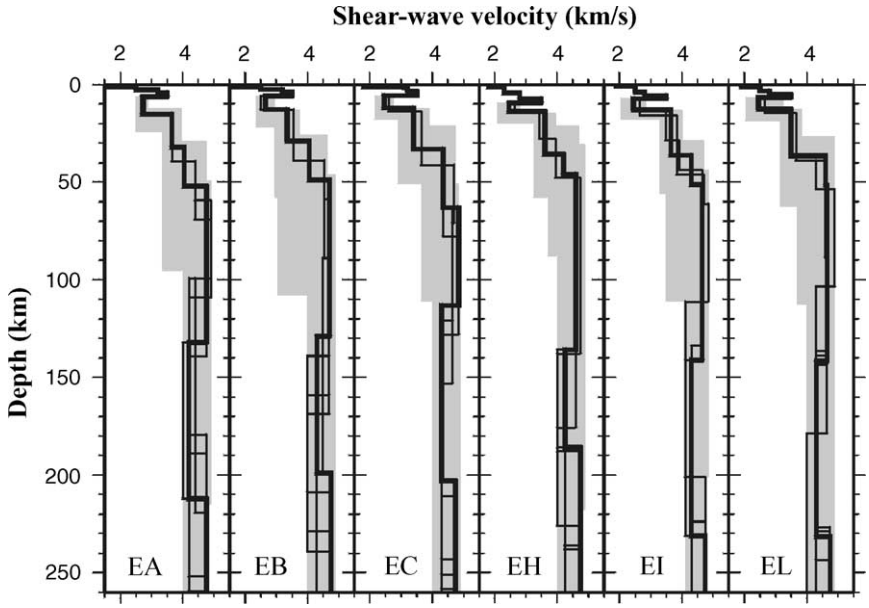

Fig. 8. The solutions of the 'hedgehog' inversions for the six regions (named EA, EB, EC, EH, EI and EL as in Fig. 3) of Umbria–Marche area along the section. For each inversion, all the solutions (thin lines), the selected solution (bold line) and the investigated parameters space (gray area) are shown.

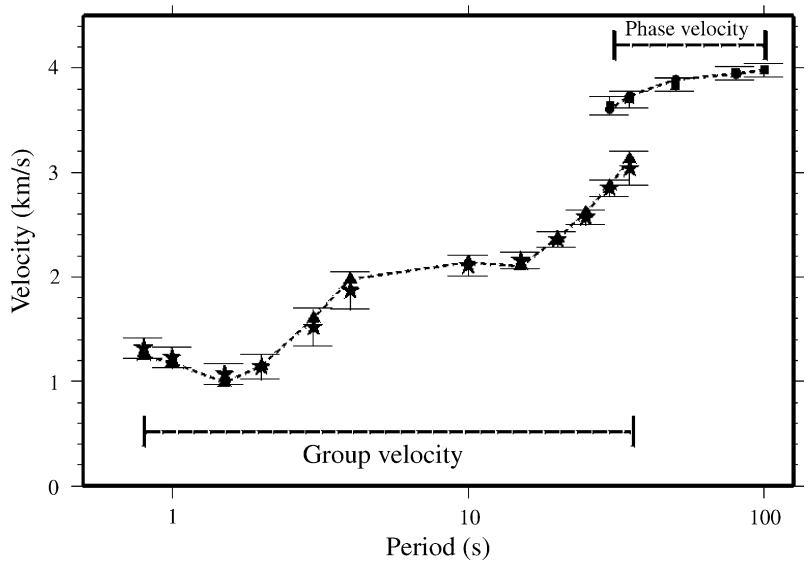

Fig. 9. Region EA. Observed group velocity (V_g) in the range 0.8–35 s (stars) and phase velocity (V_{ph}) in the range 30–100 s (squares) compared with the values corresponding to the chosen model (V_g (triangles), V_{ph} (circles)). The vertical bars indicate measurement error.

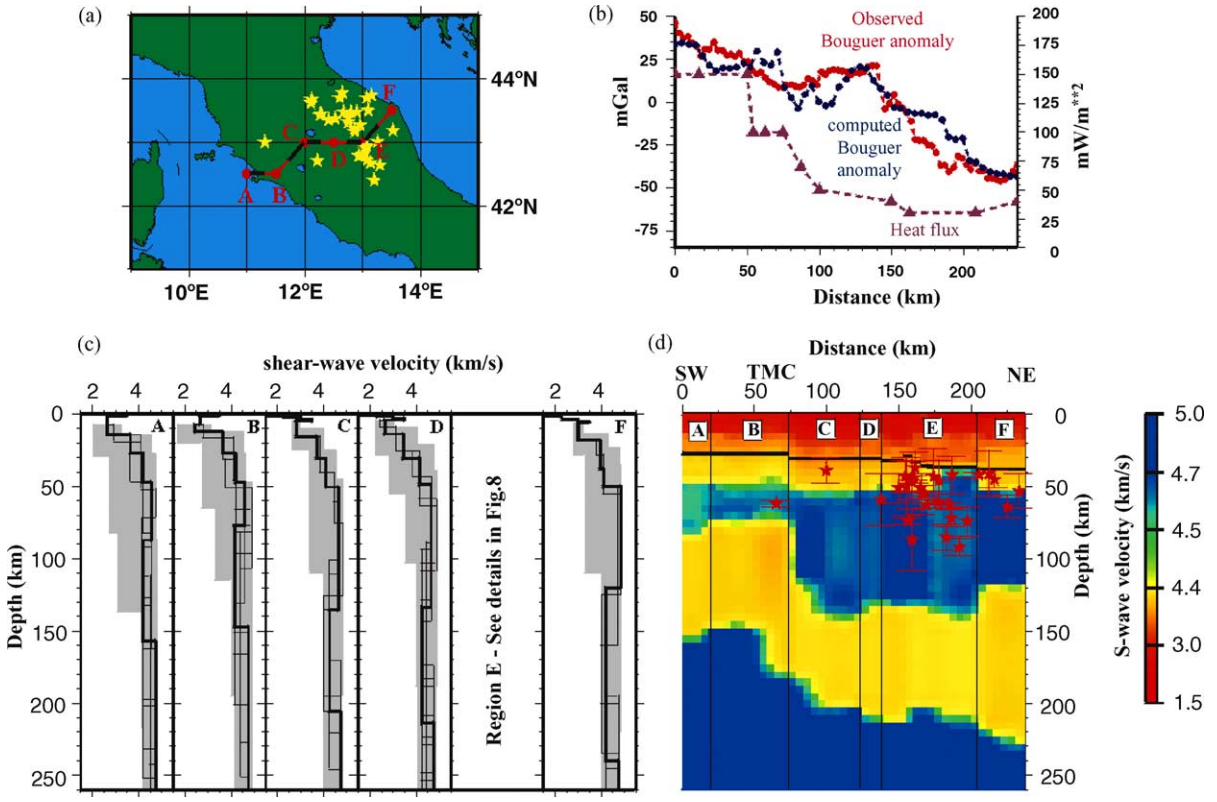

Fig. 10. (a) Location of the study profile. The points from A to F are the centers of the $1^\circ \times 1^\circ$ regions over which dispersion relations have been averaged and then used in 'hedgehog' inversions. The stars represent the location of the deep seismicity shown in (d) (ISC, 1996; Selvaggi and Amato, 1992). (b) Modeled and observed (Marson et al., 1998) Bouguer anomaly along the study profile and heat flow data (Della Vedova et al., 2001). (c) For each region, all the inversion solutions (thin lines), selected solutions (bold lines) and investigated parameters space (grey area) are shown. (d) Lithosphere–asthenosphere system from the Tyrrhenian to the Adriatic coast and related deep seismicity (ISC, 1996; Selvaggi and Amato, 1992). The cross-section has been obtained from the selected solutions (shown in (c)) by a standard minimum curvature gridding algorithm.

thickness and V_S of the main layers in the upper crust are shown in Fig. 6, and of the whole crust, lid and upper asthenosphere in Fig. 10d. On the other side, the sketch in Fig. 12 is drawn from the point estimations and their uncertainties as deduced from the velocity profile ranges shown in Figs. 5, 8 and 10c.

5. Moment tensor inversion studies

We determine moment tensor solutions for earthquakes of the Umbria–Marche sequence ($M_d > 4$), which started in September 1997, using data recorded by the MEDNET network. We also study some aftershocks (Table 4) ($2.7 < M_d < 3.9$), which occurred on the Costa-Cesi and Monte Prefoglio fault (Fig. 7) that were recorded by the local GNDT/SSN and RESIL/RSM network (Govoni et al., 1999).

The moment tensor inversion method we use was developed by Sileny et al. (1992). The advantages and limitations of the method have been illustrated in several studies (Panza and Saraò, 2000; Saraò et al., 2001; Sileny et al., 1996). The inversion which does not constrain the solution with a priori assumptions, consists of two main steps: the first step is linear and inverts data using elementary seismograms computed by modal summation (Panza, 1985) for the moment tensor components to get the six moment rate

Table 4
Fault-plane solutions determined by the source moment tensor study of crustal events

No.	Event date/origin time (h)	Latitude/ longitude (°)	Depth (km)	M_L	M_O (N m)	Strike (°)	Dip (°)	Rake (°)	Network
1	26 September 1997/00:31	43.02/12.85	7.0	5.6	(5.4 ± 0.6)E+17	144	50	−100	Mednet
2	26 September 1997/09:39	43.02/12.89	5.2	5.9	(9.0 ± 0.4)E+17	157	37	−88	Mednet
3	14 October 1997/15:23	42.92/12.93	5.5	5.6	(9.0 ± 0.3)E+16	347	22	−63	Mednet
4	16 October 1997/04:52	42.94/12.92	2.0	4.2	(8.0 ± 0.6)E+14	49	24	−26	Mednet
5	16 October 1997/12:03	43.03/12.89	4.0	4.2	(2.0 ± 0.4)E+15	19	83	16	Mednet
6	19 October 1997/04:04	43.04/12.94	1.1	3.0	(3.00 ± 0.15)E+13	315	65	170	Local
7	19 October 1997/06:39	42.99/12.95	5.4	2.9	(1.0 ± 0.5)E+14	289	63	10	Local
8	20 October 1997/04:29	42.99/12.92	2.4	2.8	(2.0 ± 0.1)E+13	323	63	−21	Local
9	23 October 1997/08:58	43.03/12.94	2.7	3.9	(4.0 ± 1.4)E+14	172	64	2	Local
10a	25 October 1997/03:08	42.82/13.08	2.0	4.4	(2.0 ± 0.1)E+15	315	84	−20	Mednet
10b	25 October 1997/03:08	42.82/13.08	1.5	4.4	(1.5 ± 0.8)E+15	313	86	161	Regional
11	27 October 1997/15:45	43.00/12.93	4.0	2.7	(3.0 ± 0.9)E+13	114	81	−8	Local
12	27 October 1997/19:27	43.00/12.94	1.6	2.9	(2.0 ± 0.5)E+13	148	40	−172	Local
13	1 November 1997/00:44	42.99/12.93	5.8	2.7	(5.0 ± 0.9)E+13	92	44	9	Local
14	1 November 1997/05:56	42.99/12.93	5.7	2.8	(9.0 ± 1.2)E+13	29	27	−29	Local
15	1 November 1997/08:08	43.00/12.93	4.9	2.7	(4.0 ± 0.4)E+13	18	25	−50	Local
16	26 March 1998/16:24	43.48/12.90	31.0	5.2	(2.0 ± 0.2)E+17	335	83	−129	Mednet

functions; the hypocenter is not fixed and can move inside a pre-defined volume. The difference between real and computed seismograms is calculated by means of the L_2 norm. In the second step, the information on the focal mechanism and on the source time function is extracted from the six components of the moment tensor. The moment rate functions (MTRF) are factored into an average moment tensor and the corresponding source time function. The advantage of this approach is a simplification of the problem of fitting the input seismograms by converting it into a problem of matching the MTRFs. The number of MTRFs is fixed at six, or five when dealing with only deviatoric sources, and their length is controlled by the number of triangles used for their parameterization. Considering the MTRFs as independent functions in the first step leads to an overparameterization of the problem, which is advantageous to partially absorb poor modeling of the structure (Kravanja et al., 1999). The effects due to local heterogeneities and to wave propagation, such as attenuation, reflection or scattering, are in this way reduced. The solution of the best double couple is robust even if only two three-component stations are used (Panza and Saraò, 2000) and the level of noise is less or equal 20% of the maximum amplitude (Sileny et al., 1996).

To compute the seismic moment tensor of the MedNet data (Table 4), we use only two three-component VBB stations (Trieste and L'Aquila), whereas when inverting the data from the local network we use the vertical-component of each station. For all the cases, we limit the dimension of the null space and where to look for the solutions by constraining the epicentral locations of each event with epicentral locations taken from the literature (Ekstrom et al., 1998, Cattaneo et al., 2000). The data from the MedNet are filtered between 0.01 and 0.2 Hz whereas the data recorded by the local network are filtered between 0.2 and 5.0 Hz; the structural models, one for each path source-receiver, are one-dimensional sections gained from EurID-data set (Du et al., 1998) when inverting the long period data, and from this study when using local data. After removing the mean, tapering and filtering, we select the temporal window of the seismograms corresponding to the dominant part of the record that will be used in the inversion. For each event, we show the retrieved focal mechanism (Fig. 7) and the waveform fit (Fig. 11). In Table 4 are summarized the inversion results: the retrieved depth, the scalar seismic moment and the fault-plane solutions of each event. The 25 October 1997 earthquake has been inverted using both data from the MedNet and from the local network. The mechanisms obtained are consistent within the errors even if inverted from data with a large difference in frequency content (Table 4).

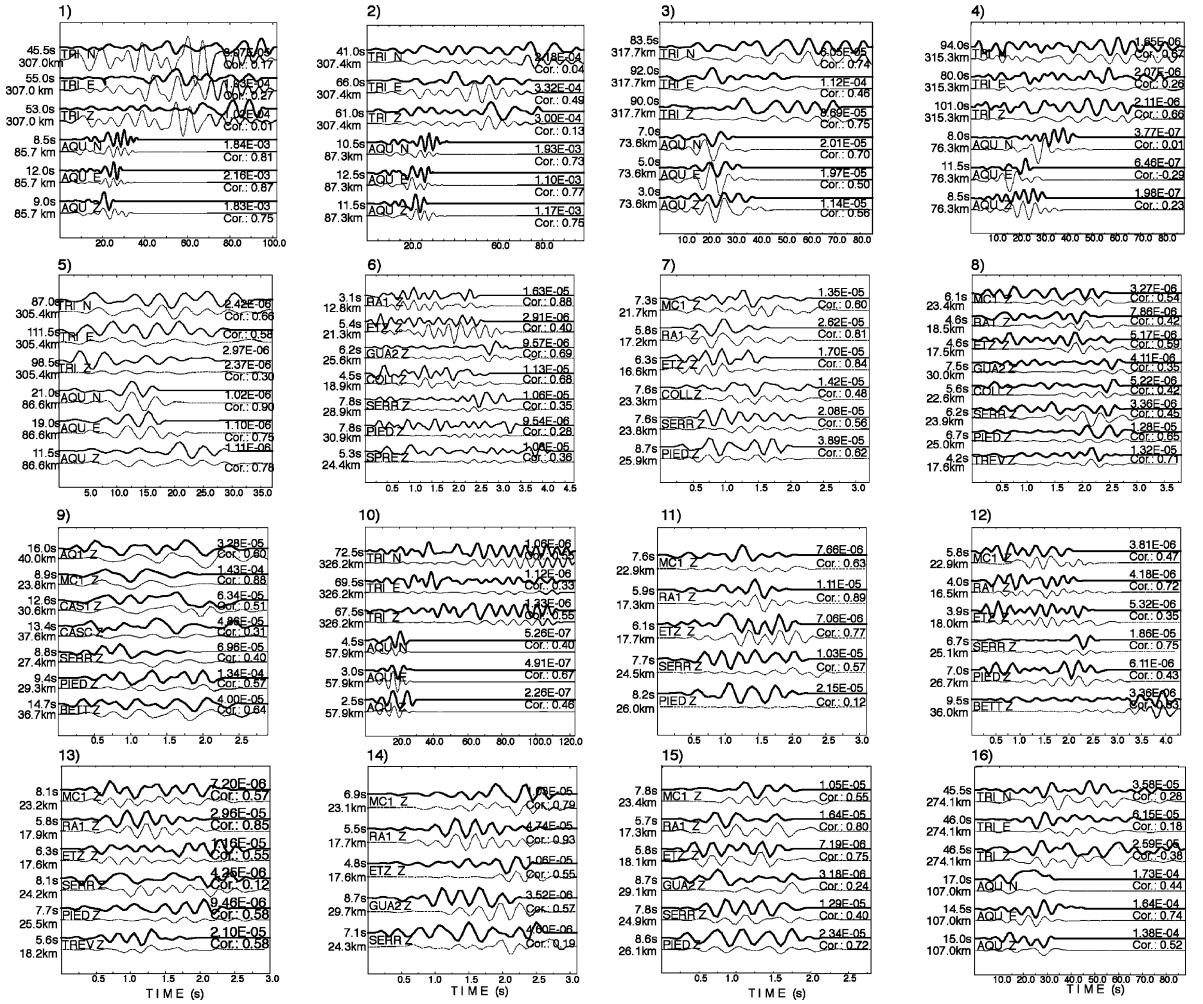

Fig. 11. Waveform fit for the events studied in this paper between real (solid bold lines) and synthetic data (thin dotted lines). The numbers on the top left correspond to those of Table 4 (event number 10 corresponds to 10a in Table 4). For each case, we report the epicentral distances (Dist) and the starting time (Dt) of the temporal window containing the signal to be inverted (left) whereas the maximum amplitudes and the correlation value (Corr) are reported on the right. The retrieved fault-plane solutions are given in Fig. 7 except for the event number 16 (3 March 1998) shown in Fig. 1.

6. Discussion and results

6.1. Umbria–Marche fault zone

The main active faults, as reported by the GNDT working group (Galadini et al., 2000), are mapped in Figs. 2 and 3. The faults recognized as seismogenic are the ones extending along a NW–SE trend, in an echelon distribution, from Gualdo Tadino to the north down to Norcia in the south, crossing the Colfiorito basin where the large 26 September 1997 events are located. These faults, dipping towards the southwest, define a half-graben structure and form a series of intermontane basins, which alternate with NW–SE trending ranges. To the southwest of this active fault system, the Foligno basin, clearly highlighted by a negative group velocity anomaly (Fig. 3) is bounded by a southeast-dipping fault to the east, and the northwest-dipping Altotiberina fault to the west. Barchi et al. (1998) and Boncio et al. (1998) interpret

the Altotiberina fault as the base of an active hanging wall block stretching towards NE from detach the Gualdo Tadino-Norcia half-graben fault system. The different panels of Fig. 3 show that positive and negative velocity anomalies follow the general trend of the geological structures and related active faults. The contrasts in velocity reflect a contrast in topography, in sediment type, and in tectonic motion, typical of active basins and ranges. Furthermore, Fig. 3 displays minor velocity contrasts evident along-strike that fragment the NW–SE trending structures into three main positive anomaly bodies that are clearly evident at periods of 1.5 and 2 s, with dimensions comparable with the correlation length of the tomography. The central velocity anomaly body contains the fault system that has been reactivated during the 1997 earthquake sequence and extends from Nocera Umbra to south of Sellano. The other two velocity anomalies have been the site of two recent moderate earthquake sequences: Norcia to the south in 1979 ($M_S = 5.8$; Deschamps et al., 1984) and Gubbio to the north in 1984 ($M_S = 5.2$; Haessler et al., 1988). At both edges of the central velocity anomaly, Calamita and Deiana (1988) report NE–SW pre-quaternary transverse structures. In particular, at the southernmost edge, Meghraoui et al. (1999) reported NE–SW trending fold axes, that bound the southernmost reactivated fault of the 1997 earthquake sequence. This also corresponds with the surface faulting of the 14 October seismic event ($M_W = 5.6$). The Umbria–Marche fold and thrust belt is therefore likely to be segmented into three main structural bodies that could explain the interplay between the 1979–1984–1997 earthquake sequences. At the scale of the 1997 reactivated fault system, the moment tensor inversions of the two large 26 September and 14 October events show dominantly normal faulting mechanisms, whereas selected aftershocks (magnitude in the range between 2.7 and 4.4) between the Costa-Cesi and Monte Prefoglio faults (Fig. 7), within the Colfiorito basin, reveal that the prevailing deformation at the step-over is of strike-slip faulting type. According to Cello et al. (1997), this step-over zone is marked by pre-existing transverse faults. Furthermore, within the same area, Cinti et al. (2000) report several differently oriented cracks interpreted as the surface effect of minor displacements along transverse structures that are likely to be oriented N–S and may correspond to western edges of the Colfiorito and Costa-Cesi basins. Therefore, it is likely that the step-over between the 1997 reactivated fault fragments (Meghraoui et al., 1999), collocated between the rupture areas of the two September 26 events, is of strike-slip type and could have controlled the lateral propagation of slip. A similar focal solution, of strike-slip type of motion, is retrieved for one of the strongest aftershocks (M_L 4.4; 25 October, 03:08 h) that took place at the southern most sector of the earthquake sequence (Fig. 7). Our solution differs considerably from the reverse focal mechanism proposed by Cattaneo et al. (2000), but corroborates the hypothesis that the present-day activity is controlled by transverse structures. The moment tensor of the 14 October (15:23, M_L 5.6) Sellano earthquake (solution 3, Fig. 7) reveals a slightly different trend with respect to the two 26 September events. This geometrical discrepancy between September and October source parameters is also observed by the SAR data (Salvi et al., 2000) and may have controlled the lateral extent of the largest rupture planes and the apparent clustering of the related aftershocks.

The NW–SE vertical oriented V_S section across the zone of the 1997 normal faulting earthquake sequence (Fig. 6) shows that the reactivated SW dipping fault zone, delineated by the earthquake foci of the September earthquakes, displays a typical thrust fault geometry, as evidenced by the lateral extent of the faulted late Triassic evaporites layer. Therefore, the 1997 Umbria–Marche normal fault zone can be interpreted as an inversion of pre-existing thrust faults. Fig. 6 shows that the imaged thrust faulted evaporite layer (blue patches 5–7 km deep) has not yet balanced the present-day normal faulting motion attesting therefore youth extensional tectonics in Umbria–Marche. A relevant feature of Fig. 6 is the marked low-velocity layer, from about 6–15 km. The transition from the overlaying high velocity evaporites to this low-velocity layer could require a net change in the dip of the fault and favor the proposed listric geometry of faulting.

Such layering in Umbria–Marche imposes a pattern and a scale on the observed coseismic and postseismic deformation (Riva et al., 2000). Therefore, the structural changes in the upper crust, as seen in Fig. 6, seem to control the present fault characteristics such as: rupture geometry, pattern of deformation and emergence towards the surface.

6.2. The lithosphere–asthenosphere system from the Tyrrhenian to the Adriatic

Fig. 10 and the interpreted model in Fig. 12 show an image of the lithosphere–asthenosphere system along a profile from the Tyrrhenian to the Adriatic coast that confirms the gross features already published in the literature (e.g. Du et al., 1998 and references therein) and better outlines significant details.

Beneath Central Italy, the proposed model (Fig. 12) shows clear evidence of lithospheric roots, reaching at least a depth of 130 over 120 km of width, from below the western edge of the thick sedimentary basins (75 km) to below the extension–compression transition (200 km). The crust exhibits clear layering and lateral variation in thickness: about 25 km below the Tuscan Metamorphic Complex (TMC), about 30 km below the extensional thick sedimentary basins, about 35 km below the Umbria–Marche geological domain (UMD). The lithospheric mantle (lid) is thin (about 30 km) below the TMC, while it is about 70 km thick below UMD. All along the profile a mantle wedge with thickness of about 20 km, is in-between the crust and the lid (Figs. 10 and 12). The wedge exhibits very low mantle velocities and hence may well decouple the underlying lid from the crust. Young magmatism at the surface and high heat flow values in the region where this low-velocity upper mantle wedge gets shallower and attains its maximum thickness (TMC) suggest that this layer may represent a partially molten mantle in agreement with petrological and geochemical data (Peccerillo et al., 2001). The subcrustal earthquakes (Selvaggi and Amato, 1992; ISC, 1996) seem to cluster in the shallower part of the thick Adriatic lid and in the eastern part of the lithospheric root, consistently with a slab-like geometry, while the part of the lithospheric root and thin lid to the west seems to be almost free of seismic activity (Fig. 10). This is seen in many P-wave tomographic images indicating the presence of a high-velocity body of significantly larger volume than that delimited by the earthquakes foci. There are two possible explanations for the existence of a large lithospheric volume with laterally varying mechanical properties under North-Central Italy: (a) the presence of lateral variations in the stiffness of the lithosphere, consistent

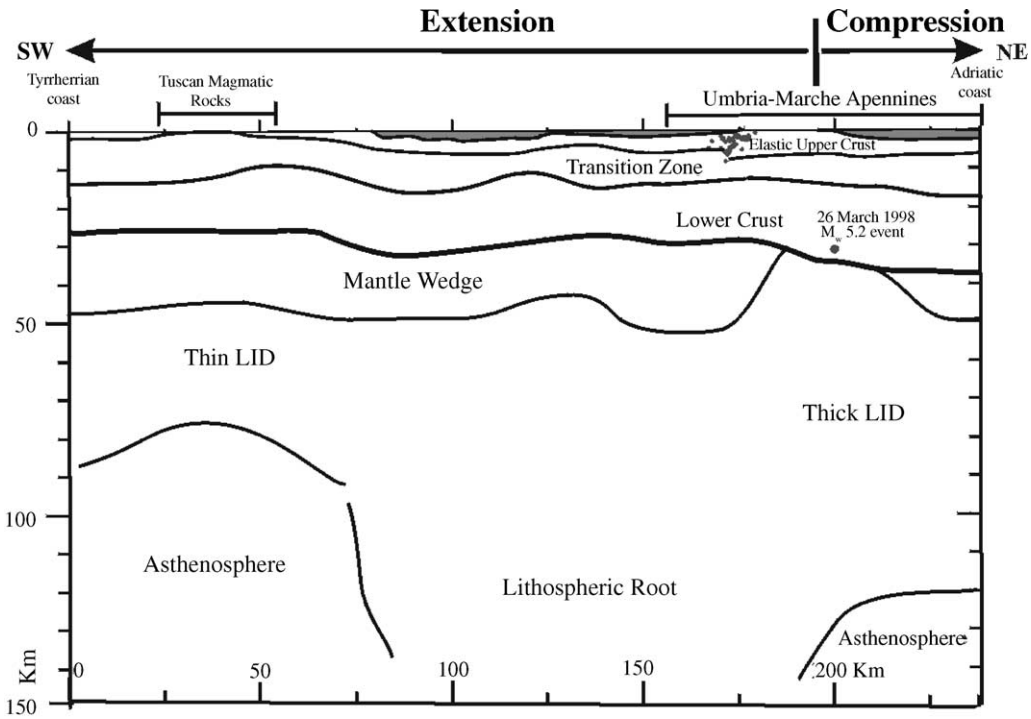

Fig. 12. Sketch of the lithosphere–asthenosphere system from the Tyrrhenian to the Adriatic sea.

with the heat flow distribution, and/or (b) the coexistence of the Adria west-dipping remnant slab with a possible relic of the old Alpine east-dipping slab consistent with geological (Boccaletti et al., 1971; Doglioni et al., 1998) and seismic reflection data (Pialli et al., 1998; Finetti et al., 2001). The crust and upper mantle structure beneath North-Central Italy provides clear evidence of a low-velocity uppermost mantle with a wedge-like geometry. From the geometry of the crust, mantle wedge and underlying lid, the subcrustal lithosphere is likely detached from the overlying crust and peels away exposing subcrustal depths to hot material. The high velocity upper mantle underlying this low-velocity layer is inferred to be subcrustal lithospheric material delaminated from the overlying crust. We argue that the eastward migrating extension–compression reported in the Italian upper crust may correspond to an eastward migrating axis of delamination in the uppermost mantle.

For the proposed model of the lithosphere–asthenosphere system beneath Central Italy, we computed the Bouguer anomaly using velocity versus density empirical relationships (Ludwig et al., 1970). The agreement, shown in Fig. 10, between observed and computed Bouguer anomaly is quite satisfactory, since it is the result of direct computation and no data fitting has been applied. The trend of the computed Bouguer anomalies is mainly controlled by the lateral variations in density within the mantle wedge, from less dense material below the TMC to more dense material beneath the UMD. A generalized lateral variation in ρ and V_S is consistent with the heat flow in the region (Della Vedova et al., 2001).

7. Conclusions

This study has provided information and details on the physical properties of the crust and upper mantle in Central Italy at three different scales: 1997 Umbria–Marche fault zone, Umbria–Marche fold and thrust belt and Central Apennines from the Tyrrhenian to the Adriatic coast.

The three largest shallow earthquakes (26 September 1997 at 00:33 h, $M_W = 5.7$; 26 September 1997 at 09:40 h, $M_W = 6.1$ and 14 October 1997 at 15:23 h, $M_W = 5.6$) of the 1997 Umbria–Marche normal faulting sequence occurred on three distinct and neighboring fault segments. The propagation of the rupture along these segments seems to be controlled by the presence of transverse structures (with strike-slip faulting mechanisms) in-between the segments and by a change in the geometry of faulting. The 1997 Umbria–Marche normal fault zone can be interpreted as an inversion of pre-existing thrust faults. The imaged thrust faulted evaporite layer has not yet balanced the present-day normal faulting motion attesting therefore youth extensional tectonics within the thrust belt. Our data are in favor of listric geometry of faulting at depth.

At the scale of the Umbria–Marche fold and thrust belt, the tomography results show an intimate relation between the lateral variations and the distribution of the active fault systems and related sedimentary basins. Furthermore, this geological domain is likely to be segmented into three main structural bodies that could explain the interplay between the 1979 Norcia–1984 Gubbio–1997 Umbria–Marche earthquake sequences. The retrieved models for the Umbria–Marche upper crust reveal the importance of the inherited compressional tectonics on the ongoing extensional deformation and related seismic activity. The structural changes in the upper crust are likely to control fault seismogenesis and rupture geometry. At the scale of the Central Apennines our study provides evidence of lithospheric roots beneath the Apenninic chain, reaching at least to a depth of 130 km along with a set of velocity models that map the lateral extent of the crust–mantle boundary and lithosphere–asthenosphere system from the Tyrrhenian to the Adriatic coast. The evidence of the lithospheric roots is based on the larger thickness of the lid in the central part of the section when compared to its eastern and western parts and to standard continental lid thickness. At shallow depth between lid and crust and along almost all the profile, we report an about 20 km thick mantle wedge, which decouples the underlying lid from the crust. This low-velocity mantle wedge separates the ongoing compressional deformation reported in the Adriatic lid from the extensional deformation reported in the upper crust between Western Tuscany and Marche. We reveal strong variations in the lithospheric thickness along the study profile that are accompanied by variations in V_S, in agreement with heat flow distribution, Bouguer anomaly and seismicity. Therefore,

the present-day configuration of the crust and upper mantle (sketched in Fig. 12) that resulted from complex evolutionary stages of thickening and thinning of the lithosphere in interaction with the underlying asthenosphere, may contribute internal forces to the regional geodynamics. Furthermore, we argue that the eastward migrating extension–compression reported in the Italian upper crust may correspond to an eastward migrating axis of delamination in the uppermost mantle. We speculate that the 31 km depth estimate of the 26 March 1998 earthquake ($M_W = 5.2$), is very close to the crust–mantle boundary, and its epicentral position at the transition extension–compression, may corroborate ongoing delamination processes in the Umbria–Marche lower crust.

Acknowledgements

We thank two anonymous reviewers for constructive comments that substantially improved this paper. We are grateful to Iginio Marson who provided the Bouguer anomalies data and to Bruno Della Vedova for the heat flow data. This research was funded by Italian MIUR Cofin funds (2001: subduction and collisional processes in the Central Mediterranean; 2000: active deformation at the northern boundary of Adria), GNDT funds (2000: determinazione dello stile di deformazione e dello stato di sforzo delle macrozone sismogenetiche italiane) and CNR project CNRC007AF8.

References

Amato, A., Alessandrini, B., Cimini, G., Frepoli, A., Selvaggi, G., 1993. Active and remnant subducted slabs beneath Italy: evidence from seismic tomography and seismicity. Annali di Geofisica 26, 210–214.

Amato, A., Azzara, R., Basili, A., Chiarabba, C., Ciaccio, M.G., Cimini, G.B., Di Bona, M., Frepoli, A., Hunstad, I., Lucente, F.P., Margheriti, L., Mariucci, M.T., Montone, P., Nostro, C., Selvaggi, G., 1998. Geodynamic evolution of the Northern Apennines from recent seismological studies. Mem. Soc. Geol. It. 52, 337–343.

Backus, G.E., Gilbert, F., 1968. The resolving power of gross Earth data. Geophys. J. 16, 169–205.

Backus, G.E., Gilbert, F., 1970. Uniqueness in the inversion of inaccurate gross Earth data. Philos. Trans. R. Soc. Lond. 266, 123–192.

Bally, A.W., Burbi, L., Cooper, C., Ghelardoni, R., 1986. Balanced sections and seismic reflection profiles across the Central Apennines. Mem. Soc. Geol. It. 35, 257–310.

Barba, S., Basili, R., 2000. Analysis of the seismological and geological observations for moderate-size earthquakes; the Colfiorito fault system (Central Apennines, Italy). Geophys. J. Int. 141, 241–252.

Barchi, M., De Feyter, A., Magnani, M.B., Minelli, G., Pialli, G., Sotera, M., 1998. Extensional tectonics in the Northern Apennines (Italy): evidences from the CROP03 deep seismic reflection line. Mem. Soc. Geol. It. 35, 527–538.

Barchi, M., Galadini, G., Lavecchia, P., Messina, P., Michetti, A.M., Peruzza, L., Pizzi, A., Tondi, E., Vittori, E., 2000. Sintesi delle conoscenze sulle faglie attive in Italia Centrale: parametrizzazione ai fini della caratterizzazione della pericolosita' sismica. CNR-Gruppo Nazionale per la Difesa dai Terremoti, Roma.

Boccaletti, M., Elter, P., Guazzone, G., 1971. Plate tectonics model for the development of the Western Alps and Northern Apennines. Nature 234, 108–111.

Boncio, M., Lavecchia, G., 2000. A geological model for the Colfiorito earthquakes (September–October 1997, Central Italy). J. Seismol. 4, 345–356.

Boncio, M., Ponziani, F., Brozzetti, F., Barchi, M., Lavecchia, G., Pialli, G., 1998. Seismicity and extensional tectonics in the Northern Umbria–Marche Apennines. Mem. Soc. Geol. It. 35, 539–555.

Calamita, F., Deiana, G., 1988. The arcuate shape of the Umbria–Marche–Sabina Apennines (Central Italy). Tectonophysics 146, 139–147.

Calcagnile, G., Panza, G.F., 1981. The main characteristics of the lithosphere–asthenosphere system in Italy and surrounding regions. Pure Appl. Geophys. 119, 865–879.

Cara, M., 1973. Filtering of dispersed wave trains. Geophys. J. R. Astron. Soc. 33, 65–80.

Carmignani, L., Decandia, F.A., Fantozzi, P.L., Lazzarotto, A., Liotta, D., Meccheri, M., 1994. Tertiary extensional tectonics in Tuscany (Northern Apennines, Italy). Tectonophysics 238, 95–315.

Carminati, E., Giunchi, C., Sabadini, R., 1998. Numerical modeling of the dynamics of the Northern Apennines. Mem. Soc. Geol. It. 35, 365–380.

Castellarin, A., Cantelli, L., Fesce, A.N., Mercier, J.L., Picotti, V., Pini, G.A., Prosser, G., Selli, L., 1992. Alpine compressional tectonics in Tuscany (Northern Apennines, Italy). Tectonophysics 238, 295–315.

Cattaneo, M., Augliera, P., De Luca, G., Gorini, A., Govoni, A., Marcucci, S., Michelini, A., Monachesi, G., Spallarossa, D., Trojani, L., XGUMS, 2000. The 1997 Umbria–Marche (Italy) earthquake sequence: analysis of the data recorded by the local and temporary networks. J. Seismol. 4, 401–414.

Cello, G., Mazzoli, S., Tondi, E., Turco, E., 1997. Active tectonics in the Central Apennines and possible implications for seismic hazard analysis in peninsular Italy. Tectonophysics 272, 43–68.

Cello, G., Deiana, G., Ferelli, L., Marchegiani, M., Maschio, L., Mazzoli, S., Michetti, A., Serva, L., Tondi, E., Vittori, T., 2000. Geological constraints for earthquake faulting studies in the Colfiorito area (Central Italy). J. Seismol. 4, 357–364.

Cinti, F.R., Cucci, L., Marra, F., Montone, P., 2000. The 1997 Umbria–Marche earthquakes (Italy): relation between the surface tectonic breaks and the area of deformation. J. Seismol. 4, 333–343.

Della Vedova, B., Marson, I., Panza, G.F., Suhadolc, P., 1991. Upper mantle properties of the Tyrrhenian area a frame work for its recent tectonic evolution. Tectonophysics 195, 311–318.

Della Vedova, B., Bellani, S., Pellis, G., Squarci, P., 2001. In: Vai, G.B., Martini, I.P. (Eds.), Anatomy of an Orogen: The Apennines and Adjacent Mediterranean Basins. Kluwer Academic Publisher, Dordrecht, pp. 65–76.

Deschamps, A., Iannaccone, G., Scarpa, R., 1984. The Umbrian earthquake (Italy). Annales Geophisicae 2 (1), 29–36.

Ditmar, P.G., Yanovskaya, T.B., 1987. A generalization of the Backus–Gilbert method for estimation of lateral variations of surface wave velocity. Izv. Akad. Nauk SSSR, Fiz. Zemli 6, 30–60.

Doglioni, C., 1991. A proposal for the kinematic modelling of W-dipping subductions—possible applications to the Tyrrhenian–Apennines system. Terra Nova 3, 423–434.

Doglioni, C., Mongelli, F., Pialli, G., 1998. Boundinage of the Alpine Belt in the Apenninic back-arc. Mem. Soc. Geol. It. 35, 457–468.

Doglioni, C., Harabaglia, P., Merlini, S., Mongelli, F., Peccerillo, A., Piromallo, C., 1999. Orogens and slabs vs. their direction of subduction. Earth-Sci. Rev. 45, 167–208.

Du, Z.J., Michelini, A., Panza, G.F., 1998. EurID: a regionalised 3D seismological model of Europe. Phys. Earth Planet. Inter. 105, 31–62.

Dziewonski, A.M., Bloch, S., Landisman, M., 1969. A technique for the analysis of transient seismic signals. Bull. Seism. Soc. Am. 59, 427–444.

Ekstrom, G., Morelli, A., Boschi, E., Dziewonski, A., 1998. Tensor analysis of the Central Italy sequence of September–October 1997. Geophys. Res. Lett. 25, 1971–1974.

Finetti, I.R., Boccaletti, M., Bonini, M., Del Ben, A., Geletti, R., Pipan, M., Sani, F., 2001. Crustal section based on CROP seismic data across the North Tyrrhenian–Northern Apennines–Adriatic Sea. Tectonophysics 343, 135–163.

Frepoli, A., Amato, A., 1997. Contemporaneous extension and compression in the Northern Apennines from earthquake fault-plane solutions. Geophys. J. Int. 129, 368–388.

Galadini, F., Galli, P., Leschiutta, I., Monachesi, G., Stucchi, M., 1999. Active tectonics and seismicity in the area of the 1997 earthquake sequence in Central Italy: a short review. J. Seismol. 3, 167–175.

Galadini, F., Meletti, C., Rebez, A. (A cura di), 2000. Le ricerche del GNDT nel campo della pericolosità sismica (1996–1999). CNR-Gruppo Nazionale per la Difesa dai Terremoti, Roma.

GNDT, and SSN, 1998. Registrazioni di aftershocks effettuate in Fabriano dal 4/11/97 al 14/11/97. CD-ROM.

Govoni, A., Spallarossa, D., Augliera, P., Trojani, L., 1999. The 1997 Umbria–Marche Earthquake Sequence: The Combined Data Set of the GNDT/SSN Temporary and the RESIL/RSM Permanent Seismic Networks. CD-ROM.

Haessler, H., Gaulon, R., Rivera, L., Console, R., Frogneux, M., Gasparini, C., Martel, L., Patau, G., Siciliano, M., Cisternas, A., 1988. The Perugia (Italy) earthquake of 29 April 1984: a microearthquake survey. Bull. Seism. Soc. Am. 78, 1948–1964.

Hunstad, I., Anzidei, M., Cocco, M., Baldi, P., Galvani, A., Pesci, A., 1999. Modelling coseismic displacements during the 1997 Umbria–Marche earthquake (Central Italy). Geophys. J. Int. 139, 283–295.

ISC, 1996. ISC Bulletin 1996 (Revised). ISC Catalogue 1964–1996. International Seismological Centre, CD-ROM.

Jolivet, L., Dubois, R., Fournier, R., Goffé, B., Michard, A., Jourdar, C., 1990. Ductile extension in Alpine Corsica. Geology 18, 1007–1010.

Keilis-Borok, V.I. (Ed.), 1989. Seismic Surface Waves in a Laterally Inhomogeneous Earth. Kluwer Academic Publisher, Dordrecht.

Knopoff, L., 1972. Observations and inversion of surface wave dispersion. In: Ritsema, A.R. (Ed.), The Upper Mantle; Tectonophysics 13 (1–4), 497–519.

Knopoff, L., Panza, G.F., 1977. Resolution of upper mantle structure using higher modes of Rayleigh waves. Ann. Geophys. 28, 211–218.

Kravanja, S., Panza, G.F., Sileny, J., 1999. Robust retrieval of seismic point source time function. Geophys. J. Int. 136, 385–394.

Lavecchia, G., Brozzetti, F., Barchi, M., Keller, J., Menichetti, M., 1994. Seismotectonic zoning in East-Central Italy deduced from the analysis of the Neogene to present deformations and related stress field. Bull. Soc. Geol. Am. 106, 1107–1120.

Levshin, A.L., Pisarenko, V.F., Pogrebinsky, G.A., 1972. On a frequency–time analysis of oscillations. Ann. Geophys. t.28 fasc.2, 211–218.

Levshin, A.L., Ratnikova, L., Berger, J., 1992. Peculiarities of surface wave propagation across Central Eurasia. Bull. Seism. Soc. Am. 82, 2464–2493.

Lucente, F.P., Chiarabba, C., Cimini, G.B., Giardini, D., 1999. Tomographic constraints on the geodynamic evolution of the Italian region. J. Geophys. Res. 104, 20307–20327.

Ludwig, W.J., Nafe, J.E., Drake, C.L., 1970. In: Maxwell, A.E. (Ed.), New Concepts of Sea Floor Evolution. Wiley/Interscience, New York, pp. 53–84.

Margheriti, L., Nostro, C., Cocco, M., Amato, A., 1996. Seismic anisotropy beneath the Northern Apennines (Italy) and its tectonic implications. Geophys. Res. Lett. 23 (20), 2721–2724.

Marson, I., Cernobori, L., Nicolich, R., Stoka, M., Liotta, D., Palmieri, F., Velicogna, I., 1998. CROP03 profile: a geophysical analysis of data and results. Mem. Soc. Geol. It. 52, 123–137.

Meghraoui, M., Bosi, V., Camelbeeck, T., 1999. Fault fragment control in Umbria–Marche, Central Italy, earthquake sequence. Geophys. Res. Lett. 26, 1069–1072.

Montone, P., Amato, A., Frepoli, A., Mariucci, M.T., Cesaro, M., 1997. Crustal stress regime in Italy. Annali di Geofisica 40 (3), 741–757.

Negredo, A.M., Barba, S., Carminati, E., Sabadini, R., Giunchi, C., 1999. Contribution of numeric dynamic modelling to the understanding of the seismotectonic regime of the Northern Apennines. Tectonophysics 315, 15–30.

Olivieri, M., Ekstrom, G., 1999. Rupture depths and source processes of the 1997–1998 earthquake sequence in Central Italy. Bull. Seism. Soc. Am. 89, 305–310.

Pantosti, D., Valensise, G., 1990. Faulting mechanism and complexity of the November 23, 1980, Campania–Lucania earthquake, inferred from surface observations. J. Geophys. Res. 95, 15319–15341.

Panza, G.F., 1981. The resolving power of seismic surface waves with respect to crust and upper mantle structural models. In: Cassinis, R. (Ed.), The Solution of the Inverse Problem in Geophysical Interpretation. Plenum Press, New York.

Panza, G.F., 1985. Synthetic seismograms: the Rayleigh waves modal summation. J. Geophys. Res. 58, 125–145.

Panza, G.F., Saraò, A., 2000. Monitoring volcanic and geothermal areas by full seismic moment tensor inversion: are non-double couple components always artifacts of modeling? Geophys. J. Int. 143, 353–364.

Panza, G.F., Schwab, F., Knopoff, L., 1973. Multimode surface waves for selected focal mechanism. I. Dip-slip sources on a vertical fault-plane. Geophys. J. R. Astron. Soc. 34, 265–278.

Panza, G.F., Schwab, F., Knopoff, L., 1975a. Multimode surface waves for selected focal mechanisms. II. Dip-slip sources. Geophys. J. R. Astron. Soc. 42, 931–943.

Panza, G.F., Schwab, F., Knopoff, L., 1975b. Multimode surface waves for selected focal mechanisms. III. Strike-slip sources. Geophys. J. R. Astron. Soc. 42, 945–955.

Panza, G.F., Mueller, S., Calcagnile, G., 1980. The gross features of the lithosphere–asthenosphere system in Europe from seismic surface waves and body waves. Pure Appl. Geophys. 118, 1209–1213.

Panza, G.F., Mueller, St., Calcagnile, G., Knopoff, L., 1982. Delineation of the north central Italian upper mantle anomaly. Nature 296, 238–239.

Peccerillo, A., Poli, G., Donati, C., 2001. The plio-quaternary magmatism of Southern Tuscany and Northern Latium: compositional characteristics, genesis and geodynamic significance. Ofioliti 26 (2a), 229–238.

Pialli, G., Barchi, M., Minelli, G., 1998. Results of the CROP03 deep seismic profile. Mem. Soc. Geol. It. 52, 657.

Piromallo, C., Morelli, A., 1997. Imaging upper mantle by P-wave travel time tomography. Annali di Geofisica 40, 963–979.

Pontevivo, A., Panza, G.F., 2002. Group velocity tomography and regionalization in Italy and bordering areas. Phys. Planet. Inter. 134, 1–15.

Riva, R., Aoudia, A., Vermeersen, L.L.A., Sabadini, R., Panza, G.F., 2000. Crustal versus asthenospheric relaxation and post-seismic deformation for shallow normal faulting earthquakes: the Umbria–Marche (Central Italy) case. Geophys. J. Int. 141, F7–F11.

Royden, L., Patacca, E., Scandone, P., 1987. Segmentation and configuration of subducted lithosphere in Italy: an important control on thrust-belt and foredeep-basin evolution. Geology 15, 714–717.

Salvi, S., Stramondo, S., Cocco, M., Tesauro, M., Hunstad, I., Anzidei, M., Briole, P., Baldi, P., Sansosti, E., Fornaro, G., Lanari, R., Doumaz, F., Pesci, A., Galvani, A., 2000. Modeling coseismic displacements resulting from SAR interferometry and GPS measurements during the 1997 Umbria–Marche seismic sequence. J. Seismol. 4, 479–499.

Saraò, A., Panza, G.F., Privitera, E., Cocina, O., 2001. Non-double couple mechanisms in the seismicity preceding 1991–1993 Etna volcano. Geophys. J. Int. 145, 319–335.

Scandone, P., 1979. Origin of the Tyrrhenian sea and Calabrian arc. Boll. Soc. Geol. It. 98, 27–34.

Selvaggi, G., Amato, A., 1992. Subcrustal earthquakes in the Northern Apennines (Italy): evidence for a still active subduction? Geophys. Res. Lett. 19, 2127–2130.

Selvaggi, G., Chiarabba, C., 1995. Seismicity and P-wave velocity image of the southern Tyrrhenian subduction zone. Geophys. J. Int. 121, 818–826.

Shapiro, N.M., Ritzwoller, M.H., 2002. Monte Carlo inversion for global shear velocity model of the crust and upper mantle. Geophys. J. Int. 151, 88–105.

Sileny, J., Panza, G.F., Campus, P., 1992. Waveform inversion for point source moment tensor retrieval with optimization of hypocentral depth and structural model. Geophys. J. Int. 108, 259–274.

Sileny, J., Campus, P., Panza, G.F., 1996. Seismic moment tensor resolution by waveform inversion of a few local noisy records. I. Synthetic tests. Geophys. J. Int. 126, 605–619.

Spakman, W., Van der Lee, S., Van der Hilst, R., 1993. Traveltime tomography of the European–Mediterranean mantle down to 1400 km. Phys. Earth Planet. Inter. 79, 3–74.

SSN and ENEL, 1998. Elaborazioni delle principali registrazioni accelerometriche della sequenza sismica umbro-marchigiana del settembre-ottobre 1997. CD-ROM.

Suhadolc, P., Panza, G.F., 1989. Physical properties of the lithosphere–asthenosphere system in Europe from geophysical data. In: Boriani, A., et al. (Eds.), The Lithosphere in Italy; Accad. Naz. Lincei 80, 15–40.

Urban, L., Cichowicz, A., Vaccari, F., 1993. Computation of analytical partial derivatives of phase and group velocities for Rayleigh waves respect to structural parameters. Stud. Geophys. Geod. 36, 14–36.

Valyus, V.P., Keilis-Borok, V.I., Levshin, A.L., 1969. Determination of the velocity profile of the upper mantle in Europe. Proc. Acad. Sci. USSR 185, 3.

Wortel, M.J.R., Spakman, W., 1992. Structure and dynamics of subducted lithosphere in the Mediterranean region. Proc. Kon. Ned. Akad. Wetensch. 95 (3), 325–347.

Wortel, M.J.R., Spakman, W., 2000. Subduction and slab detachment in the Mediterranean–Carpathian region. Science 290, 1910–1917.

Yanovskaya, T.B., Antonava, L.M., 2000. Lateral variations in the structure of the crust and upper mantle in the asian region from data on the group velocity of Rayleigh WAVES. Phys. Solid Earth 36, 121–128.

Yanovskaya, T.B., Ditmar, P.G., 1990. Smoothness criteria in surface wave tomography. Geophys. J. Int. 102, 63–72.

Yanovskaya, T.B., Kizima, E.S., Antonova, L.M., 1998. Structure of the crust in the Black Sea and adjoining regions from surface wave data. J. Seismol. 2, 303–316.

Yanovskaya, T.B., Antonova, L.M., Kozhevnikov, V.M., 2000. Lateral variations of the upper mantle structure in Eurasia from group velocities of surface waves. Phys. Earth Planet. Inter. 122, 19–32.

Buoyancy-Driven Deformations and Contemporary Tectonic Stress in the Lithosphere beneath North-Central Italy

A. Aoudia, A. T. Ismail-Zadeh and G. F. Panza

Abstract. On the basis of a revisited crust and uppermost mantle Earth structure that supports delamination processes beneath North-Central Italy we study the continental deformation and model the contemporary flow and stress distribution in the lithosphere. The rate of the modeled lithospheric flow is in agreement with GPS data and its patterns explain the heat flux, the regional geology and provide a new background for the genesis and age of the recent Tuscan magmatism. The modeled stress in the lithosphere is spatially correlated with gravitational potential energy patterns and show that internal buoyancy forces, solely, can explain the coexisting regional contraction and extension and the unusual intermediate depth seismicity.

Introduction

The juxtaposed contraction and extension observed in the crust of the North-Central Italian Apennines (Fig. 1) and elsewhere has, for a long time, attracted the attention of geoscientists and is a long-standing enigmatic feature. Several models, invoking mainly external forces, have been put forward to explain the close association of these two end-member deformation mechanisms clearly observed by seismological and geological investigations [*e.g. Frepoli and Amato, 1997; Montone et al., 1999*; *Doglioni et al., 1999*]. These models appeal to interactions along plate margins or at the base of the lithosphere, or to subduction processes [*e.g. Negredo et al., 1999; Wortel and Spakman, 2000*]. Some of the geodynamic models were constrained by earth models that resolve fairly well either the crust [*e.g. Pialli et al., 1998*] or the mantle structures [*e.g. Wortel and Spakman, 2000*] but not the crust-uppermost mantle structures [*e.g. Agostinetti et al., 2002; Chimera et al., 2003*].

The geodynamic complexity of the Central part of Italy makes the kinematics of the present day deformation and its relationships with the recent magmatism and seismicity less well understood. To unravel some of these aspects, geophysical models of the earth structure, compatible with independent gravity, heat-flow, petrological and geochemical data, that provide enough resolving power to the investigated deformation are required.

We study the contemporary continental tectonic stress along a west-east transect crossing the whole Peninsula from the Tyrrhenian coast, via the Umbria-Marche geological domain, to the Adriatic coast. We make use of a recently published crust/lithosphere-asthenosphere structural earth model [*Chimera et al., 2003*]. Although external forces must have been important in the building up of the North-Central Apennines, we investigate the contribution of internal

buoyancy forces with respect to the ongoing slow and complex lithospheric deformations, as revealed by very recent GPS solutions and by the unusual intermediate depth seismicity distribution [*Selvaggi and Amato, 1992*] that does not define a classical Benioff zone. Our study brings additional constraints to the recent magmatism [*Peccerillo, 2002*] observed in Tuscany and highlights the importance of gravitational body forces in the geodynamics of the Central Mediterranean.

Set up of the numerical models

The earth model we use is the S-wave velocity model by Chimera et al. [*2003*] retrieved by using deep seismic sounding profiles, crossing the whole Peninsula [*Pialli et al., 1998*] from the Tyrrhenian via the Tuscan Metamorphic Complex (TMC) and the Umbria-Marche geological domain (UMD) [*Bally et al., 1986*] to the Adriatic, as a priori constraints of new shallow and deep tomographic inversions of surface waves. The retrieved crust and lithospheric mantle (lid) exhibit lateral variation in thickness. Lithospheric roots, more than 120 km wide, between the TMC and UMD, reach a depth of at least 130 km. A sharp and well-developed low-velocity zone in the uppermost mantle (mantle wedge), from the Tyrrhenian dying out beneath the Apennines, separates crust and lid. The lateral variation in the Moho geometry by Chimera et al. [*2003*] is in agreement with the one computed by Agostinetti et al. [*2002*] using receiver functions from broad-band seismic stations beneath the same study transect.

In the uppermost 50 km of the model given in Fig. 1, we use density values estimated from a high-resolution gravimetry survey [*Marson et al., 1998*] made along the study profile. For the deeper structures we convert the S-wave velocity model [*Chimera et al., 2003*] into density [*Ludwig et al., 1970*] considering temperature effects. The concordance between the gravity anomaly directly computed from our density model (no data fitting) and the observed Bouguer anomaly (Fig. 1) is a measure of the reliability of our assumptions linked to the density estimates. Doing so, we fix the density and geometry of the crust-mantle structure, and the viscosity is the only variable parameter in our models.

Viscosity is an important physical parameter in stress modeling, because it influences the stress state and results in strengthening or weakening of Earth's material. The viscosity model of the UMD crust is consistent with the findings of Aoudia et al. [*2003*] computed from the viscoelastic relaxation of the 1997 Umbria-Marche normal faulting earthquake sequence. Being the least-known physical parameter of the model, the effective viscosity of the lithospheric mantle beneath the UMD can be constrained considering the observed regional strain rates. Sub-crustal earthquakes in the region provide an indirect measure of the rate of strain release within the seismogenic body. To compute the observed seismic moment released beneath the UMD in the depth range 30 - 80 km, we used the Harvard Centroid-Moment Tensor Catalog (1977-2002) which contains events with M≥5. Two large shocks occurred in the region: in 19.09.1979 (M_W=5.8) and in 26.03.1998

(M_W=5.4). The remaining UMD sub-crustal earthquakes have lower magnitudes, and their contribution to the cumulative seismic moment release (CSMR) is very low. The CSMR is estimated to be about 8.5×10^{17} N m for the region. Using Kostrov's formula the strain rate, within a volume V (50 km × 50 km × 50 km) over a time interval t (20 years), is 8.5×10^{-17} s^{-1}. This strain rate is used as a constraint on the viscosity of the lid in our test computations vs. the modeled strain rate for various viscosity ratios between lid and asthenosphere. Based on these tests we adopted the effective viscosity of the lid beneath the UMD to be 5×10^{22} Pa s.

To constrain the lateral variation in the viscosity of the lithosphere (Fig. 2), we converted the S-wave velocity model of Chimera et al. [*2003*] to temperature using an approach similar to Goes et al. [*2000*] with a variable compositional rock structure as given in Peccerillo [*2002*].

Slow viscous flow and tectonic (deviatoric) stress are found from the momentum conservation and continuity equations. By defining the stream function ψ as a velocity potential $\mathbf{v} = (\partial\psi/\partial x_2, -\partial\psi/\partial x_1)^{\mathrm{T}}$ the governing equations can be combined to form:

$$\left(\frac{\partial^2}{\partial x_2^2}-\frac{\partial^2}{\partial x_1^2}\right)\eta\left(\frac{\partial^2\psi}{\partial x_2^2}-\frac{\partial^2\psi}{\partial x_1^2}\right)+4\frac{\partial^2}{\partial x_1\partial x_2}\eta\frac{\partial^2\psi}{\partial x_1\partial x_2}=-g\frac{\partial\rho}{\partial x_1} \quad (1)$$

Here (x_1, x_2), ρ, η, and g are the Cartesian co-ordinates, density, viscosity, and acceleration due to gravity, respectively. The equations are solved together with the appropriate boundary and initial conditions. A two-dimensional Eulerian finite element approach [*Naimark et al., 1998*] is used to solve the corresponding discrete problem derived from Eq. (1). This is based on the Galerkin method and bi-cubic spline interpolations of unknown variables. The method has been successfully applied to model stress field in a descending slab [*e.g. Ismail-Zadeh et al., 2000*].

The maximum shear stress is determined from the computed components of the tectonic stress tensor τ_{ij} $(i, j = x_1, x_2)$:

$$\tau_{\max}=\left[\frac{1}{2}\left(\tau_{11}^2+\tau_{22}^2+2\tau_{12}^2\right)\right]^{1/2}=\eta\left[4\left(\frac{\partial^2\psi}{\partial x_1\partial x_2}\right)^2+\left(\frac{\partial^2\psi}{\partial x_2^2}-\frac{\partial^2\psi}{\partial x_1^2}\right)^2\right]^{1/2} \quad (2)$$

To minimize boundary effects, the studied cross-section has been extended along the horizontal (100 km leftward and 100 km rightward) and vertical (10 km upward and 190 km downward) directions. We prescribe free slip conditions at the boundary of this extended model domain. We use zero-density and 10^{15} Pa s viscosity for the layer above the

seismic section as an approximation to the physical parameters of air. Horizontally and downward, the density and viscosity of the extended regions are kept constant and equal to that at the relevant portion of the boundary of the cross-section. The model domain is divided into 98x94 elements in the horizontal and vertical directions, with a spatial resolution of 4.46 km × 4.89 km.

Model results

The modeled flow field responds directly to the density and viscosity distributions (Fig. 2). The motion of the crust and mantle is caused by the negative buoyancy of the lid and the positive buoyancy of the mantle wedge. The downward motion due to the denser lid sinking in the mantle can be responsible for the subsidence of the Adriatic realm, and the up-welling predicted at the western part of the profile contributes to the tectonic uplift in Tuscany, where the horst-graben structure is observed. Therefore the predicted flow field is in agreement with the regional geological observations [*Pialli et al, 1998*].

The velocities predicted by the numerical model in the upper crust of the region (about 3 mm yr^{-1} as a maximum horizontal velocity at the surface) correlate in magnitude with the preliminary results from the two continuous GPS stations CAME and ELBA (Fig. 1) we deliberately installed, in late 2000, along the transect to monitor the ongoing continental deformation [Gardi et al., 2003]. CAME (Camerino) and ELBA (Elba Island) stations are located at both edges of the continental extension. CAME is right in-between the juxtaposed extension and compression. The CAME-ELBA baseline computed from the ASImed (geodaf.mt.asi.it) GPS-VLBI-SLR combined solution is extending at a rate of 2.6 ± 2.3 mm yr^{-1} [*Devoti, personal communication*].

The computed upward and downward flow field, visible in the western and the eastern parts of the transect, respectively, is well in agreement with the sharp decrease of the heat flow values from west to east (Fig. 2). The horizontal eastward flow field observed within the low velocity mantle wedge (between 0 and 150 km distance, Fig. 2) that decouples the crust from the lid (between 30 and 50 km depth, Fig. 2) is compatible with a delamination process and it may explain the mantle wedge emplacement. The magmatic rocks, at the surface, rich in incompatible elements and their crustal-like isotopic signatures consistent with a genesis in a sub-crustal anomalous mantle [*Peccerillo, 2002*], and the high heat flow values (in agreement with the computed upward flow field) suggest that this mantle wedge is a partially molten mantle that feeds the TMC. The clear decrease in the ages of the TMC rocks ranging from 8-7 to 0.2 Ma from west to east along the transect [*Peccerillo, 2002*], is compatible with the predicted eastward flow in the mantle wedge.

As shown in Fig. 2, the lateral variation in the viscosity of the lithosphere corresponds to the rather sharp heat flow difference (> 100 mW/m^2) observed in the area. To test the stability of our results (Fig. 3) we consider three models of

viscosity profiles: (i) model *a* viscosity distribution is shown in Fig. 2; (ii) in model *b* the effective viscosity of the TMC upper crust is less than that in model *a* by a factor of 5; and (iii) in model *c*, the effective viscosity of the UMD upper crust is higher than that in model *a* by a factor of 5. Figure 3 shows the state of tectonic stress in the study transect. A decrease in the effective viscosity of the upper crust beneath TMC does not affect strongly the stress field (compare *a* and *b*). The higher effective viscosity of the upper crust beneath the UMD, the larger shear stress (*c*). The maximum horizontal compressional stress is associated with the lid below the UMD, in the depth range from 50 to 80 km. This finding is in good agreement with the compressional mechanisms of well-constrained fault-plane solutions [*Selvaggi and Amato, 1992*]. The region of high shear stress in the models correlates well with the distribution of the sub-crustal seismicity reported in the literature [*e.g. Chimera et al., 2003*]. The puzzling hypocenter location of the sub-crustal seismicity, which does not define a Wadati-Benioff seismic zone, can now be explained by the particular geometry and buoyancy of the delaminating lithosphere. In the crust the models predict compressional regime at the eastern part of the profile, as already reported in the literature, and tension just below the Umbria-Marche Apennines, where the 1997 normal faulting earthquake sequence took place. Our stress models predict tension below the Quaternary extensional sedimentary basins (Fig. 3) as well. The crust exhibits tension where the TMC outcrops and where the underlying mantle wedge and the asthenospheric low velocity layer are uprisen. This localized uplift-subsidence type of motion is in agreement with a radial extension in proximity of Quaternary vertical intrusions [*Patacca and Scandone, 1989*]. The geoid, with a centimeter precision [*Barzaghi et al., 2002*], that is a proxy for the amount of gravitational potential energy (GPE) available to drive deformation in the lithosphere, exhibits its steepest gradient (Fig. 3) where the lithosphere is highly deformed (km 150-200 distance, Fig 3). The deformation patterns, either observed or modeled, are spatially correlated with GPE patterns.

Conclusions and discussion

We have shown here that the buoyancy forces that result from the density distribution in the lithosphere govern the present day deformation within North-Central Italy and can explain regional coexisting contraction and extension and the shallow depth and unusual distribution of intermediate depth earthquakes. The modeled uppermost mantle flow supports the lithospheric delamination beneath the peninsula and provides a unifying background for petrological and geochemical studies of recent magmatism and volcanism in Tuscany.

The reported unchanged time-space stress field, inferred from the magnetic anisotropy of Plio-Pleistocene sediments [*Sagnotti et al., 1999*] in the compressional part, and the distribution of the thick extensional Quaternary sedimentary basins, in places where our model predicts high magnitude

tension, makes us think that buoyancy is the prevailing mechanism in this slow-rate deforming area since, at least, Pleistocene times. This is further supported by the compatibility between the eastward flow within the mantle wedge delaminating the lid from the crust and the clear eastward decrease in the ages of the Plio-Quaternary magmatism (8-7Ma – 0.2Ma).

Acknowledgments. The work benefited from discussions with R. Barzaghi, R. Devoti and A. Peccerillo. Constructive criticism by G. Houseman substantially improved an initial version of the manuscript. We thank two anonymous reviewers for their helpful comments. This research was funded by Italian MIUR Cofin-2002. A.T.I-Z was supported by the Alexander von Humboldt-Stiftung.

References

Agostinetti, N. P., F. P. Lucente, G. Selvaggi, and M. Di Bona, Crustal structure and Moho geometry beneath the Northern Apennines (Italy), *Geophys. Res. Lett., 29 (20)*, 60-1/4, 2002.

Aoudia, A., et al., Postseismic deformation following the 1997 Umbria-Marche (Italy) moderate normal faulting earthquakes, *Geophys. Res. Lett., 70*, 1390-1393, 2003.

Barzaghi, R., B. Betti, A. Borghi, G. Sona, and V. Tornatore. The Italian quasi-geoid ITALGEO99. *Bollettino di Geodesia e Scienze Affini, 1*, 33-51, 2002.

Bally, A.W., L. Burbi, C. Cooper, and R. Ghelardoni, Balanced sections and seismic reflection profiles across the Central Apennines, *Mem. Soc. Geol. It., 35*, 257-310, 1986..

Chimera, G., A. Aoudia, A. Sarao', and G.F. Panza, Active Tectonics in Central Italy: constraints from surface wave tomography and source moment tensor inversion, *Phys. Earth Planet. Inter., 138*, 241-262, 2003.

Gardi, A., R. Sabadini, C. Ferraro, and A. Aoudia, The interplay between global tectonic processes and the seismic cycle in the Umbria–Marche seismogenic region, *Geophys. J. Int., 155*, 1093 – 1104, 2003.

Goes, S., R. Govers, and P. Vacher, Shallow mantle temperatures under Europe from *P* and *S* wave tomography. *J. Geophys. Res.* 105, 111, 53-11169, 2000.

Della Vedova, B., S. Bellani, G. Pellis, and P. Squarci, In: Vai, G.B., and Martini, I.P., (Editors). *Anatomy of an Orogen*: the Apennines and Adjacent Mediterranean Basins. Kluwer Academic Publisher, 65-76, 2001.

Doglioni, C., P. Harabaglia, S. Merlini, F. Mongelli, A. Peccerillo, and C. Piromallo, Orogens and slabs vs. their direction of subduction. *Earth-Science Reviews, 45*, 167-208, 1999.

Frepoli, A., and A. Amato, Contemporaneous extension and compression in the Northern Apennines from earthquake fault-plane solutions, *Geophys. J. Int., 129*, 368-388, 1997.

Ismail-Zadeh, A.T., G.F. Panza, and B. N. Naimark, Stress in the descending relic slab beneath the Vrancea region, Romania, *Pure Appl. Geophys. 157*, 111-130, 2000.

Ludwig, W.J., J.E. Nafe, and C.L. Drake, In: Maxwell, A.E., (Editor). *New concepts of sea floor evolution*. Wiley-Interscience, New York: 53-84, 1970.

Marson, I., L. Cernobori, R. Nicolich, M. Stoka, D. Liotta, F. Palmieri, and I. Velicogna, CROP-03 profile: a geophysical analysis of data and results, *Mem. Soc. Geol. It., 52*, 123-137, 1998.

Montone, P., A. Amato, and S. Pondrelli, Active stress map of Italy, *J. Geophys. Res. 104*, 25595-25610, 1999.

Naimark, B.N., A.T. Ismail-Zadeh, and W.R. Jacoby, Numerical approach to problems of gravitational instability of geostructures with advected material boundaries, *Geophys. J. Int.* 134, 473-483, 1998.

Negredo, A.M., S. Barba, E. Carminati, R. Sabadini, and C. Giunchi, Contribution of numeric dynamic modelling to the

understanding of the seismotectonic regime of the Northern Apennines, *Tectonophysics, 315*, 15-30, 1999.
Patacca, E. and P. Scandone, In: The lithosphere in Italy. (eds Boriani et al.) 157-176 (Acc. Naz. Lincei., 80), 1989.
Peccerillo, A., Quaternary magmatism in central-southern Italy: a new classification scheme for volcanic provinces and its geodynamic implications, *Boll. Soc. Geol. It.*, 1, 113-127, 2002.
Pialli, G., M. Barchi, and G. Minelli (eds), Results of the CROP03 Deep Seismic Reflection Profile, *Mem. Soc. Geol. It.*, *LII*, 657 pp., 1998.
Sagnotti *et al*. Magnetic anisotropy of Plio-Pleistocene sediments from the Adriatic margin of the northern Apennines (Italy): implications for the time-space evolution of the stress field. *Tectonophysics*, 311, 139-153, 1999.
Selvaggi, G., and A. Amato, Subcrustal earthquakes in the Northern Apennines (Italy): evidence for a still active subduction? *Geophys. Res. Lett.*, 19, 2127-2130, 1992.
Wortel, M.J.R., and W. Spakman, Subduction and slab detachment in the Mediterranean-Carpathian region. *Science, 290*, 1910-1917, 2000.

A. Aoudia, G.F. Panza, Abdus Salam International Centre for Theoretical Physics, SAND Group, Trieste, Italy & Dept. of Earth Sciences, University of Trieste, Italy. (e-mail: aoudia@dst.units.it, panza@dst.units.it)

A. T. Ismail-Zadeh, International Institute of Earthquake Prediction Theory and Mathematical Geophysics, Russian Academy of Sciences, Moscow, Russia & Geophysikalisches Institut, Universität Karlsruhe, Germany (e-mail:. Alik.Ismail-Zadeh@gpi.uni-karlsruhe.de).

(Received ?, 2004; revised ?,?; accepted ?, ?)

AOUDIA ET AL.: BUOYANCY-DRIVEN DEFORMATIONS

AOUDIA ET AL.: BUOYANCY-DRIVEN DEFORMATIONS

Figure 1.
(a) Density model of the crust and uppermost mantle beneath North-Central Italy and the hypocentres of the sub-crustal earthquakes (vertical bars indicate the depth error) recorded in the period 1965-1998 (Selvaggi and Amato, 1992; ISC) within a stripe 150 km wide along the study profile (red line in the inset). The study profile, from the Tyrrhenian to the Adriatic coastlines, crosses the Tuscan Metamorphic Complex (TMC) and the Umbria-Marche geological Domain (UMD). The bold black segment indicates the Moho depth (Chimera et al. 2003). The topmost line presents the surface topography.
(b) Observed (Marson et al., 1998) Bouguer gravity anomaly (blue) vs. gravity (red) predicted from our density model.
(**c, d**) study profile and schematic geological model after Patacca and Scandone (1989) and locations of continuous GPS stations.

Figure 2.
Effective viscosity used and predicted flow field (bottom panel). A reduction of the effective viscosity of the crust and mantle lithosphere at the left of the model correlates with a high heat flow observed in the region (Della

Vedova et al., 2001 - upper panel) and with the recent magmatism (Peccerillo, 2002).

Figure 3.
Tectonic shear stress and compressional axes (ticks) predicted by models (a), (b) and (c) along the studied profile (tensional axes are perpendicular to the compressional ones). The horizontal ticks indicate thrusting and vertical ticks indicate normal faulting. The viscosity profile for model (a) is shown in Fig. 2. See text for models (b) & (c). The geoid height computed from Barzaghi et al. (2002) exhibits its steepest gradient along the study profile and above the area of maximum deformation predicted in model (a).

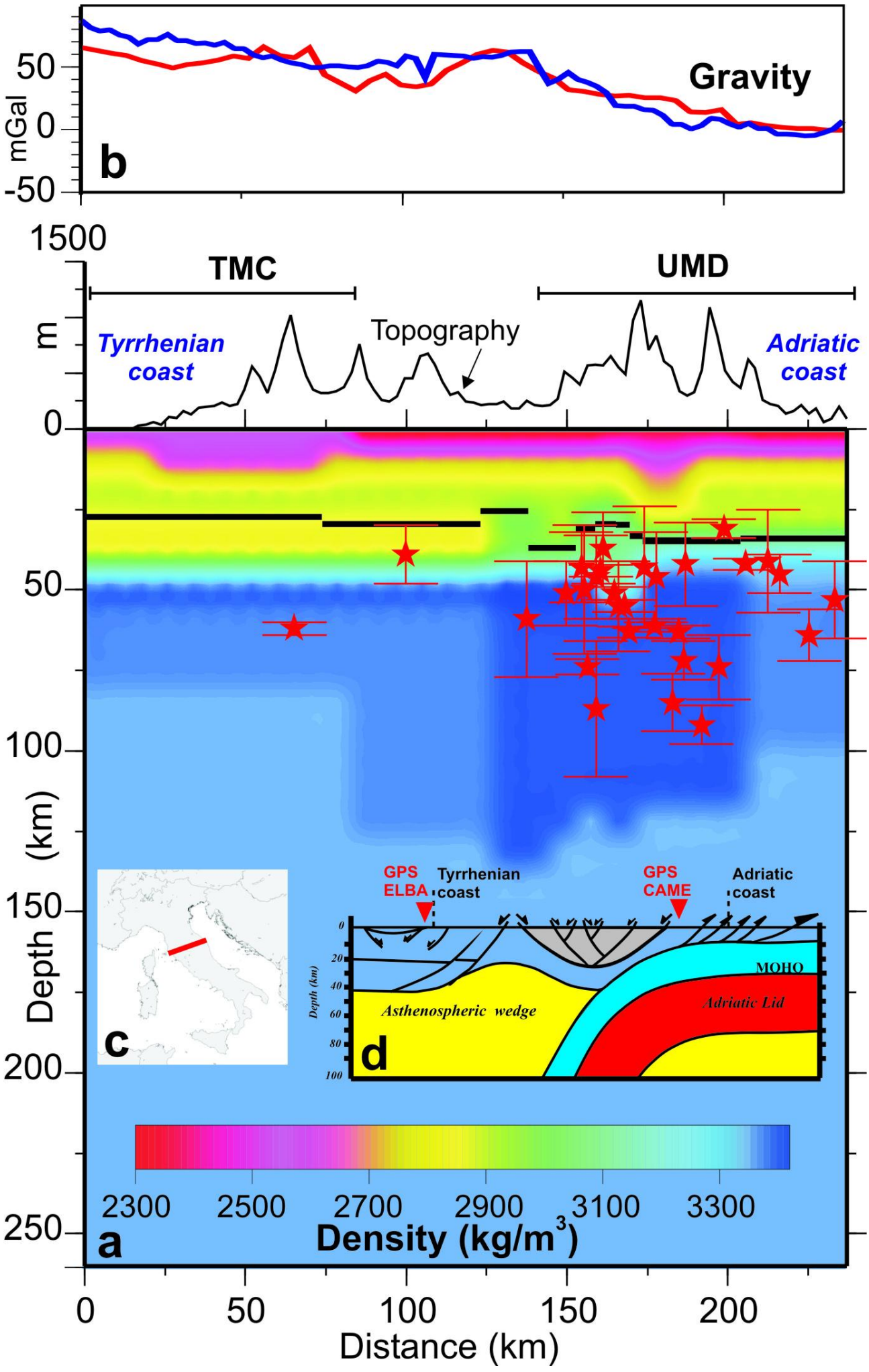
Gravity
mGal
50
0
-50
b
1500
TMC
UMD
Topography
Tyrrhenian coast
Adriatic coast
m
0
50
100
150
200
250
Depth (km)
GPS ELBA
Tyrrhenian coast
GPS CAME
Adriatic coast
MOHO
Asthenospheric wedge
Adriatic Lid
Depth (km)
0
20
40
60
80
100
c
d
2300
2500
2700
2900
3100
3300
Density (kg/m3)
a
0
50
100
150
200
Distance (km)

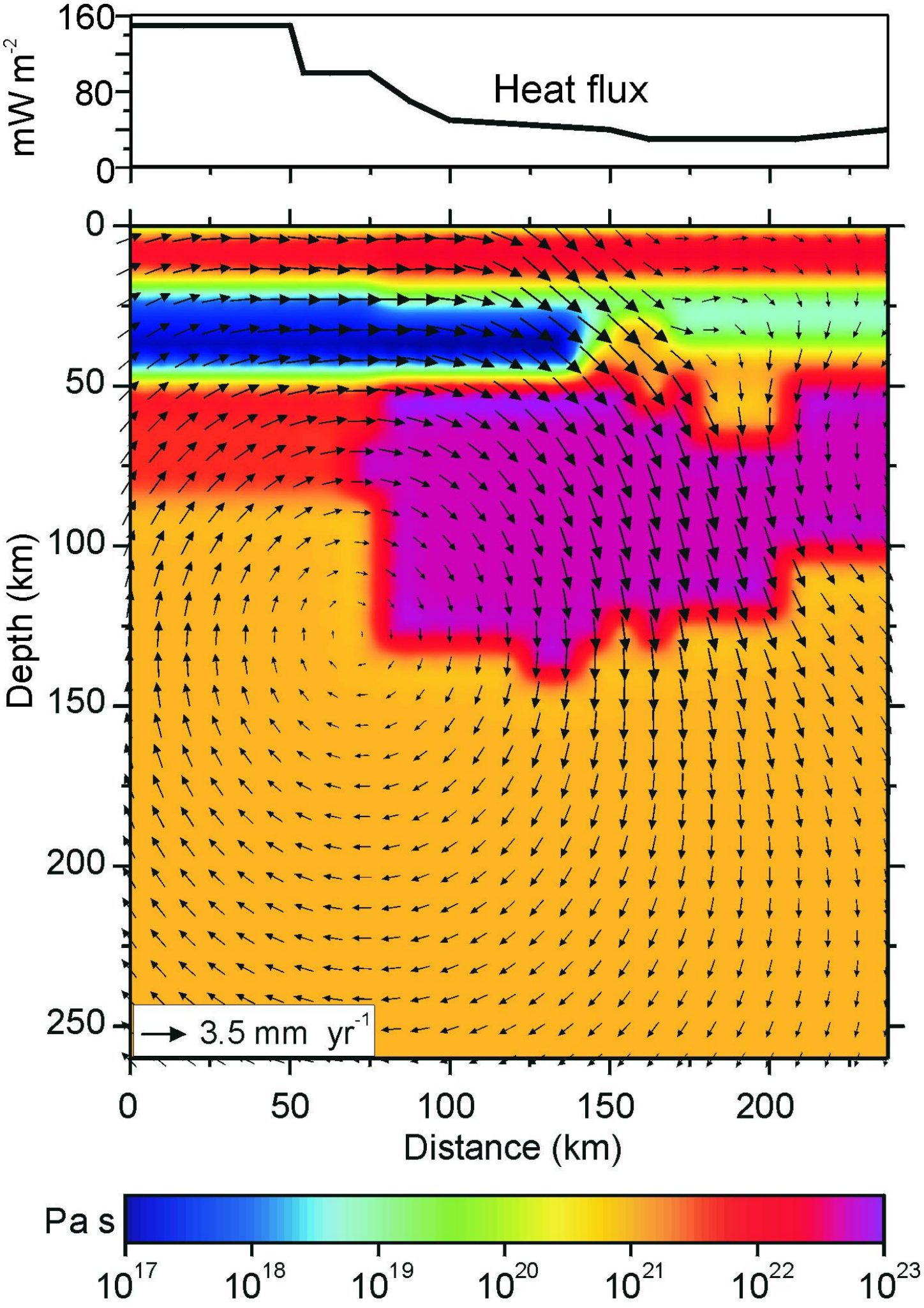
160
80
0
mW m-2
Heat flux
0
50
100
150
200
250
Depth (km)
3.5 mm yr-1
0
50
100
150
200
Distance (km)
Pa s
10^17
10^18
10^19
10^20
10^21
10^22
10^23

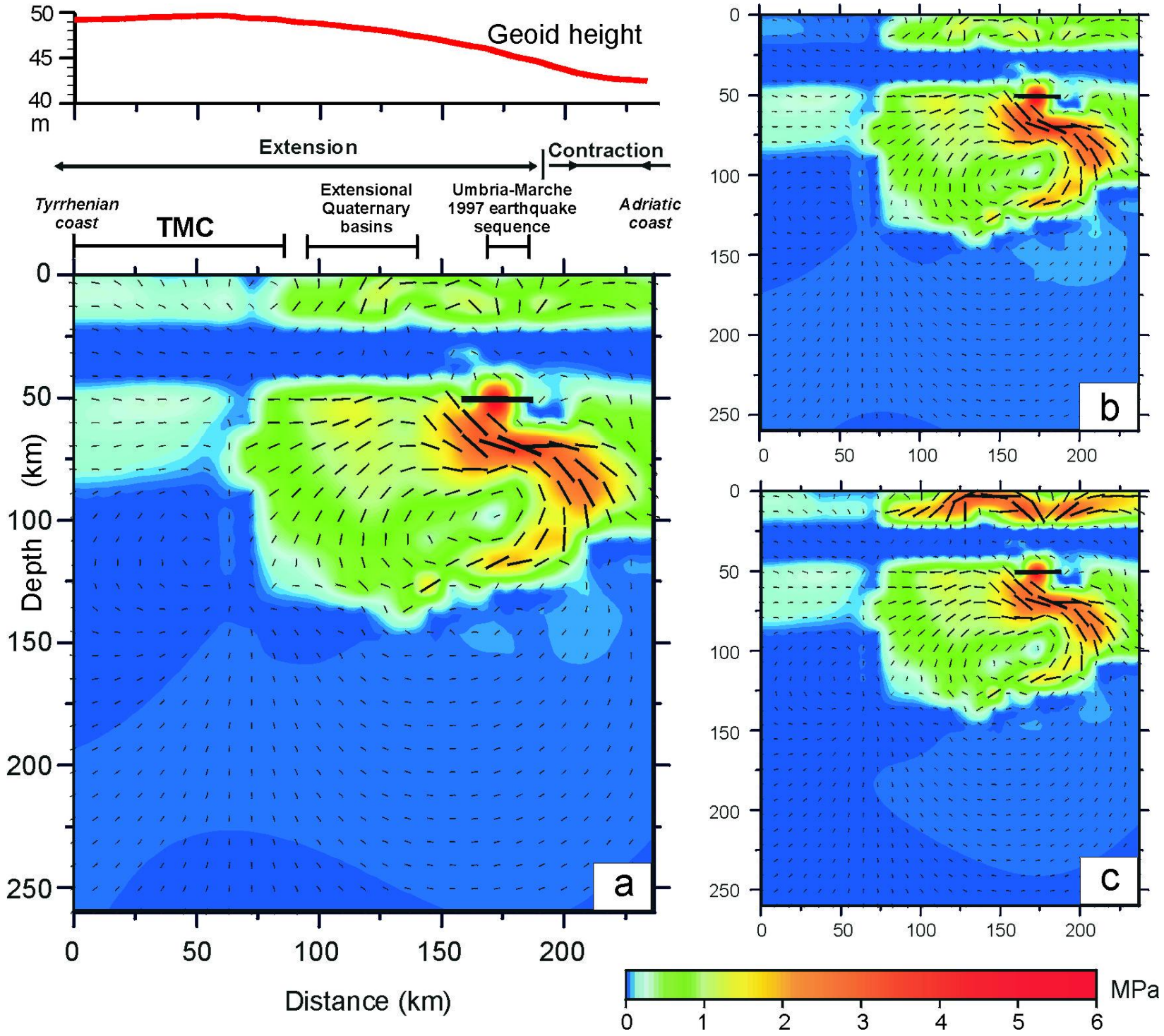
Geoid height
50
45
40
m
Extension
Contraction
Tyrrhenian coast
TMC
Extensional Quaternary basins
Umbria-Marche 1997 earthquake sequence
Adriatic coast
Depth (km)
Distance (km)
a
b
c
MPa
0
1
2
3
4
5
6